Three-Zone in-cylinder process model for DI diesel engines

SDPO.14.010.m

Sebastián Galindo López

Master of Science Thesis

Mechanical Systems and Integration

Three-Zone in-cylinder process model for DI diesel engines

SDPO.14.010.m

Master of Science Thesis

For the degree of Master of Science in Mechanical Engineering at Delft University of Technology

Sebastián Galindo López

April 17, 2014

Faculty of Mechanical, Maritime and Materials Engineering (3mE) · Delft University of Technology

Delft University of Technology
Department of
Marine technology (mt)

The undersigned hereby certify that they have read and recommend to the Faculty of Mechanical, Maritime and Materials Engineering (3mE) for acceptance a thesis entitled

THREE-ZONE IN-CYLINDER PROCESS MODEL FOR DI DIESEL ENGINES

by

SEBASTIÁN GALINDO LÓPEZ

in partial fulfillment of the requirements for the degree of

MASTER OF SCIENCE MECHANICAL ENGINEERING

Dated: April 17, 2014

Supervisor(s):

Prof.ir. Douwe Stapersma

Reader(s):

Prof.ir. Douwe Stapersma

Prof.dr.ir. Bendiks Jan Boersma

Ir. Klaas Visser

Ir. Peter de Vos

Table of Contents

List of Figures

Summary

The need to reduce harmful emissions to the environment is been addressed on different fronts. Diesel engines, as one of the prime movers in transport industry, has become an active research focus for several years in order to improve their efficiency while keeping the harmful emissions the lowest possible. The inclusion of more stringent regulations and emission control areas such as NECA in the north sea demands for a better understanding of the combustion process in the cylinder in order to reduce emissions. To study such problem an approach is to regard the cylinder as a perfectly mixed volume. This concept is very simple and allows for fast calculations but it lacks the physics and the resolution necessary to study pollutants formation.

The main objective of this thesis is to propose a model where the cylinder volume is divided into a few volumes, so the cylinder process can be studied in more detail and some resolution is included to calculate NO emissions.

A model with three control volumes, called zones, is introduced. One zone represents the liquid fuel in the cylinder and two zones represent the gas mixture. In one of the gaseous zones the mixture preparation and combustion reaction occur; the second gaseous zone provides the oxidant to the previous zone and the combustion products are further mixed with air.

The detailed model and the equations necessary to simulate the process are introduced. The required sub-models are proposed and the implementation of the complete model is done in different steps. First the liquid volume is treated and tested under a set of different conditions. In a second step the gas phase is simulated by neglecting the existence of liquid fuel in the cylinder. Finally, the complete model is assembled and NO formation mechanism is coupled with the model, testing is done allowing to evaluate the concept.

Acknowledgements

This work is the result of a long year of work that took me trough an exciting yet challenging journey, and it would have not been possible without the support of many people surrounding me. First of all, I would like to thank my supervisor Prof.ir. Douwe Stapersma for his assistance during the writing of this thesis. From him I have learnt many lessons that I will bring with me wherever I am. I cannot thank enough for the extensive hours he spent with me debating ideas and helping me with the difficulties that arouse while working on this project, also the particular interest he took on this project.

None of this would have been possible without the love and support of my family, especially my parents. Thanks for the patience when things were not going as expected and believing in me unconditionally. I could not have better parents.

This experience in The Netherlands would not have been the same without the company of many friends with whom I have shared a beer or discussion when not burning the midnight oil. I hope we all keep in contact.

I am grateful to COLFUTURO who financed my living and studying in the Netherlands, this allowed me to achieve an important goal in my life and opened the doors to an amazing personal experience.

Finally, I want to thank my flatmates Sergio and Liliana, they have been a great support this year.

Delft, University of Technology — Sebastián Galindo López
April 17, 2014

Chapter 1

Introduction

This study contributes to the development of diesel engines simulation, and in this particular case combustion modelling. The reason is based on the public need for maintaining, or even improving, current prosperity, while preserving the environment and the health of mankind.

On a daily basis this means, amongst others, that one has to comply with stringent regulations concerning internal combustion engine emissions. These emissions include pollutants like nitrogen oxides (NO_x) and soot. Not to forget CO_2 emissions that contribute to green house effect. Another implication of this public need, together with an increase of the global energy demand, is the depletion of fossil fuels, which makes a call for efficient use of organic fuels.

The reduction of harmful emissions together with the efficient use of fossil fuels is linked to the research on diesel engines, which are the prime mover on shipping, rail, heavy-duty transport, and increasingly in passenger cars. Conventional engine design approaches that rely on prototype development are too time-consuming and expensive, development of predictive and efficient computational tools would represent a significant step forward in the ability to rapidly design high efficiency, low emission systems. Modern diesel technology consists of direct liquid fuel injection under high pressure, which forms a non-homogeneous mixture leading to relatively high levels of soot. This spray formation process may seem straightforward, but in reality it is dauntingly complex. And also the combustion presents especially difficult and complex challenges.

The in-cylinder process modelling covers different levels which increases in complexity as well as computational time with the level of detail needed. On the one side the zero dimensional analysis that brings low computational cost but no possibility to compute emissions and to the other extreme computational fluid Mechanics (CFD) modelling which solves for detailed flow phenomena and chemistry but with a high computational cost. In between this two, is allocated the so-called phenomenological models that permit to compute emissions levels with a degree of accuracy but without the need to solve the complex flow phenomena in the cylinder thus reducing computational time, making them a very attractive tool to develop propulsion or generation systems.

The aim of this study is to produce a three-zone model to simulate the in-cylinder process of DI diesel engines. It means the use of techniques to simulate the in-cylinder process in Diesel

engines introducing a number of zones to describe mean effects of different sub-processes present in the cylinder, allowing to have a temperature distribution. This temperature distribution in the hope that there is a zone where temperatures are high enough to activate the chemical mechanism by which NO_x is produced, and if so the temperature path is correct to reproduce emission trends.

1-1 Literature Review

The chemical reaction kinetics, which describes the formation of nitrogen oxides and soot particles in diesel engine combustion, is a highly non-linear example of temperature and material composition dependent problem. It follows that with a simple averaging of diesel states over the entire combustion chamber with known burning rate leads to unreliable calculations of pollutant emissions. To compute pollutant emissions, additionally to the time discretization, a spatial discretization is required. For the reason mentioned above, the so-called phenomenological, multi-zone combustion models have been developed, where a compromise between accuracy and computational effort is shown.

In the literature has been reported in the past, a number of such simulation models. The following is a selection of these models, some of them in relation to the subdivision of the combustion chamber volume in a number of zones, and others as a reference to the generic modelling of heat release on very different assumptions and simplifications.

Thermodynamic Two-Zone Models

The models presented in this section are based in the exposition made by Merker and colleagues in [1, 6, 7].

1-1-1 Hohlbaum Model

In this model [1], the combustion chamber is divided into two zones of equal pressure, which one should imagine as being divided by the flame front and a direct boundary. Strictly speaking, the flame front itself represents a zone onto itself, i.e. the third zone (fig. 1-1).

Zone 1 contains unburned mixture, i.e. air and fuel, which will in the following be designated as unburned zone and described with the state quantities $p, V_1, T_1, n_{1,i}$, and λ_1.

Zone 2 should contain burned mixture, consisting of incompletely oxidized fuel, and will in the following be designated as burned zone and described with the state quantities $p, V_2, T_2, n_{2,i}$,and λ_2. In zone 2, secondary oxidation occurs. For this, reaction kinetic models are necessary. Thermal NOx formation also takes place in zone 2, which is described by the Zeldovich mechanism.

The flame front separates both of these zones. It is assumed to be infinitely thin and without mass. Primary oxidation takes place in the flame front until equilibrium, i.e. the components $\mathrm{O}, \mathrm{H}, \mathrm{O_2}, \mathrm{H_2O}, \mathrm{CO}, \mathrm{CO_2}$ and OH are in chemical equilibrium in the flame front. Parallel to the mixture that goes to the flame front and reacts, there is an amount of air that bypasses the flame front via the direct boundary previously mentioned.

By means of a balancing of the relevant mass and energy flows, the equations for the mass and energy in both are obtained. Valid thereby for the mass balance in zone 1 is

$$dm_1 = dm_f - dm_{1F} - dm_{12} \tag{1-1}$$

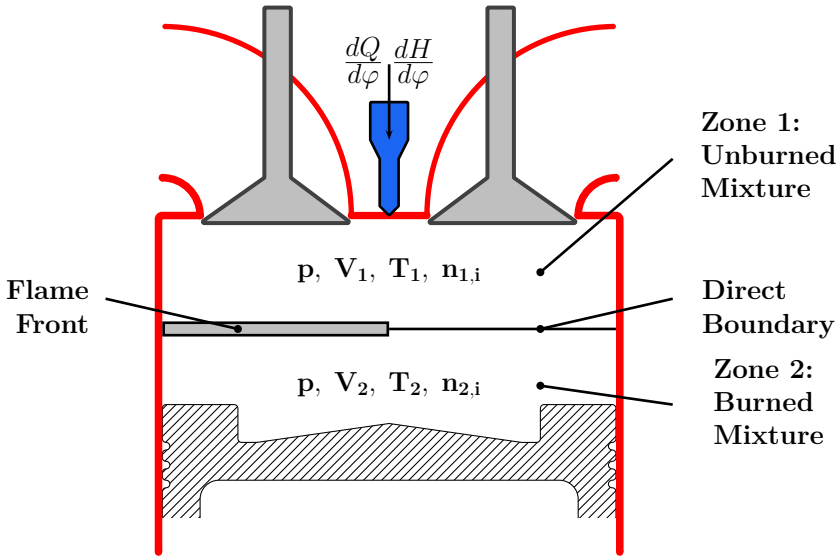

Figure 1-1: Thermodynamic Model Hohlbaum [1]

with

- dm_f: injected fuel mass
- dm_{1F}: mass added to the flame front (fuel+air)
- dm_{12}: air mass passing by the flame front and added directly to zone 2 across the direct boundary (must appear because of $\lambda_1 > 1$); it can also go through the flame front, however without participating in the reactions occurring there and without heat absorption. Here the subscript f denotes fuel, 1 refers to zone 1 and F is used to indicate the Flame front zone

The energy balance can be written in this way

$$dU_1 = dm_f \cdot h_f - dm_{1F} \cdot h_{1F} - dm_{12} \cdot h_{12} + dQ_1 - p \cdot dV_1 \tag{1-2}$$

Analogously, for the mass balance of zone 2 is valid

$$dm_2 = dm_{F2} + dm_{12} \tag{1-3}$$

with dm_{F2} composed by the elements of partial chemical balance.

The energy law reads:

$$dU_2 = dm_{F2} \cdot h_{F2} + dm_{12} \cdot h_{12} + dQ_2 - p \cdot dV_2 \tag{1-4}$$

Because the flame front is assumed to be without mass, it is furthermore valid

$$dm_{1F} = dm_{F2} = dm_F \tag{1-5}$$

The specific enthalpy of the mass transported from the flame front to zone 2 dm_{F2} is reaction-enthalpy Δh_R larger than the gas that is transported from zone 1 into the flame front, i.e.

$$h_{F2} = h_{1F} + \Delta h_R \tag{1-6}$$

The terms dQ_1 and dQ_2 describe the energy losses of both zones via heat transfer as a result of radiation and convection to the wall limiting the combustion chamber. The total transferred heat

$$dQ = dQ_1 + dQ_2 = \alpha \cdot A \cdot (T_w - T) \cdot dt \tag{1-7}$$

can, for example, be calculated again according to Woschni's method, whereby T is the energetic mean temperature, which can be determined for the caloric mixture from the relation

$$(m_1 + m_2) \cdot u\,(T) = m_1 \cdot u_1\,(T_1) + m_2 \cdot u_2\,(T_2) \tag{1-8}$$

However, for the subdivision of the total transferred heat dQ in dQ_1 and dQ_2, it is required a model, because the surface of the flame front and thus the size of the surface of both zones is not defined in the two-zone model. Hohlbaum proposes for this distribution the following relation

$$\frac{dQ_1}{dQ_2} = \left(\frac{m_1}{m_2}\right)^2 \cdot \frac{T_1}{T_2} \tag{1-9}$$

On the one hand, this approach takes into consideration that the burned zone contributes more to the total heat loss because of the higher temperature T_2 than unburned zone 1. On the other hand, the method considers the fact that at the beginning of combustion, the mass of zone 2 and thus its contribution to heat transfer is minimal. Finally, the temporal progression of the bypass air mass flow dm_{12} must still be determined. The quantity designated as mixture stoichiometry λ^* is defined as the ratio of air-mass to fuel-mass elements escaping from zone 1 per time slice,

$$\lambda^* = \frac{dm_{air,1F} + dm_{12}}{L_{min} \cdot dm_{f,1F}} \tag{1-10}$$

The air ratio of the mixture going into the flame front is defined as (λ_F), and it is assumed to be < 1 and temporally constant, thus $\lambda_F \neq f\,(\varphi)$, the mixture stoichiometry on the other hand is increasing in linear proportion to the crank angle, such that at the start of diffusion combustion $\lambda^* = \lambda_F$ and the excess air has at the end of diffusion combustion just completely intermixed with the unburned in zone 2.

Especially this assumption for the mixture stoichiometry makes clear the problematic nature of this simple zero-dimensional model; the lack of model depth (lacking physics) has to be substituted with more or less arbitrary assumptions. Same observation must be made to the heat transfer to the walls, although based on what the differences between the two zones at some specific stages, there is no further physical explanation on the expression proposed by Hohlbaum in eq.(1-9).

1-1-2 Heider Model

Heider [2] has introduced another way to calculate the conditions in both zones. He distinguishes thereby between two zones (figure 1-2). In zone 1, which is designated as the reaction zone, energy conversion takes place. In the reaction zone, the air-fuel ratio λ_0 is assumed to

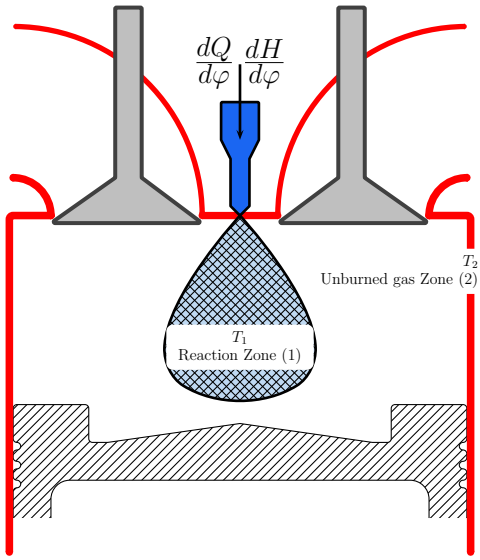

Figure 1-2: Thermodynamic Model Heider [2]

be constant throughout the working cycle. The mass in the reaction zone is thus fixed by means of equation (1-12) over the heat release rate. Zone 2 describes the unburned and thus occupies the remaining volume of the combustion chamber. No combustion occurs here.

As opposed to Hohlbaums model, in the case of Heider, the results are based on the process calculation of the zero-dimensional single-zone model. These results can be calculated in advance with the working process calculation. The paths of the swept volume, of pressure, and of mass mean temperature as well as the cylinder mass, compression air-fuel ratio, heat release rate, and wall heat losses are assumed to be known. The following assumptions are valid as conditions of compatibility.

$$V_1 + V_2 = V(\varphi) \tag{1-11a}$$

$$m_1 + m_2 = m(\varphi) \tag{1-11b}$$

$$p_1 = p_2 = p(\varphi) \tag{1-11c}$$

Provided the air-fuel ratio λ_0 is known, the mass of air in the reaction zone can be calculated

$$\lambda_0 = \frac{m_{air1}(\varphi)}{L_{min} \cdot m_f(\varphi)} = \text{const.} \tag{1-12}$$

For the fuel mass is valid in the case of a known heat release rate,

$$m_f(\varphi) = \frac{1}{I_{hv}} \int \frac{dQ_f}{d\varphi} + m_{f,0} \tag{1-13}$$

where $m_{f,0}$ is the residual mass of fuel from previous cycles and I_{hv} is the heating value of the fuel.

With this, for the mass of zone 1 can be calculated as follows:

$$m_1(\varphi) = m_{air1}(\varphi) + m_f(\varphi) = (\lambda_0 \cdot L_{min} + 1) \cdot m_f(\varphi) \tag{1-14}$$

and the ideal state equation is valid for both zones.

$$\begin{aligned} p_1 \cdot V_1 &= m_1 \cdot R_1 \cdot T_1 \\ p_2 \cdot V_2 &= m_2 \cdot R_2 \cdot T_2 \end{aligned} \tag{1-15}$$

In the final analysis it must be determined which part of the energy released in the reaction zone is transferred to zone 2. This happens in the model representation essentially via turbulent mixing and less so via radiation and convection. For this, the following boundary conditions must be kept:

At the beginning of combustion, the temperature difference between both zones as a result of the high temperature difference between the flame and the unburned mass is maximal. Furthermore, this temperature difference is contingent on heat release via combustion. The turbulent mixing of both zones leads, with progressing combustion, to a lowering of temperature in the reaction zone and an increase of temperature in the zone with the unburned substance. At the end of the combustion, the temperature difference is around zero, since both zones are then completely intermixed.

These considerations lead to the following empirical method for the temperature difference between both of these zones

$$T_1(\varphi) - T_2(\varphi) = B(\varphi) \cdot A^* \tag{1-16}$$

For the function $B(\varphi)$ is valid

$$B(\varphi) = 1 - \frac{\int_{\varphi_{SOC}}^{\varphi} [p(\varphi) - p_0(\varphi)] \cdot m_1 \cdot d\varphi}{\int_{\varphi_{SOC}}^{\varphi_{EO}} [p(\varphi) - p_0(\varphi)] \cdot m_1 \cdot d\varphi} \tag{1-17}$$

As in the determination of the heat transfer coefficient according to Woschni, here too, the difference between the cylinder pressure $p(\varphi)$ and the theoretical pressure of the motored engine $p_0(\varphi)$ is utilized for the consideration of the influence of combustion. A^* describes the temperature level in the reaction zone at the start of combustion. Detailed investigations have shown that minimal adjustments of the A^*value and the air-fuel ratio λ_0 are necessary for varying engines and combustion processes. For small to medium-sized diesel engines possessing an intake swirl

$$\begin{aligned} \lambda_0 &= 1, \\ A^* &= A \cdot \frac{1.2 + (\lambda_{gl} - 1.2)^{C_{gl}}}{2.2 \cdot \lambda_0} \end{aligned} \tag{1-18}$$

is applicable. A is an engine-specific factor, which has to be determined once for the respective engine. For C_{gl} is valid

Bore [mm]	Stroke [mm]	Cycle	Compression Ratio	Rated speed [rpm]	A value [K]
79.5	95.5	4	19.5	4000	1650
128	142	4	16	2100	1740
160	180	4	14	1500	1580
480	600	4	14	450	1650
580	1700	2	17	127	1655

Table 1-1: Typical A values

- $C_{gl} = 0.15$ for engines with 4-valve technology and central injection nozzle
- $C_{gl} = 0.07$ for engines with 2-valve technology and a side injection nozzle

λ_{gl} describes the global air-fuel ratio.

Valid for large diesel engines without intake swirl is

$$\lambda_0 = 1.03 \text{ and } \lambda_0 = 1.03 - 0.24 \cdot \frac{EGR}{100}$$

in the case of external exhaust gas recycling. In large diesel engines, the A^* value can be assumed to be constant

$$A^* = A = \text{const.}$$

Although this model was first developed only for the diesel engine, it can also be applied to SI engines with favourable results. Then

$$\lambda_0 = \lambda_{gl} \text{ and } A^* = \text{const}$$

is valid.

Table 1-1 has been reproduced from [7]. It provides A values for different engines.

Despite the obvious empirical nature of this model, it offers a very good basis for nitrogen oxide calculation. Additionally, its simplicity makes it a very appealing model. With this model, no assumptions have to be made regarding the distribution of the wall heat losses to the two zones, which can only be determined as a whole by means of the single zone model. The temperatures in both zones are calculated in simple manner with the empirical formula proposed. Last but not least, Merker [7] states that calculation model is appealing because of its short calculation times.

Phenomenological models

In this section will be provided information of models that describe the rate of heat release (ROHR), and packet models. This is done because some models combine these two concepts to produce in-cylinder combustion models. At the same time they provide concepts that are important to understand the combustion process.

1-2 Zero-Dimensional Heat Release Function

1-2-1 Chmela Model

A relatively simple and thus time-efficient calculation model for heat release in the diesel engine has been presented by Chmela et al. and Lakshminarayanan [8–11]. Although, this model does not carry division of the combustion space into different volumes, it does relate the heat release to some parameters of importance. These parameters are availability of fuel mass at every point in time, hence the difference between injected and burned fuel mass, secondly the specific turbulent kinetic energy, which is taken as representative for the mixing speed of air and fuel [12].

$$\frac{dQ_B}{d\varphi} = C_{model} \cdot f_1\left(m_B\right) \cdot f_2\left(k\right) = C_{model} \cdot \left(m_B - \frac{Q_B}{H_u}\right) \cdot \exp\left(C_{rate} \cdot \frac{\sqrt{k}}{\sqrt[3]{V_{cyl}}}\right) \tag{1-19}$$

where m_B is the cumulative mass of fuel injected, Q_B the cumulative heat release and H_u is the lower calorific value of fuel. Additionally, the constants values are $C_{model} = 1000\,kJ/kg$ and $C_{rate} = 0.002s$.

The turbulent kinetic energy k is derived only from the injection, since a quantitative estimate shows that the kinetic energy of the injection is about two orders of magnitude more than that of the inlet and quench flow. The production rate of the kinetic energy via injection is

$$\frac{dE_{kin,prod}}{dt} = C_{turb} \cdot \frac{1}{2} \cdot \dot{m}_f \cdot \left(v_{inj}\right)^2 \tag{1-20}$$

with,

$$\dot{m}_f = C_D \cdot \rho_f \cdot n_{noz} \cdot A_{noz} \cdot v_{inj} \tag{1-21}$$

and injection velocity computed form Bernoulli equation,

$$v_{inj} = \sqrt{\frac{2 \cdot \left(p_{inj} - p_{cyl}\right)}{\rho_f}} \tag{1-22}$$

The dissipation rate of the kinetic energy is treated in a simplified way as proportional to the absolute amount of kinetic energy itself. Then the change in kinetic energy is expressed as,

$$\frac{dE_{kin}}{dt} = \frac{dE_{kin,prod}}{dt} - C_{diss} \cdot E_{kin} \tag{1-23}$$

The specific turbulent kinetic energy k is finally approximated as the ratio of the kinetic energy available for mixing and the sum of the air and fuel mass in the diffusion flame. The air ratio in the flame is assumed to be stoichiometric:

$$k = C_{turb} \cdot \frac{E_{kin}}{m_f \cdot \left(1 + L_{min}\right)} \tag{1-24}$$

Values of C_{turb} have been reported for different engines in [9], and it ranges from 0.18 to 0.25.

The attractiveness of this models lies in the short calculation time and simplicity, added to the link made to the injection system parameters. On the other hand, there is also the restriction that neither the ignition delay nor the typical premixed fraction of diesel engine combustion can be described with this model. Both phenomena are substantially influenced by the evaporation speed of the fuel, the additional consideration of which in the model would cause a significantly higher requirement in calculation time [12].

1-2-2 Whitehouse Model

This model was developed by Whitehouse and Way [13], is one of the first attempts to obtain a simple formula for heat release to be suitable for performance calculations, based on the single zone concept. The hypothesis of this model lies in the idea that at any time the rate of combustion must depend on the amount of fuel to be burnt and the amount of oxygen available to burn.

The concept states that if combustion is assumed to take place at the surface of a number of droplets, the rate of combustion would be proportional to the surface area of the droplets. Taking all droplets to be identical, then

$$M_i = n \cdot \rho \cdot \pi \cdot \frac{D_0^3}{6} \tag{1-25a}$$

$$M_u = n \cdot \rho \cdot \pi \cdot \frac{D^3}{6} \tag{1-25b}$$

M_i and M_u are the mass of fuel injected and mass of fuel unburnt respectively, D_0 and D are the droplet initial diameter and fuel droplet diameter.

$$\begin{aligned} \text{total area} = n \cdot \pi \cdot D^2 = n \cdot \pi \cdot \left(\frac{6M_u}{n \cdot \rho \cdot \pi}\right)^{2/3} = (n \cdot \pi)^{1/3} \cdot \left(\frac{6 \cdot M_u}{\rho}\right)^{2/3} \\ = \left(\frac{6 \cdot M_i}{\rho \cdot D_o^3}\right)^{1/3} \cdot \left(\frac{6 \cdot M_u}{\rho}\right)^{2/3} = \frac{6 \cdot M_i^{1/3} \cdot M_u^{2/3}}{\rho \cdot D_o} \end{aligned} \tag{1-26}$$

thus area $\propto M_i^{1/3} \cdot M_u^{1/3}$ if ρ and D_0 are constant.

Then the combustion heat release is assumed to be of the form

$$R = K \cdot M_i^{1/3} \cdot M_{iu}^{2/3} \cdot P_0^m \tag{1-27}$$

P_0 is the partial pressure of oxygen and K to be a function of such variables as fuel injection characteristics, air movement, and combustion chamber shape, but in the paper it was taken as a constant for a particular engine.

Whitehouse based on the work of Austen and Lyn [14], where an analysis of the heat release in DI engines is made, and after a series of measurements, states that both physical and chemical effects are involved in the process of heat release. Fuel is injected into the engine in liquid form; before it can be burnt, it must be heated, and mixed with sufficient quantity of oxygen for burning.

These two physical processes are referred to collectively as preparation. The prepared fuel may then burn at a rate given by the chemical kinetic equations.

Whitehouse mentions that at high temperatures the burning time is negligible compared to preparation time, so that the preparation rate can be taken as the heat release rate $P = R$. In addition at the beginning of the burning period when temperature is low, chemical kinetics are important. Subsequently the burning rate increases due to temperature rise until it is controlled by lack of fuel prepared, and then fuel burns at the rate at which fuel is prepared.

Based on this description and derivation showed above, it is defined first a preparation rate of fuel, and second a chemical reaction rate.

The fuel preparation rate following the form of equation 1-27 is written in general form as

$$P = K \cdot m_i^{1-x} \cdot m_u^x \cdot P_0^m \tag{1-28}$$

where x, m are empirical constants and K is a factor to be determined for each individual case. Typical values of x and m are $x = 2/3$ $m = 0.4$; $x = 1/3$ $m = 0.55$.

For the chemical reaction rate, an empirical relation is used since diesel fuel is not a pure substance. This equation is based on the Arrhenius equation.

$$R = \frac{K^{'}}{N} \cdot \frac{P_0}{\sqrt{T}} \cdot \int (P - R) \cdot dx \cdot e^{-act/T} \tag{1-29}$$

The term $\int (P - R) \cdot dx$ is equal to the quantity of fuel in the cylinder that has been prepared but not burnt. N is the engine speed [rev/min]. The value of R is computed from the value of $\sum (P - R)$ up to the beginning of the step being computed. $K^{'}$ and act are constants.

As general conclusion Whitehouse mentions the need for two zone models for further understanding of heat release to take into account variations of the temperature and gas composition within the cylinder. In a latter work, Williams and Whitehouse [15] provide comparison between two-zone models looking into computational aspects.

1-2-3 Rakopoulos two-zone model

Rakopoulos et al. [16, 17] depict two zones where the volumes are defined by the study of the fuel spray phenomenology. Based on empirical relations, that will be described later in this document under the packet models, the spray volume and subsequently the air mass eentrained are computed. In this spray zone, the combustion takes place and the combustion model of Whitehouse and Way [13] is used to describe preparation and reaction rates.

1-3 Packet Models

One of the models most frequently used to describe DI diesel engines combustion is the packet model developed by Hiroyasu et al. [3, 18–20]. In this approach the injection jet is subdivided into many small zones (packets), which as a whole depict the jet contour (figure 1-3). Usually, only one injection jet is calculated per cylinder, and it is assumed that all the other jets are identical in behaviour [12].

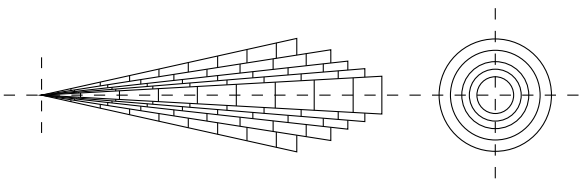

Figure 1-3: Packet Model [3]

The heat release rate of the cylinder is computed by addition of the contribution of each packet. The packets are considered individual open control volumes where mass and energy balances are solved. Moreover, within these limits, the most important sub processes like drop evaporation, air mixture, combustion, and pollutant formation rates are calculated [3].

In this document the revised model of [3] by Stiesch [21, 22] will be presented, but only spray discretization and sub models will be described. Reference to related models will be provided later for a more detailed description. During the compression stroke, only one zone exists, which extends itself over the entire combustion chamber and is viewed as ideally mixed. Fresh charge air and, in the case of EGR, combustion products are found in this zone. During the injection spray packets are continuously generated, which reproduce the global form of the injection spray and subdivide it in both axial and radial directions. Independently of the number of nozzle holes, only one single fuel spray is viewed; an interaction of various sprays can thus not be considered. Once injection starts, every time step a fuel disk is generated and subdivided radially into packets. At the generation instant, only liquid fuel is found in the packet. After the progression of a characteristic time, the liquid fuel is atomized into small drops, and the entrainment of gases from the surrounding zone of fresh air to the single spray packets begins. The fuel droplets are heated up by the hot gases, which have entered the packets and evaporate. After the end of the ignition delay, the fuel-air-mixture begins to burn, by means of which the packet temperature increases again and pollutant formation (NO and soot) begins as well [12, 21].

Once combustion have started, the packets can thus contain not only liquid fuel and fresh air, but also fuel vapour and combustion products. Mixing of various spray packets or an exchange of energy between them does not occur. With exception of air-entrainment into the spray (and thus to the packets) and wall heat transfer, all transport processes occur within the packets.

Pressure is viewed as independent of location and only as a function of time. This assumption is justified because of the high speed of sound at high pressures during the combustion phase [7].

1-3-1 Stiesch Model

Development and Mixture Formation

Immediately after start of injection, one spray packet is viewed as a continuous liquid phase, which moves into the combustion chamber with the constant speed

$$v_{inj} = C_D \cdot \sqrt{\frac{2 \cdot \Delta p_{inj}}{\rho_{B,fl}}} \tag{1-30}$$

until atomization begins. A common value used for C_D is 0.39

The liquid fuel mass per packet is computed with help of the momentary injection rate $\dot{m}_{inj}$, the number of packets in the radial direction k_{max} and the length of time interval Δt,

$$m_{B,P} = \frac{\dot{m}_{inj} \cdot \Delta t}{k_{max}} \tag{1-31}$$

After a characteristic time span (break-up time), the liquid phase breaks into small drops.

$$t_{bu,c} = 28.65 \cdot \frac{\rho_{B,fl} \cdot D_D}{\sqrt{\rho_L \cdot \Delta p_{inj}}} \tag{1-32}$$

It has to be mentioned apart from stating that the expression was obtained by experimental observations neither Hiroyasu nor Stiesch explain the nature of this equation.

To account for the stronger interaction between fuel and air at the spray boundary compared to the spray axis, spray breakup in the outer packets begins earlier, if a linear decrease in breakup time is assumed over the spray radius the breakup time is

$$t_{bu,k} = t_{bu,c} \cdot \left(1 - \frac{k-1}{k_{max}}\right) \tag{1-33}$$

As a result of air entrainment from the fresh air zone into the spray packet, the packet speed is reduced. For packets on the spray axis

$$v_{tip,c} = 1.48 \cdot \left(\frac{\Delta p_{inj} \cdot D_D^2}{\rho_L}\right)^{1/4} \cdot \frac{1}{\sqrt{t}} \tag{1-34}$$

is valid, and for packets further outside, the assumption of a decreasing exponentially speed profile towards the spray border.

$$v_{tip,k} = v_{tip,c} \cdot \exp\left(-C_{rad} \cdot (k-1)^2\right) \tag{1-35}$$

The injection process itself also changes the flow pattern in the combustion chamber decisively. The kinetic energy of the injection jets is approximately two orders of magnitude above the kinetic energy of swirl and squish flows at injection start. As a result of this, the spray packets generated first are much more strongly slowed down by the surrounding gas phase than the ones created towards the end of injection.

The packet speed after spray breakup is therefore corrected according to

$$v_{i,k} = C_1 \cdot v_{tip,k} \cdot \left[1 + \left(\frac{i-1}{i_{max}-1}\right)^{C_2} \cdot \frac{\Delta t_{inj}}{C_3}\right] \tag{1-36}$$

whereby $i = 1$ designates the packet generated first and i=imax the last. The constant C_1 can be slightly higher than 1, C_2 has the approximate value of 0.5 and C_3 describes the absolute speed difference between the first and the last packet.

The air entrainment rate is calculated with the principle of impulse conservation of the spray packets

$$v_{i,k} \cdot (m_{B,P} + m_{L,P}) = \text{const} \tag{1-37}$$

Distribution Spectrum

After the spray breakup time, the liquid fuel of the spray packet disintegrates into many small drops, the integral behaviour of which can be described with the Sauter mean diameter. The Sauter mean diameter is the diameter of a representative drop, which has the same volume to

surface area ratio as all drops integrated over the entire spray. The next relation is presented by Stiech, but there are several other relations in the literature, a comprehensive amount of such expressions can be found in [19].

$$\mathrm{SMD} = 6156 \times 10^{-6} \cdot \nu_{B,fl}^{0.385} \cdot \rho_{B,fl}^{0.737} \cdot \rho_{L}^{0.06} \cdot \Delta p_{inj}^{-0.54} \tag{1-38}$$

with SMD in $[m]$, ν in $[m^2/s]$, ρ in $[kg/m^3]$ and pressure difference Δp_{inj} in $[kPa]$. The number of fuel drops in a packet under the assumption that all drops are equally large amounts to

$$N_{Tr,P} = \frac{m_{B,P}}{\frac{\pi}{6} \cdot \mathrm{SMD}^3 \cdot \rho_{B,fl}} \tag{1-39}$$

For a more detailed description of atomization and thus also of the following evaporation process, the drop size distribution function

$$g(r) = \frac{r^3}{6\bar{r}^4} \cdot \exp\left(\frac{-r}{\bar{r}}\right) \tag{1-40}$$

can be utilized with the radius

$$\bar{r} = \frac{\mathrm{SMD}}{6} \tag{1-41}$$

of the most frequently appearing drop.

Drop Evaporation

In describing evaporation, the mixing model is often used, in which the inside of the drop is always assumed to be isothermal.

With this, the convective heat transfer from the gas phase to the drop with the help of the Nusselt number.

$$\frac{dQ_{Tr}}{dt} = \pi \cdot \mathrm{SMD} \cdot \kappa_s \cdot (T_P - T_{Tr}) \cdot \frac{z}{e^z - 1} \cdot \mathrm{Nu} \tag{1-42}$$

whereby z represents a dimensionless correction factor, which diminishes the transferred heat flux under the simultaneous appearance of mass transfer via evaporation.

$$z = \frac{c_{p,B,g} \cdot \frac{dm_{Tr}}{dt}}{\pi \cdot \mathrm{SMD} \cdot \kappa_s \cdot \mathrm{Nu}} \tag{1-43}$$

The evaporation rate of a drop is computed with the help of the relation for mass transfer as

$$\frac{dm_{Tr}}{dt} = -\pi \cdot \mathrm{SMD} \cdot \rho_s \cdot C_{diff} \cdot \ln\left(\frac{p_{cyl}}{p_{cyl} - p_{B,g}}\right) \cdot \mathrm{Sh} \tag{1-44}$$

For the Nusselt and Sherwood number is valid

$$\mathrm{Nu} = \frac{\tilde{h} \cdot d}{\kappa_f} = 2 + 0.6 \cdot \mathrm{Re}^{1/2} \cdot \mathrm{Pr}^{1/3} \tag{1-45a}$$

$$\mathrm{Sh} = \frac{\tilde{h}_D \cdot d}{D_{fa}} = 2 + 0.6 \cdot \mathrm{Re}^{1/2} \cdot \mathrm{Sc}^{1/3} \tag{1-45b}$$

whereby the Reynolds number is calculated with a relative speed between drop and gas phase, which is assumed to be up to 30% of the momentary packet speed $v_{i,k}$, the Prandtl number Pr=$\mu \cdot C_p/k_f$ and the Schmidt number Sc=$\mu/\rho \cdot D_{fa}$.

Temperature change of the liquid fuel drops results finally from an energy balance over a drop

$$\frac{dT_{Tr}}{dt} = \frac{1}{m_{Tr} \cdot c_{p,Tr}} \cdot \left(\frac{dQ_{Tr}}{dt} + \frac{dm_{Tr}}{dt} \cdot \Delta h_v \right) \tag{1-46}$$

with drop mass contingent on diameter and drop temperature:

$$m_{Tr} = \frac{\pi}{6} \cdot \rho_{Tr} \cdot \mathrm{SMD}^3 \tag{1-47}$$

Ignition Delay

Ignition delay is often described by means of a simple Arrhenius method

$$\tau_{zv} = C_1 \cdot \frac{\lambda_P}{p_{cyl}^2} \cdot \exp\left(\frac{C_2}{T_P}\right) \tag{1-48}$$

with $C_1 = 18$ and $C_2 = 6000$.

Heat Release

The maximum combustion rate in the packet is limited by the strictest three criteria. Only the vaporous fraction of fuel can be burned, the quantity of air in the packet and maximal chemical conversion rate for premixed flames.

$$\dot{m}_{B,Ox,P} \leq \min\left[\frac{m_{B,g,P}}{\Delta t}, \frac{m_{L,P}}{L_{min} \cdot \Delta t}, 5 \times 10^5 \cdot \rho_{mix} \cdot x_{B,g,P} \cdot x_{O_2,P}^5 \cdot \exp\left(-\frac{12000}{T_P}\right) \cdot V_P \right] \tag{1-49}$$

1-3-2 Jung and Assanis Model

Jung and Assanis [23, 24] present a model based on the packet concept where the spray is divided in multiple packets and each packet is subject to air entrainment, droplet evaporation and combustion. This model differs from the one developed by Hiroyasu [3] in the combustion model. The model proposes a premixed and a mixing-controlled combustion rate. The rates are described by an Arrhenius type kinetic equation.

During the ignition delay, an amount of fuel and air mixes. After ignition delay the premixed combustion start at a rate

$$RR_p = B_1 \cdot \rho_{mix}^2 \cdot x_{fv} \cdot x_{ox}^5 \cdot \exp\left(-\frac{1200}{T_z}\right) \cdot V_z \tag{1-50}$$

where B_1 is frequency factor; ρ_{mix} is density of the mixture; x_{fv} is the mass fraction of fuel vapour and x_{ox} is mass fraction of oxidizer; T_z is temperature of the zone; V_z is the volume of the zone. This equation is valid until the premixed fuel is completely consumed.

Later once the premixed fuel is consumed, combustion proceeds as a mixing controlled and late combustion phases. The rate to describe these two processes is

$$RR_m = B_2 \cdot m_{fv} \cdot \frac{P_{ox}}{P} \cdot P^{0.25} \cdot \exp\left(-\frac{2500}{T_z}\right) \tag{1-51}$$

where B_2 is a constant; m_{fv} is the mass of fuel vapor; P_{ox} is the partial pressure of oxygen; P is the total pressure. Here if the amount of fuel available is less than the one described by equation (1-51) only the available fuel is burned, otherwise is burned at rate RR_m.

Also worth mentioning is the work proposed by Jung and Assanis [25] where a simplified version of their model is presented. They mention that computational time is increased due to emissions modelling in a number of zones compared to the zero dimensional model.

In their analysis, Assanis and Jung [25] portray two fundamental causes for the increased computational time. A first source is the fuel evaporation process that is described by a set of relatively stiff equations thus requiring small time steps for integration during the evaporation period, thus increasing the computational time. A second cause of the increased computational time is the NO formation model, which is based on extended Zeldovich mechanism. To overcome these problems, based on several sources they conclude that the evaporation of the injected fuel is fast and is possible to consider the fuel jet as a gas jet under normal operating conditions $\dot{m}_{inj} = \dot{m}_{fv}$. As for the NOx formation process, based on the observation that the temperature difference between the spray tip and tail is not significant, an aggregated spray zone concept is introduced.

1-3-3 Im and Huh Model

Similarly to the work of Jung and Assanis, Im and Huh [26] propose a packet model where spray is described with the same formulas but a different formulation for the reaction rates.

The premixed combustion rate is defined as follows

$$\left(\frac{dM_b}{dt}\right)_p = C_p \cdot \left(\frac{M_{mix}}{\tau_c}\right) \tag{1-52a}$$

$$\tau_c = \frac{\lambda}{S_l} \tag{1-52b}$$

where λ is the Taylor microscale and S_l is the laminar flame speed. M_{mix} is the mass of fuel-air mixture in the given element. C_p is an arbitrary tuning constant.

The Diffusion combustion rate is determined principally by fuel-air mixing, here a turbulent mixing time scale is introduced to represent the rate of fuel-air mixing as,

$$\left(\frac{dM_b}{dt}\right)_d = \left(\frac{dM_e}{dt}\right) \cdot \left(\frac{\tau_{ca}}{\tau_c}\right) \quad \text{if } \tau_{ca} < \tau_c \tag{1-53a}$$

$$\left(\frac{dM_b}{dt}\right)_d = \left(\frac{dM_e}{dt}\right) \quad \text{if } \tau_{ca} > \tau_c \tag{1-53b}$$

$$\frac{dM_e}{dt} = C_e \cdot \left(\frac{M_e}{\tau_c}\right) \tag{1-53c}$$

$$\tau_e = \left(\frac{L^2}{\epsilon}\right)^{1/3} \tag{1-53d}$$

where M_b and M_e are the masses of burned fuel and entrained air in the element. The time scales τ_e and τ_{ca}, denote the mixing time and the time corresponding to one-degree crank angle.

1-3-4 Rakopoulos Multi-zone model

Rakopoulos et al. [27, 28] present a model of a two-dimensional fuel spray development in the cylinder, with the issuing jet divided into several volumes, called zones, formed along the direction of the fuel injection as well as across it. The model follows each zone, with its own time history, as the spray penetrates into the swirling air environment of the combustion chamber before and after wall impingement.

As in other models presented, after ignition delay, combustion starts first by the premixed fuel and air produced before combustion starts. Rakopoulos propose an Arrhenius type equation as follows:

If $(m_{f,ev} - m_{f,bu}) \leq (m_a - AF_{st} \cdot m_{f,bu}) / AF_{st}$, then

$$\frac{dm_{f,bu}}{dt} = K_{bu} \cdot p^{0.757} \cdot (m_{f,ev} - m_{f,bu}) \cdot \exp(-5500/T) \tag{1-54}$$

otherwise,

$$\frac{dm_{f,bu}}{dt} = K_{bu} \cdot p^{0.757} \cdot [(m_a - AF_{st} \cdot m_{f,bu}) / AF_{st}] \cdot \exp(-5500/T) \tag{1-55}$$

where K_{bu} is a constant to be evaluated.

1-4 Other sources

Another packet models have been developed and used to simulate the in-cylinder process. Examples of them can be found in references [29–34]. An exhaustive review on numerical modelling of CI engines can be found in [35], in this reference elements presented in this document as well as an extensive table containing a wide range of combustion models ranging from single zone models to multidimensional models are summarized. Extra information related to two-zone models and combustion rate can be found in [31, 36–43] In addition Pariotis et al. [44] provide a comparison between three different approaches to simulate internal combustion engines, providing the benefits and shortcomings associated to each method.

1-5 Research Objectives

This thesis focuses on the simulation of the in-cylinder process of direct injection diesel engines. The main objective is to simulate the process introducing few zones to have a sufficiently hot control volume where the chemical mechanisms of thermal NOx can be incorporated to compute engine emissions. The basic idea is promoted by Stapersma [4]; in his work he proposes a few number of zones (fig. 1-4) contrary to the great number of zones in the packet models. This, because it is of interest to use mean values instead of following the individual history of multiple volumes.

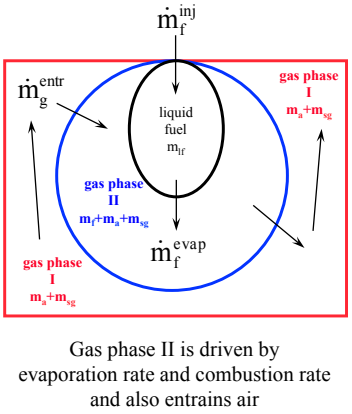

Figure 1-4: Stapersma concept [4]

In addition, it is desired to study the flows related to the fuel in the liquid phase (injection and evaporation) to see how different injection schemes affect the in-cylinder process, then the previously mentioned few zone model (Holhbaum and Heider) cannot be used but some of their concepts can be incorporated.

In this project the model will be implemented using elements of the Matlab/simulink single zone model developed in the ship design, propulsion and operation (SDPO) section of the department of Marine Technology in TU Delft and provided by Stapersma, particularly the properties library. Furthermore, the proposed model will be evaluated to study its capacity to simulate the in-cylinder process but no further validation is made.

In order to achieve the main objective the following tasks must be completed.

- Establish the fundamental model and zones in which the cylinder volume will be divided.
- Establish the thermodynamic and mathematical background of the model.
- Model the transport terms that arise from the model proposed.
- Implement the proposed model in Matlab/Simulink
- Introduce NOx mechanism to compute emissions.
- Evaluate the adequacy of the model to simulate the in-cylinder process.

1-6 Thesis Outline

After presenting in this chapter a literature review of the different models existent and showing some basic equations that may be used in the model adopted in this thesis, the following work is organized as follows. First, in chapter two, the model to simulate the in-cylinder process will be described and the equations needed to describe the system will be derived. After this chapter, chapter three and four will cover sub-models, their implementation and results of tests performed to ensure the assumptions made were valid. Once validity of the separate parts of the model is presented, the parts will be put together in chapter five to run some study cases. Finally in the last chapter conclusions about the model and recommendations for future work will be presented.

Chapter 2

Three-zone model and Cylinder Thermodynamics

In this chapter the Three-zone in-cylinder process model used in this project will be described and the basic equations necessary to model the system will be derived. First, the model proposed to describe the In-cylinder process will be depicted, providing the fundamental ideas and assumptions. In a second stage, the general formulas for mass and energy balances of a control volume will be presented and used to derive the equations for the different control volumes in the model, along with further assumptions.

2-1 Multi-zone Model

The model used in this project is intended to describe the in-cylinder process once inlet and outlet valve close. This process comprises air compression, fuel injection, evaporation, fuel air mixing, combustion and expansion until exhaust valve open (EO). Additionally it is considered that fuel is injected directly into the cylinder.

The space inside the cylinder is discretized in three volumes or zones as depicted in Figure 2-1. Two zones are used to describe the gaseous phase present in the cylinder, and one to describe the liquid present in the chamber.

The liquid zone is composed solely by liquid fuel. This zone does not exist until fuel injection starts and disappears once the total amount of fuel is evaporated. Then, the flows coming in and out of the volume are, liquid fuel coming from the injector and evaporated fuel leaving the volume. In addition heat must flow into the zone to provide the energy necessary to evaporate the fuel.

As mentioned above, the gaseous phase is described by two zones. One called Flame Zone and the second Bulk Zone. This is done similarly to the model of Heider, and the same numbering he used to refer to the zones is taken.

The flame zone (1) surrounds the Liquid Zone and is composed by air, evaporated fuel and stoichiometric gas. The flame volume is the most important because here it is where the

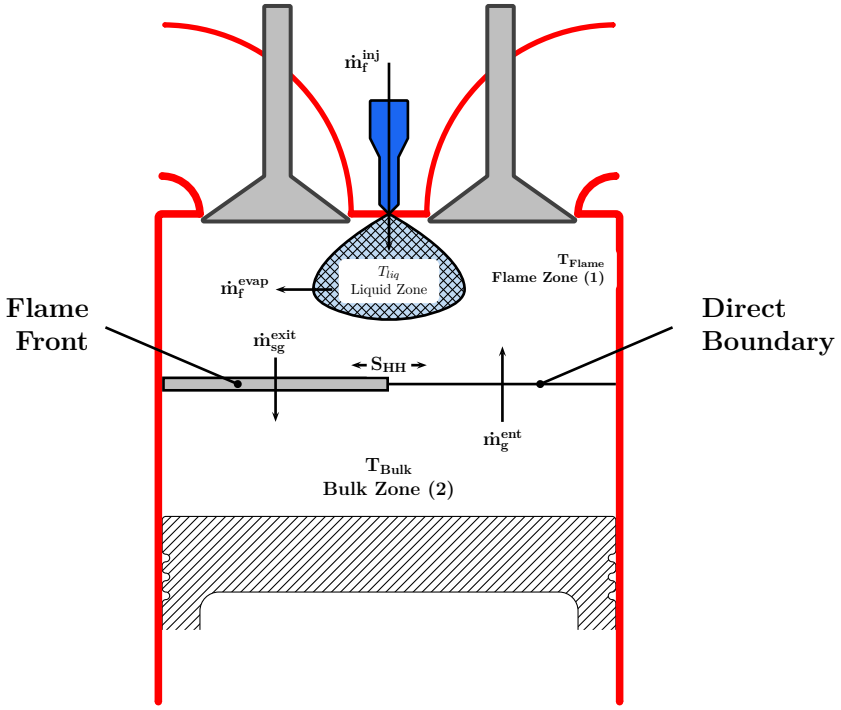

Figure 2-1: Three Zone Model

mixing process and combustion occurs. In this control volume, evaporated fuel flows in from the liquid zone, gas mixture comes in from the Bulk zone. Moreover, the gases produced by combustion (stoichiometric gas) may or may not leave the system, this will be explained in more detail later in this work. Additionally, the volume exchanges heat with the cylinder walls and provides the heat to evaporate the fuel. Together the Liquid and Flame zone describe the fuel spray, present in every direct injection (DI) diesel engine.

Finally, the Bulk Zone is the remaining gas present in the cylinder. This zone is composed by air and stoichiometric gas, no vaporous fuel is allowed to go in. Initially the composition is dictated by the trapped condition and in this model such condition is supplied as an initial condition. The volume generally is the biggest at the beginning of the simulation, and mainly provides air to the spray in order to achieve an ignitable mixture. The mass flows in and out of the volume are gases leaving as entrained gas to the Flame Zone and stoichiometric gas coming from the Flame as a result of combustion. Furthermore, the zone exchanges heat with the walls of the cylinder.

The Flame and Bulk zones can be regarded as they are separated partly by the flame front and the rest of the area by a membrane. The basic mass flows proceed between the two zones through one of these boundaries depending on their nature.

2-2 Basic equations

The basic equations considered for the thermodynamic analysis of the cylinder are the mass balance, and the energy balance that can be written in terms of internal energy or enthalpy. In the energy balances specific quantities will be used, it means values per kilogram of the

substance considered.

1. Mass Balance
$$\frac{dm}{dt} = \sum_i \dot{m}_i^{in} - \sum_i \dot{m}_i^{out} \tag{2-1}$$

2. Energy Balance - Internal Energy
$$\frac{d\left(m \cdot u\right)}{dt} = \sum_i \left(h^{in} \cdot \dot{m}^{in}\right)_i - \sum_i \left(h^{out} \cdot \dot{m}^{out}\right)_i + \dot{Q} - \dot{W}_T - p \cdot \frac{dV}{dt} \tag{2-2}$$

3. Energy Balance - Enthalpy
$$\frac{d\left(m \cdot h\right)}{dt} = \sum_i \left(h^{in} \cdot \dot{m}^{in}\right)_i - \sum_i \left(h^{out} \cdot \dot{m}^{out}\right)_i + \dot{Q} - \dot{W}_T - V \cdot \frac{dp}{dt} \tag{2-3}$$

2-3 Liquid zone

The liquid zone constitutes the core of the fuel spray where only liquid fuel is present and no gas is diffused into the liquid. The subscript "liq" will be used to symbolize this zone.

2-3-1 Mass Balance

$$\frac{dm_{liq}}{dt} = \dot{m}_f^{inj} + \dot{m}_a + \dot{m}_{sg} - \dot{m}_f^{evap} \tag{2-4}$$

As mentioned in this zone it is assumed that no gas diffuses into the liquid fuel then $\dot{m}_{sg}$ and $\dot{m}_a$ are zero.

$$\frac{dm_{liq}}{dt} = \dot{m}_f^{inj} - \dot{m}_f^{evap} \tag{2-5}$$

The two terms in the right hand size to be modelled latter in this work.

2-3-2 Energy Balance

$$\frac{d\left(m \cdot u\right)_{liq}}{dt} = \dot{m}_f^{inj} \cdot h_{f,liq}^{inj} - \dot{m}_f^{evap} \cdot h_{f,g}^{evap} + \dot{Q} + \dot{W}_T - p \cdot \frac{dV_{liq}}{dt} \tag{2-6}$$

Where $\dot{W}_T = 0$, and $\dot{Q}$ is the heat transferred from the surrounding gas (Flame Zone), and it has to be modelled.

$$\dot{Q} = \dot{Q}_{1 \to liq} \tag{2-7}$$

Then the energy balance reduces to

$$\frac{d\left(m \cdot u\right)_{liq}}{dt} = \dot{m}_f^{inj} \cdot h_{f,liq}^{inj} - \dot{m}_f^{evap} \cdot h_{f,g}^{evap} + \dot{Q}_{1 \to liq} - p \cdot \frac{dV_{liq}}{dt} \tag{2-8}$$

Expanding the differential term of the internal energy, substituting the mass balance and grouping terms in equation (2-8) produces,

$$m_{f,liq} \cdot \frac{du_{f,liq}}{dt} = \dot{m}_f^{inj} \cdot \left(h_{f,liq}^{inj} - u_{f,liq}\right) - \dot{m}_f^{evap} \cdot \left(h_{f,g}^{evap} - u_{f,liq}\right) + \dot{Q}_{1\to liq} - p \cdot \frac{dV_{liq}}{dt} \quad (2\text{-}9)$$

and defining the heat capacity of the liquid fuel as

$$c_{f,liq} \overset{\text{def}}{=} \frac{du_{f,liq}}{dT} \quad (2\text{-}10)$$

Finally the energy balance is

$$m_{f,liq} \cdot c_{f,liq} \frac{dT_{f,liq}}{dt} = \dot{m}_f^{inj} \left(h_{f,liq}^{inj} - u_{f,liq}\right) - \dot{m}_f^{evap} \left(h_{f,g}^{evap} - u_{f,liq}\right) + \dot{Q}_{I\to liq} - p \cdot \frac{dV_{liq}}{dt} \quad (2\text{-}11)$$

where the properties of the liquid fuel can be computed from the property block, as functions of temperature.

2-4 Zone 1 (FLAME)

In this zone fuel is only present in gas phase, in addition combustion proceeds in this volume thus the contents of this volume include air, stoichiometric gas and vaporous fuel. The subscript 1 or *"Flame"* will be used to describe quantities related to this region. It is important to note that in the model is mentioned a flame front but it only acts as a barrier for the produced stoichiometric gas to leave the volume. In essence the model is completely different from the Houlbaum model where partial oxidation occurs in the flame front, and the gas leaves to complete oxidation and further mixing in zone (2).

2-4-1 Mass Balance

In this volume the partial mass balances, the reaction mass balance and the general gas phase balance are defined as follows.

1. Partial mass balances for gas phase

$$\frac{dm_{f,1}}{dt} = \dot{m}_f^{evap} - \frac{dm_{f,1}^{comb}}{dt} \quad (2\text{-}12a)$$

$$\frac{dm_{a,1}}{dt} = \dot{m}_a^{ent} - \frac{dm_{a,1}^{comb}}{dt} \quad (2\text{-}12b)$$

$$\frac{dm_{sg,1}}{dt} = \dot{m}_{sg}^{ent} + \frac{dm_{sg,1}^{comb}}{dt} - \dot{m}_{sg}^{exit} \quad (2\text{-}12c)$$

2. Reaction mass balance

$$m_{f,1} + m_{a,1} \to m_{sg,1} \quad (2\text{-}13a)$$

$$\frac{dm_{f,1}^{comb}}{dt} + \frac{dm_{a,1}^{comb}}{dt} = \frac{dm_{sg,1}^{comb}}{dt} \quad (2\text{-}13b)$$

Introducing the stoichiometric ratio (σ), equations (2-13a) and (2-13b) can be rewritten in the following way,

$$m_{f,1} + \sigma \cdot m_{f,1} \rightarrow (1+\sigma) \cdot m_{f,1} \tag{2-14a}$$

$$\frac{dm_{f,1}^{comb}}{dt} + \sigma \cdot \frac{dm_{f,1}^{comb}}{dt} = (1+\sigma) \cdot \frac{dm_{f,1}^{comb}}{dt} \tag{2-14b}$$

In addition, if ξ is defined as the combustion rate and using equation (2-14b) the partial mass balances can be written as follows,

$$\xi \overset{\text{def}}{=} \frac{dm_{f,1}^{comb}}{dt} \tag{2-15}$$

$$\frac{dm_{f,1}}{dt} = \dot{m}_f^{evap} - \xi \tag{2-16a}$$

$$\frac{dm_{a,1}}{dt} = \dot{m}_a^{ent} - \sigma \cdot \xi \tag{2-16b}$$

$$\frac{dm_{sg,1}}{dt} = \dot{m}_{sg}^{ent} - \dot{m}_{sg}^{exit} + (1+\sigma) \cdot \xi \tag{2-16c}$$

3. Gas phase mass balance

$$\frac{dm_1}{dt} = \dot{m}_f^{evap} + \underbrace{\dot{m}_a^{ent} + \dot{m}_{sg}^{ent}}_{\dot{m}_g^{ent}} - \dot{m}_{sg}^{exit} \tag{2-17}$$

The mass in flame zone is a mixture of air, stoichiometric gas and fuel vapour.

$$m_1 = m_{a,1} + m_{sg,1} + m_{f,1} \tag{2-18}$$

2-4-2 Energy Balance

$$\frac{d\,(m \cdot u)_1}{dt} = \dot{m}_f^{evap} \cdot h_{f,g}^{evap} + \underbrace{\dot{m}_a^{ent} \cdot h_a^{ent} + \dot{m}_{sg}^{ent} \cdot h_{sg}^{ent}}_{\dot{m}_g^{ent} \cdot h_g^{ent}} - \dot{m}_{sg}^{exit} \cdot h_{sg}^{exit} + \dot{Q} - p \cdot \frac{dV_1}{dt} \tag{2-19}$$

The Heat flow term is composed by two flows. The heat transfer to the liquid zone and the heat loss to the wall.

$$\dot{Q} = -\dot{Q}_{1 \rightarrow liq} - \dot{Q}_{1 \rightarrow wall} \tag{2-20}$$

The accumulation term $\frac{d(m \cdot u)_1}{dt}$ is decomposed in the following way

$$\begin{aligned} \frac{d\,(m \cdot u)_1}{dt} = {} & m_{a,1} \cdot \frac{du_{a,1}}{dt} + m_{f,1} \cdot \frac{du_{f,1}}{dt} + m_{sg,1} \cdot \frac{du_{sg,1}}{dt} \\ & + \frac{dm_{a,1}}{dt} \cdot u_{a,1} + \frac{dm_{f,1}}{dt} \cdot u_{f,1} + \frac{dm_{sg,1}}{dt} \cdot u_{sg,1} \end{aligned} \tag{2-21}$$

Where the terms with internal energy derivatives in the right hand side of the equation (2-21) are rewritten by means of the heat capacity of the air, gaseous fuel and stoichiometric gas,

$$c_v \overset{\text{def}}{=} \left(\frac{\partial u}{\partial T}\right)_v \tag{2-22}$$

and the heat capacity of the mixture is defined as a mass average.

$$\left(\frac{\partial u_1}{\partial T}\right)_v = c_{v,1} = \frac{(m \cdot c_v)_{a,1} + (m \cdot c_v)_{f,1} + (m \cdot c_v)_{sg,1}}{m_{a,1} + m_{f,1} + m_{sg,1}} \tag{2-23}$$

Working out equation (2-19), and sorting terms produces,

$$\begin{aligned} m_1 \cdot c_{v,1} \cdot \frac{dT_1}{dt} = \dot{m}_f^{evap} \cdot h_{f,g}^{evap} + \underbrace{\dot{m}_a^{ent} \cdot h_a^{ent} + \dot{m}_{sg}^{ent} \cdot h_{sg}^{ent}}_{\dot{m}_g^{ent} \cdot h_g^{ent}} - \dot{m}_{sg}^{exit} \cdot h_{sg}^{exit} - \frac{dm_{a,1}}{dt} \\ \cdot u_{a,1} - \frac{dm_{f,1}}{dt} \cdot u_{f,1} - \frac{dm_{sg,1}}{dt} \cdot u_{sg,1} - \dot{Q}_{1\to liq} - \dot{Q}_{1\to wall} - p \cdot \frac{dV_1}{dt} \end{aligned} \tag{2-24}$$

Substituting the partial mass balances (eq 2-16a) to (eq.2-16c)

$$\begin{aligned} m_1 \cdot c_{v,1} \cdot \frac{dT_1}{dt} = \dot{m}_f^{evap} \cdot h_{f,g}^{evap} + \underbrace{\dot{m}_a^{ent} \cdot h_a^{ent} + \dot{m}_{sg}^{ent} \cdot h_{sg}^{ent}}_{\dot{m}_g^{ent} \cdot h_g^{ent}} - \dot{m}_{sg}^{exit} \cdot h_{sg}^{exit} \\ - \left(\dot{m}_f^{evap} - \xi\right) \cdot u_{f,1} - \left(\dot{m}_a^{ent} - \sigma \cdot \xi\right) \cdot u_{a,1} - \left\langle \dot{m}_{sg}^{ent} - \dot{m}_{sg}^{exit} + (1+\sigma) \cdot \xi \right\rangle \cdot u_{sg,1} \\ - \dot{Q}_{I\to liq} - \dot{Q}_{I\to wall} - p \cdot \frac{dV_1}{dt} \end{aligned} \tag{2-25}$$

Grouping similar terms,

$$\begin{aligned} m_1 \cdot c_{v,1} \cdot \frac{dT_1}{dt} = \dot{m}_f^{evap} \cdot \left(h_{f,g}^{evap} - u_{f,1}\right) + \dot{m}_a^{ent} \cdot \left(h_a^{ent} - u_{a,I}\right) + \dot{m}_{sg}^{ent} \cdot \left(h_{sg}^{ent} - u_{sg,1}\right) \\ - \dot{m}_{sg}^{exit} \cdot \left(h_{sg}^{exit} - u_{sg,1}\right) - \langle (1+\sigma) \cdot u_{sg,1} - \sigma \cdot u_{a,1} - u_{f,1} \rangle \cdot \xi \\ - \dot{Q}_{I\to liq} - \dot{Q}_{I\to wall} - p \cdot \frac{dV_1}{dt} \end{aligned} \tag{2-26}$$

In this equation the heat of combustion can be recognized from the terms next to the combustion rate and it can be noted that it is temperature dependent. The properties of the gases in the volume can be computed in the property block as functions of temperature and mass fractions assuming they are mixtures of ideal gases. So, once the transport terms are modelled, the temperature in the zone can be computed integrating numerically.

2-5 Zone 2 (BULK)

In this zone only gaseous components exist, but in this volume combustion does not proceed. In addition, it is assumed that only stoichiometric gas may enter the volume. In this zone there is heat transfer to the cylinder walls. The subscript 2 or "Bulk" will be used to describe quantities related to this region.

2-5-1 Mass Balance

Mass balances are derived in a similar way to the zone 1. It is important to be careful with the signs of the flows since the inflows in the preceding zone now are outflows, and outflows of zone 1 now feed the Zone 2.

1. Partial mass balances for gas phase

$$\frac{dm_{a,2}}{dt} = -\dot{m}_a^{ent} \tag{2-27a}$$

$$\frac{dm_{sg,2}}{dt} = -\dot{m}_{sg}^{ent} + \dot{m}_{sg}^{exit} \tag{2-27b}$$

2. Gas phase mass balance

$$\frac{dm_2}{dt} = -\underbrace{\left(\dot{m}_a^{ent} + \dot{m}_{sg}^{ent}\right)}_{\dot{m}_g^{ent}} + \dot{m}_{sg}^{exit} \tag{2-28}$$

The mass in the bulk zone is composed of air and stoichiometric gas.

$$m_2 = m_{a,2} + m_{sg,2} \tag{2-29}$$

2-5-2 Energy Balance

$$\frac{d\left(m \cdot u\right)_2}{dt} = -\underbrace{\left(\dot{m}_a^{ent} \cdot h_a + \dot{m}_{sg}^{ent} \cdot h_{sg}\right)}_{\dot{m}_g^{ent} \cdot h_g} + \dot{m}_{sg}^{exit} \cdot h_{sg}^{exit} + \dot{Q} - p \cdot \frac{dV_2}{dt} \tag{2-30}$$

Where the heat flow term is the heat transfer to the cylinder walls

$$\dot{Q} = -\dot{Q}_{2 \to wall} \tag{2-31}$$

The accumulation term $\frac{d(m \cdot u)_2}{dt}$is

$$\frac{d\left(m \cdot u\right)_2}{dt} = m_{a,2} \cdot \frac{du_{a,2}}{dt} + m_{sg,2} \cdot \frac{du_{sg,2}}{dt} + \frac{dm_{a,2}}{dt} \cdot u_{a,2} + \frac{dm_{sg,2}}{dt} \cdot u_{sg,2} \tag{2-32}$$

The heat capacity of the mixture in zone 2 is defined in the same way as in zone 1.

$$\begin{aligned} \left(\frac{\partial u_2}{\partial T}\right)_v &= c_{v,2} \\ &= \frac{\left(m \cdot c_v\right)_{a,2} + \left(m \cdot c_v\right)_{sg,2}}{m_{a,2} + m_{sg,2}} \end{aligned} \tag{2-33}$$

Then the term is

$$m_{a,2} \cdot \frac{du_{a,2}}{dt} + m_{sg,2} \cdot \frac{du_{sg,2}}{dt} = m_2 \cdot c_{v,2} \cdot \frac{dT_2}{dt} \tag{2-34}$$

Working out this term by means of product rule, and sorting terms produces

$$\begin{aligned} m_2 \cdot c_{v,2} \cdot \frac{dT_2}{dt} = &-\dot{m}_a^{ent} \cdot h_a^{ent} - \dot{m}_{sg}^{ent} \cdot h_{sg}^{ent} + \dot{m}_{sg}^{exit} \cdot h_{sg}^{exit} \\ &- \frac{dm_{a,2}}{dt} \cdot u_{a,2} - \frac{dm_{sg,2}}{dt} u_{sg,2} - \dot{Q}_{2\to wall} - p \cdot \frac{dV_2}{dt} \end{aligned} \tag{2-35}$$

Substitute the partial mass balances (2-27a) and (2-27b)

$$\begin{aligned} m_2 \cdot c_{v,2} \cdot \frac{dT_2}{dt} = &-\dot{m}_a^{ent} \cdot h_a^{ent} - \dot{m}_{sg}^{ent} \cdot h_{sg}^{ent} + \dot{m}_{sg}^{exit} \cdot h_{sg}^{exit} - \left(-\dot{m}_a^{ent}\right) \\ &\cdot u_{a,2} - \left(-\dot{m}_{sg}^{ent} + \dot{m}_{sg}^{exit}\right) \cdot u_{sg,2} - \dot{Q}_{2\to wall} - p \cdot \frac{dV_2}{dt} \end{aligned} \tag{2-36}$$

Grouping similar terms

$$\begin{aligned} m_2 \cdot c_{v,2} \cdot \frac{dT_2}{dt} = &-\dot{m}_a^{ent} \cdot \left(h_a^{ent} - u_{a,2}\right) - \dot{m}_{sg}^{ent} \cdot \left(h_{sg}^{ent} - u_{sg,2}\right) \\ &+ \dot{m}_{sg}^{exit} \cdot \left(h_{sg}^{exit} - u_{sg,2}\right) - \dot{Q}_{2\to wall} - p \cdot \frac{dV_2}{dt} \end{aligned} \tag{2-37}$$

Finally, as with the equations for the flame and liquid zones, this differential equation can be integrated numerically since all the properties of the gases can be computed in the property block as functions of temperature and mass fractions, and the transport terms will be modelled.

2-6 Total cylinder

The mass rate of change of the cylinder is equal to the injection rate and the cylinder mass is equal to the sum of the three zones.

2-6-1 Mass Balance

$$\frac{dm}{dt} = \dot{m}_f^{inj} \tag{2-38}$$

$$\begin{aligned} m &= m_1 + m_2 + m_{liq} \\ &= m_a + m_f + m_{sg} \end{aligned} \tag{2-39}$$

2-6-2 Volume Balance

Additionally the sum of the different zone volumes cannot be larger than the cylinder volume at a given crank angle φ.

$$V_{cyl}(\varphi) = V_{liq}(\varphi) + V_1(\varphi) + V_2(\varphi) \tag{2-40}$$

$$V_{cyl}(\varphi) = V_{TDC} + \frac{\pi}{4} \cdot D_B^2 \cdot L_p(\varphi) \tag{2-41}$$

$$L_p(\varphi) = r \cdot \left\langle (1 - \cos(\varphi)) + \frac{1}{\lambda_s} \cdot \left(1 - \sqrt{1 - \lambda_s^2 \cdot \sin^2(\varphi)}\right) \right\rangle \tag{2-42}$$

With $\lambda_s = r/l$.

Chapter 3

Liquid Zone Model

In this chapter the liquid volume will be described in detail. In particular the different transport terms present in Eq. (2-5) and Eq. (2-11). The equations used and their derivation will be presented for completeness, in order to understand better the limits under which the models used are valid. Particular attention is paid to the evaporation rate and the heat transfer from the surrounding to the liquid fuel. In addition, the equations will be implemented and results will be shown for a diverse set of conditions.

First, the most important concept is that the liquid zone represent the generality of the liquid phase in the cylinder once injection starts. In reality, the liquid fuel follows a very complex process and its phenomenology is considered in general as follows. First, fuel is injected under specific conditions via one or multiple nozzle holes. Next, a liquid jet is formed and after a small period of time the jet breaks-up into small droplets. The droplets continue to travel, and evaporation of the fuel starts and continues until all of the injected fuel is evaporated. The gaseous fuel produced mixes and heats up with the gases present in the cylinder to produce an ignitable mixture.

Since the objective of this project is to produce a model with short computational times, the great complexity of this two phase problem will not be modelled nor the individual history of individual droplets or packets of droplets. Instead the model proposed tries to describe the overall process of the liquid phase by dividing the entire liquid zone into small droplets with an average size. The physical processes then occur at the droplet scale and together they conform the overall transport terms required to solve the mass and energy balance (Eqns. (2-5) and (2-11)) of this volume.

3-1 Injection Rate

The injection rate is an important element to be considered in the liquid zone since it depends on the technology used in the engine. Today, two main groups of high-pressure injection systems exist. The common rail injection system and the plunger system.

3-1-1 Plunger System

In the plunger system the generation of injection pressure and the injection itself occur synchronously. These systems are driven by a camshaft, which is mechanically coupled with the engine. A basic characteristic of these systems is the intermittent pressure generation: high pressure is only available during a small crank angle interval [45].

In the model, the movement of the plunger caused by the cam is represented as a mathematical function of crank angle. The function is normalised so that the product of the function derivative and the mass of fuel to be injected compute the injection rate. Moreover, the fuel is incompressible, thus once the volume in the plunger changes the pressure builds up or down. It means that once the derivative is positive, fuel flows to the nozzle and when is negative a check valve must close to avoid back flow (see figs. 3-15 and 3-16). Hence in the plunger model, the movement of the cam fixes the volumetric flow and injection velocity, and the injection pressure comes as a result of the flow restriction in the nozzle.

$$h'(\varphi) = \frac{h_{cam}(\varphi)}{h_{cam,max}} \tag{3-1a}$$

$$\dot{m}_f^{inj} = \begin{cases} \frac{dh'}{dt} \cdot m_{f,comb} & \text{if } \frac{dh'}{dt} \geq 0 \\ 0 & \text{if } \frac{dh'}{dt} < 0 \end{cases} \tag{3-1b}$$

$$\dot{V}_f^{inj} = \frac{\dot{m}_f^{inj}}{\rho_f^{inj}} \tag{3-1c}$$

$$v_{inj} = \frac{\dot{V}_f^{inj}}{A_{nozzle}} \tag{3-1d}$$

$$p_{inj} = p_{cyl} + \frac{1}{2} \cdot \rho_{f,inj} \cdot \left(\frac{v_{inj}}{C_D} \right)^2 \tag{3-1e}$$

where C_D is the discharge coefficient and a value of 0.39 is often used in literature.

3-1-2 Common rail

In the common rail system, pressure generation and the injection event are not coupled, and the injection pressure is not dependent on engine speed. Fuel under high pressure is stored inside the rail, which usually consists of a thick-walled closed pipe. A high-pressure fuel pump continuously feeds the rail. A pressure sensor adjusts the desired rail pressure via an additional valve that controls the mass flow of excess fuel back to the fuel tank. Hence, the rail pressure is not dependent on engine speed, and an optimal adjustment to the actual operating point of the engine can be achieved. Short pipes connect the rail with the injectors. The volume of the rail is large enough to suppress pressure fluctuations due to injection. Injection timing and duration are controlled by solenoid valves and are independent of the pressure generation [45].

Contrary to the plunger model, here injection pressure is fixed and enters as a parameter, whereas injection rate and volumetric flow are a result of an effective area. In a similar

manner to the plunger lift, here the effective flow area is defined by means of a mathematical function of the crank angle hence controlling the volumetric flow and the injection rate.

$$p_{inj} = \text{Constant} \tag{3-2a}$$

$$v_{inj} = C_D \cdot \sqrt{\frac{2 \cdot (p_{inj} - p_{cyl})}{\rho_f^{inj}}} \tag{3-2b}$$

$$\dot{V}_f^{inj} = v_{inj} \cdot A_{eff}^{inj} \tag{3-2c}$$

$$A_{eff}^{inj} = A_{nozzle} \cdot \begin{cases} 0 & \text{if } \varphi < SOI \\ A'_{open}(\varphi) & \text{if } m_{inj} < m_{f,comb} \text{ and } \varphi \geq SOI \\ A'_{close}(\varphi) & \text{if } m_{inj} = m_{f,comb} \end{cases} \tag{3-2d}$$

$$\dot{m}_f^{inj} = \dot{V}_f^{inj} \cdot \rho_f^{inj} \tag{3-2e}$$

where $m_{f,comb}$ is the total fuel to be combusted.

3-2 Drop diameter

In order to divide the liquid zone into small droplets of average size, it is necessary to determine the mean droplet size. One quantity characterizing the average droplet size of a spray, and thus the success of spray break-up, is the sauter mean diameter (SMD). The SMD is the diameter of a model drop whose volume-to-surface-area ratio is equal to the ratio of the sum of all droplet volumes (V) in the spray to the sum of all droplet surface areas (A). The smaller the SMD, the more surface per unit volume and the more effective evaporation and mixture formation. An important remark about this concept is that it does not offer any information about the droplet size distribution [45]. In the literature several expressions can be found, in this project the expression proposed by Hiroyasu [18], Varde [22] and Elktob [46] were considered. In addition it was observed that at low velocities the expressions produce very high values, thus it was introduced an extra expression stating that the drop diameter is a factor of the nozzle diameter. Thus during the injection process the droplet size is selected as the smallest of the values calculated.

Hiroyasu,

$$\text{SMD}_1 = 2.33 \times 10^{-3} \Delta p^{-0.135} \rho_a^{0.121} V^{0.131} \tag{3-3a}$$

Varde,

$$\text{SMD}_2 = 8.7 \cdot d_{nozzle} \cdot (\text{Re}_\text{l} \cdot \text{We}_\text{l})^{-0.28} \tag{3-3b}$$

Elktob,

$$\text{SMD}_3 = 3.08 \cdot 10^{-6} \cdot \nu_{fl}^{0.385} \cdot \rho_{fl}^{0.737} \cdot \rho_a^{0.06} \cdot \Delta p_{noz}^{-0.54} \tag{3-3c}$$

Finally,

$$\text{SMD} = \min\left[\text{SMD}_1,\, \text{SMD}_2,\, \text{SMD}_3,\, C_{SMD} \cdot d_{nozzle}\right] \tag{3-3d}$$

where the Webber number and Reynolds number of the liquid fuel are defined as,

$$\mathrm{We}_{\mathrm{f}}^{\mathrm{inj}} = \frac{v_{inj}^2 \cdot d_{nozzle} \cdot \rho_f^{inj}}{\sigma_f^{inj}} \tag{3-4a}$$

$$\mathrm{Re}_{\mathrm{f}}^{\mathrm{inj}} = \frac{v_{inj} \cdot d_{nozzle} \cdot \rho_f^{inj}}{\mu_f^{inj}} \tag{3-4b}$$

The number of droplets then is calculated from the instantaneous mass in the liquid Zone and the mass of a single droplet.

$$N_{drop} = \frac{m_{liq}}{\frac{\pi}{6} \cdot \rho_{f,liq} \cdot \mathrm{SMD}^3} \tag{3-5}$$

3-3 Droplet Heating and Evaporation

The process of heating and evaporation of the liquid fuel droplets is not a new problem and there are several models in the literature addressing the topic, from very simple to quite detailed models [47]. Following the purpose of this project to have fast calculations, a compromise between accuracy and computational time must be made. For this reason the model described by Wakil [48] is used. In his work it is described the evaporation rate and heat transfer from the surroundings to heat-up the liquid fuel. This rates are used in the model of Borman and Johnson [49], which is used in many of the models presented in Section 1-3.

Figure 3-1 presents a spherically symmetrical droplet surrounded by a film containing an air-fuel vapour mixture. At any one instant, the mixture fuel composition varies from a maximum at the droplet surface to a minimum at the outer edge of the film. The shape of the temperature gradient curve depends on the relative temperatures of the fuel droplet and air and the mass of vapour being diffused out at that instant.

3-3-1 Heat Transfer

Referring to figure 3-1, and assuming that the initial temperature of the droplet is lower than the air temperature and lower than its own wet-bulb temperature, in which case the droplet heats up continuously during the unsteady-state portion of the vaporization time, the total or net heat transfer $\dot{Q}$ from the air to the film surrounding the droplet, prior to ignition, goes three ways:

1. To heat up the liquid droplet, $\dot{Q}_{liq}$
2. To vaporize the liquid, $\dot{Q}_{\lambda}$
3. To be carried back with the diffusing vapour in the form of superheat, $\dot{Q}_s$.

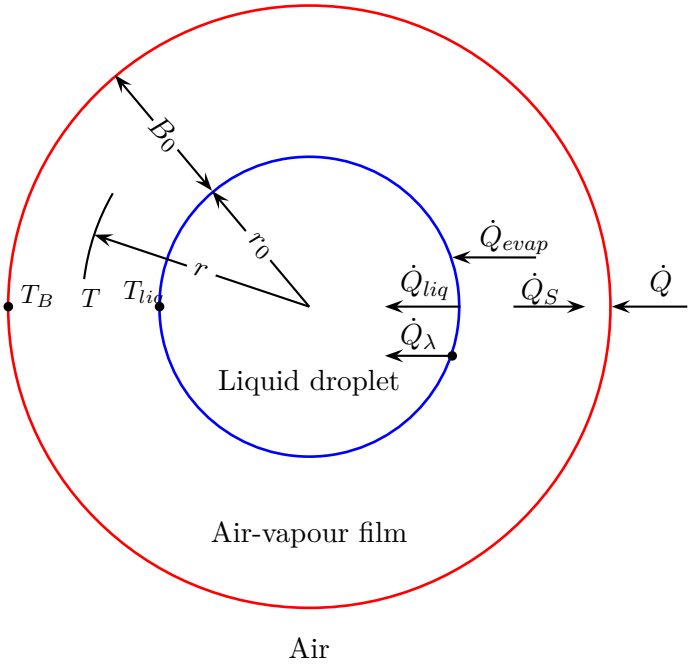

Figure 3-1: Heat transfer to droplet

The heat that arrives at the droplet surface is denoted by $\dot{Q}_{evap}$ and equals the sum of $\dot{Q}_{liq}$ and $\dot{Q}_\lambda$. It should be noted that in developing the relationship used, $\dot{Q}$ does not include radiant heat transfer.

If at any instant during vaporization a point in the air-vapour film at a radius r from the center of the droplet and at temperature T is considered

$$\dot{Q}_{evap} = \dot{Q}_{liq} + \dot{Q}_\lambda = \dot{Q} - \dot{Q}_s \tag{3-6a}$$

$$\dot{Q}_{evap} = \alpha_{drop} \cdot A_{drop} \cdot \frac{dT}{dy} - \dot{m}_f^{evap} \cdot c_{p,f} \cdot (T - T_{liq}) \tag{3-6b}$$

here $\dot{m}_f^{evap}$ is the rate at which the vapour is diffusing out, y is the fraction of the film thickness at radius r_0 , α_{drop} is the coefficient of heat transfer through the film in the absence of mass transfer, $c_{p,f}$ is the specific heat of the fuel vapour, T is the temperature of the mixture at the position y, and T_{liq} is the temperature of the surface of the droplet.

Rearranging equation (3-6b) gives:

$$dy = \frac{\alpha_{drop} \cdot A_{drop}}{\dot{Q}_{evap} - \dot{m}_f^{evap} \cdot c_{p,f} \cdot T_{liq} + \dot{m}_f^{evap} \cdot c_{p,f} \cdot T} \cdot dT \tag{3-7}$$

Integrating across the film between $y = 0$ to $y = 1.0$ where $T = T_{liq}$ to $T = T_B$ and considering the specific heat of the fuel vapor $c_{p,f}$ to be constant throughout the film:

$$1 = \frac{\alpha_{drop} \cdot A_{drop}}{\dot{m}_f^{evap} \cdot c_{p,f}} \ln\left(\frac{\dot{Q}_{evap} + \dot{m}_f^{evap} \cdot c_{p,f} \cdot (T_B - T_{liq})}{\dot{Q}_{evap}}\right) \tag{3-8}$$

or by rearranging and expressing as an exponential:

$$e^z = \frac{\dot{Q}_{evap} + \dot{m}_f^{evap} \cdot c_{p,f} \cdot (T_B - T_{liq})}{\dot{Q}_{evap}} \tag{3-9}$$

with $z = \frac{\dot{m}_f^{evap} \cdot c_{p,f}}{\alpha_{drop} \cdot A_{drop}}$. Now solving for $\dot{Q}_{evap}$

$$\begin{aligned} \dot{Q}_{evap} &= \frac{\dot{m}_f^{evap} \cdot c_{p,f} \cdot (T_B - T_{liq})}{e^z - 1} \\ &= \alpha_{drop} \cdot A_{drop} \cdot (T_B - T_{liq}) \cdot \frac{z}{e^z - 1} \end{aligned} \tag{3-10a}$$

$$\dot{Q}_{evap} = \dot{Q} \cdot \left(\frac{z}{e^z - 1}\right) \tag{3-10b}$$

Thus the factor $\frac{z}{e^z-1}$ represents the fraction of the heat transfer $\dot{Q}$ from the air that finally arrives at the surface of the liquid droplet and provides the latent heat of vaporization for the vapour diffusing out as well as the sensible heat added to the liquid droplet itself. The factor $\frac{z}{e^z-1}$ therefore represents a correction factor to the heat transfer coefficient without mass transfer from the droplet.

The heat transfer coefficient α_{drop} is computed from the correlations used in Ranz and Marshall's work [50]. From their correlation the Nusselt number for heat transfer used is:

$$\mathrm{Nu} = \frac{\alpha_{drop} \cdot \mathrm{SMD}}{\kappa_m} = 2 + 0.6 \cdot \mathrm{Re}_{drop}^{1/2} \cdot \mathrm{Pr}_{drop}^{1/3} \tag{3-11}$$

It is important to note that Ranz and Marshall correlations were obtained from experiments conducted at low temperatures and low vapour pressures. Wakil uses this formula considering that the correction factor $\frac{z}{e^z-1}$ was unity in the work of Ranz and Marshall.

It can be seen from the above equations that a calculation of the heat transfer through the film at any instant during the vaporization process of the droplet require the knowledge of the temperatures on both sides of the air-vapour film surrounding the droplet, of the velocity of the droplet relative to the air, and of its radius and on the droplet temperature.

After substitution of the Nusselt number and droplet surface area, z can be written as follows:

$$z = \frac{c_{p,fg} \cdot \dot{m}_f^{evap}}{\pi \cdot \mathrm{SMD} \cdot \kappa_m \cdot \mathrm{Nu}} \tag{3-12}$$

with $\dot{Q}_{1\to liq} = \dot{Q}_{evap}$ and $T_B = T_1$

$$\dot{Q}_{1\to liq} = \pi \cdot \mathrm{SMD} \cdot \kappa_m \cdot (T_1 - T_{liq}) \cdot \frac{z}{e^z - 1} \cdot \mathrm{Nu} \tag{1-42}$$

3-3-2 Mass Transfer

The transfer of vapour mass from the liquid surface is influenced by convection and molecular driving force of the concentration gradient. The vapour concentration at the liquid surface is determined by the vapour pressure of the liquid for the ideal low-pressure case. The difference in partial pressure between the surface and the ambient is then a driving force for mass transfer similar to $T_1 - T_{liq}$ for the heat transfer:

$$\dot{m}_f^{evap} = \tilde{h_D} \cdot A_{drop} \cdot (p_{vap,f,0} - p_{vap,f,\infty}) \tag{3-13}$$

The mass transfer film coefficient, $\tilde{h_D}$, is obtained by using the Sherwood number:

$$\mathrm{Sh} = \frac{\tilde{h_D} \cdot d_{drop}}{D_{fa}} = 2 + 0.6 \cdot \mathrm{Re}^{1/2} \cdot \mathrm{Sc}^{1/3} \tag{3-14}$$

The previous equation assumes low vaporization rates. For such low rates the effect of the bulk flow rate of vapour is not important. For higher rates of mass transfer the mass coefficient must be corrected, this is done according to Borman as follows:

$$\frac{\tilde{h_D^*}}{\tilde{h_D}} = \ln\left(\frac{p - p_{vap,f,\infty}}{p - p_{vap,f,0}}\right) \cdot \left(\frac{p}{p_{vap,f,0} - p_{vap,f,\infty}}\right) \tag{3-15}$$

Substitution of eqs. (3-14) and (3-15) in eq. (3-13) and with the assumption that $p_{f,vap,\infty}$ is zero, the evaporation rate is:

$$\dot{m}_f^{evap} = \pi \cdot SMD \cdot \rho_{f,v} \cdot \ln\left(\frac{p}{p - p_{vap,f,0}}\right) \cdot \mathrm{Sh} \tag{3-16}$$

where $\rho_{f,v} = \frac{p}{R_f \cdot T_m}$ and $p_{vap,f,0}$ is the fuel vapour pressure at the drop temperature

3-3-3 Film Properties Calculation

The properties of the gas phase inside the boundary layer are calculated as proposed by Borman [49].

$$T_m = \frac{T_B - T_{liq}}{2} \tag{3-17}$$

$$\kappa_m = \left(1 - \frac{p_{vap,f,0}}{2 \cdot p_{cyl}}\right) \cdot \kappa_a + \frac{p_{vap,f,0}}{2 \cdot p_{cyl}} \cdot \kappa_f \tag{3-18}$$

$$\mu_m = \left(1 - \frac{p_{vap,f,0}}{2 \cdot p_{cyl}}\right) \cdot \mu_a + \frac{p_{vap,f,0}}{2 \cdot p_{cyl}} \cdot \mu_f \tag{3-19}$$

$$\begin{aligned} \rho_m &= \frac{p_{cyl} \cdot M_m}{R_u \cdot T} \\ &= \frac{p_{cyl}}{R_u \cdot T_m}\left[\left(1 - \frac{p_{vap,f,0}}{2 \cdot p_{cyl}}\right) \cdot M_a + \frac{p_{vap,f,0}}{2 \cdot p_{cyl}} \cdot M_f\right] \end{aligned} \tag{3-20}$$

$$\begin{aligned} c_{p,m} &= g_a \cdot c_{p,a} + g_f \cdot c_{p,f} \\ &= \left(1 - \frac{p_{vap,f,0}}{2 \cdot p_T}\right) \cdot \frac{M_a}{M_m} \cdot c_{p,a} + \frac{p_{vap,f,0}}{2 \cdot p_T} \cdot \frac{M_f}{M_m} \cdot c_{p,f} \end{aligned} \tag{3-21}$$

3-4 Liquid Zone Analysis

In order to examine the validity of the modelling of the liquid zone, this block will be tested under different conditions to observe the response of the liquid phase and the limitations of the model. The analysis will be divided in two according to the two types of injection systems (plunger, common rail). For this analysis the gas conditions will be set constant during the simulation. The main driver will be crank angle and depending on the type of injection system the plunger lift or the effective area for common rail.

The data of the engine nominal speed, start of injection angle, exhaust valve open, and the fuel injection temperature are presented in table 3-1.

Table 3-1: Engine parameters used for simulation

Parameter	
Nominal engine speed	1000 rpm
SOI	4° before TDC
EO	300° after BDC
T_{inj}	40° C

The surrounding gas temperature variation was made from 600K to 2500K with constant gas pressure of 85.5 bar. Pressure variation was from 50 bar to 100 bar with constant gas temperature of 1550 K.

3-4-1 Common Rail Injection System

As mentioned before the common rail system depends on the effective area, this area is computed by multiplying the nozzle area and a normalized formula to simulate the valve opening of the system. Since this model does not consider the dynamics of the valve nor the control system required by the common rail, then it must be adjusted manually to comply with the amount of fuel that must be injected. The nozzle diameter and rail pressure are selected to achieve reasonable technical values.

Inputs

The figures presented below show the main parameters of the injection block, which can be seen as the driving inputs of the model. The injection pressure of the common rail system is selected to be 1600 bar and remains constant throughout the simulation as observed in figure 3-2.

The pressure of the surrounding gas is varied to see the influence on the fuel injection. The figure 3-3 shows the injection velocity and as it was expected the higher the gas pressure the smaller the pressure difference thus lower injection velocity. Figure 3-4 presents the effective area or area opening of the injector and figure 3-5 shows the fuel injection rate. It can be seen from both pictures that the injection time increases as the gas pressure increases, this as a result of the smaller pressure difference in the injector nozzle.

In figure 3-6 the integrated fuel injection rate is observed. The figure shows that the injected fuel varies for different gas pressures, but it must be noted that this variation is a result of the need to adjust manually when the injector starts to close. Moreover, the calibration of this point was done only one time and kept equal for the other study cases.

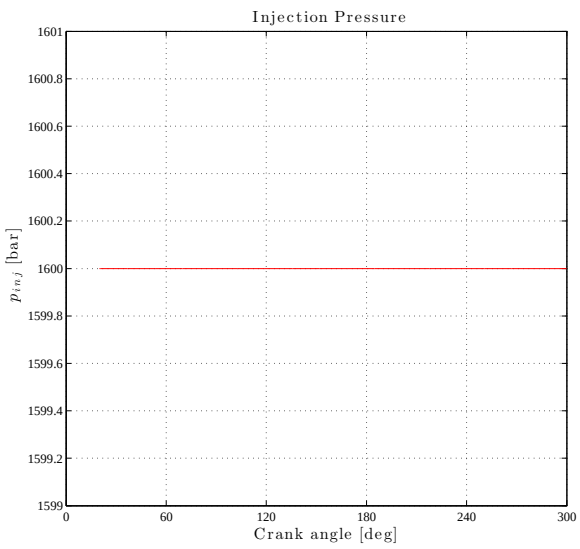

Figure 3-2: Injection Pressure CR

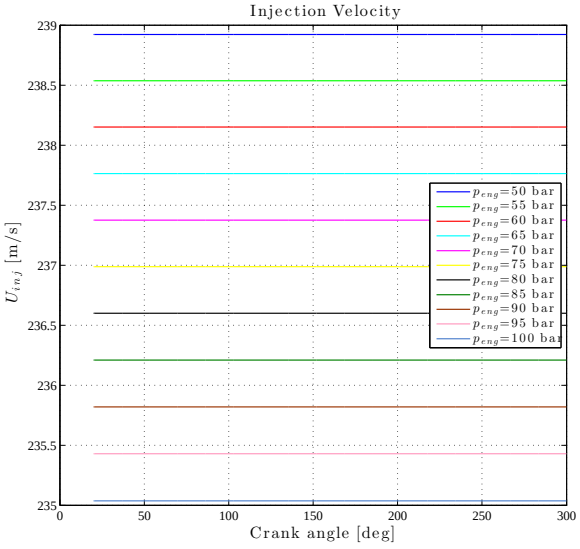

Figure 3-3: Injection Velocity CR

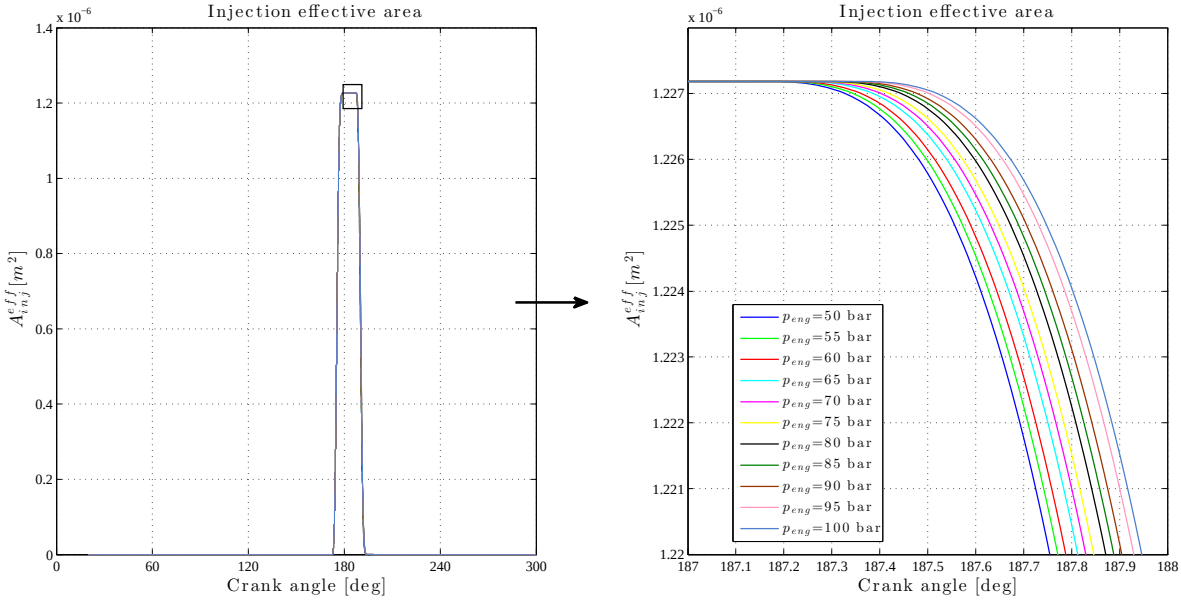

Figure 3-4: Injection effective area CR

Atomization Block

The primary outputs of the atomization block are presented in fig. 3-7 and fig. 3-8. In figure 3-7 the average droplet diameter in the cylinder is represented by the SMD. The gas pressure increase translates into larger droplets as a consequence of the lower injection velocity and less effective atomization.

Figure 3-8 shows the number of droplets in the cylinder computed as the quotient of the mass of liquid in the cylinder and the droplet mass. Figure 3-8a presents the variation of the number of droplets for different gas pressures. As mentioned before the increase in gas

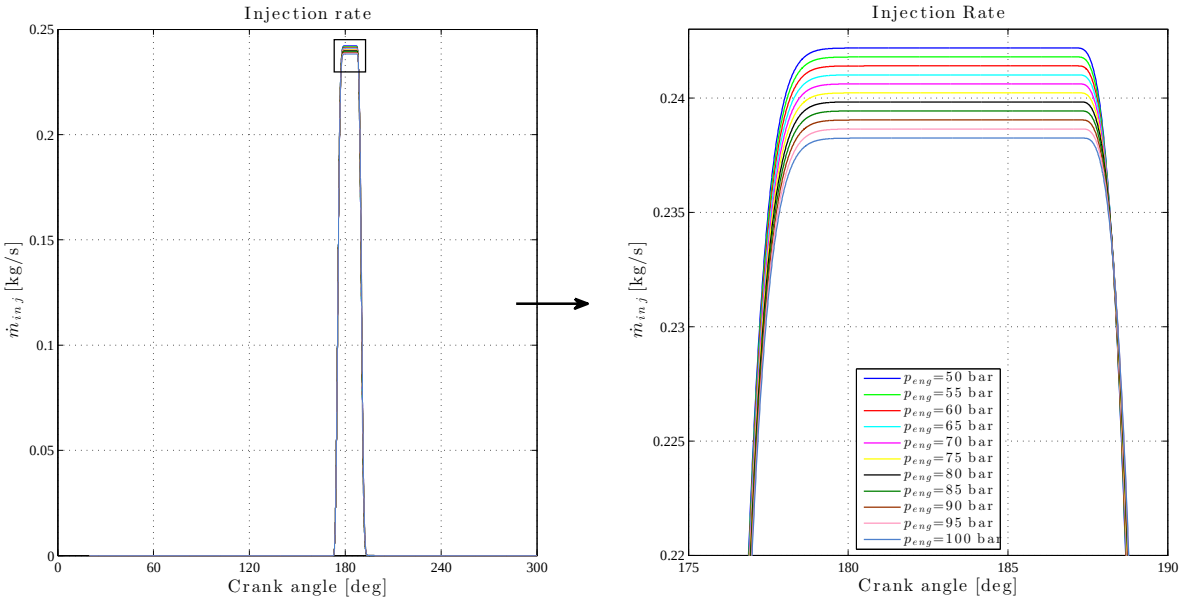

Figure 3-5: Injection Rate CR

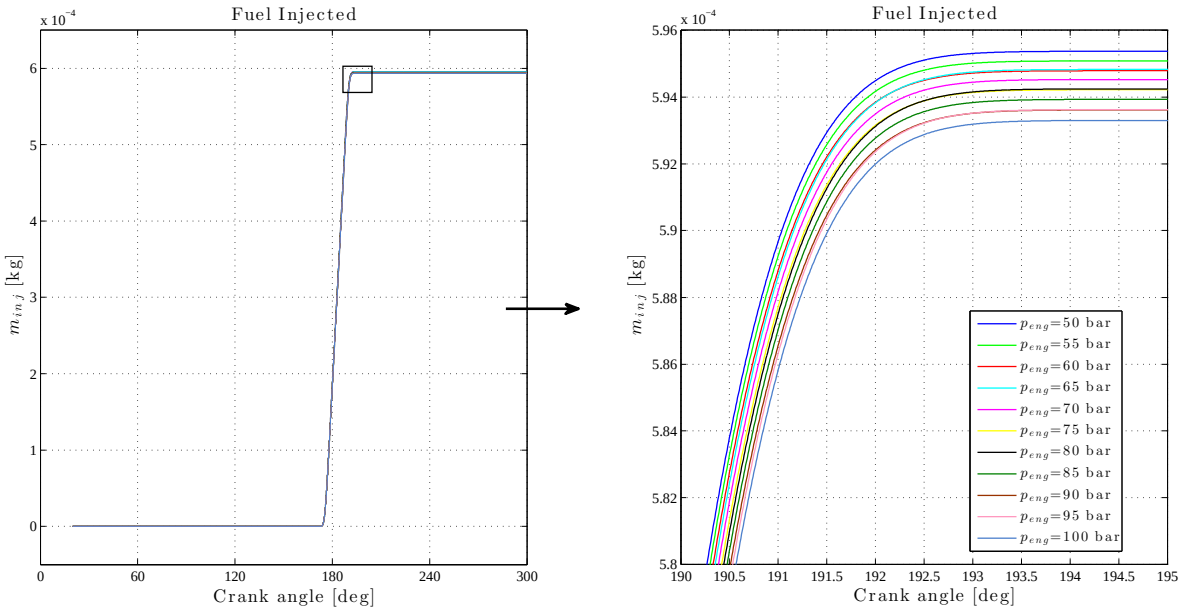

Figure 3-6: Fuel injected CR

pressure produces larger drop diameters; then the number of droplets is lower since the mass per drop is higher. Figure 3-8b shows the variation of the number of droplets as the gas temperature is increased. It can be observed that as temperature increases the number of droplets is smaller. This effect is less obvious from eq. (3-5), the higher number of droplets at lower gas temperatures is as a result of a slower evaporation rate thus the instantaneous mass of the liquid zone is larger which results in more droplets.

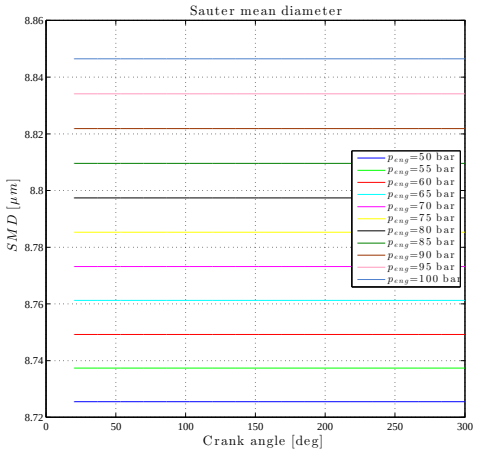

Figure 3-7: Drop diameter CR

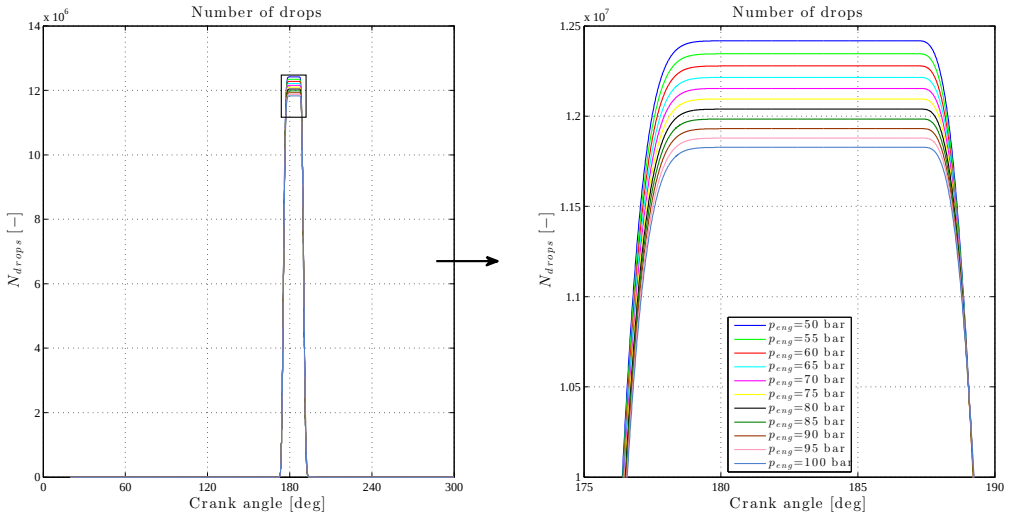

(a) Pressure variation

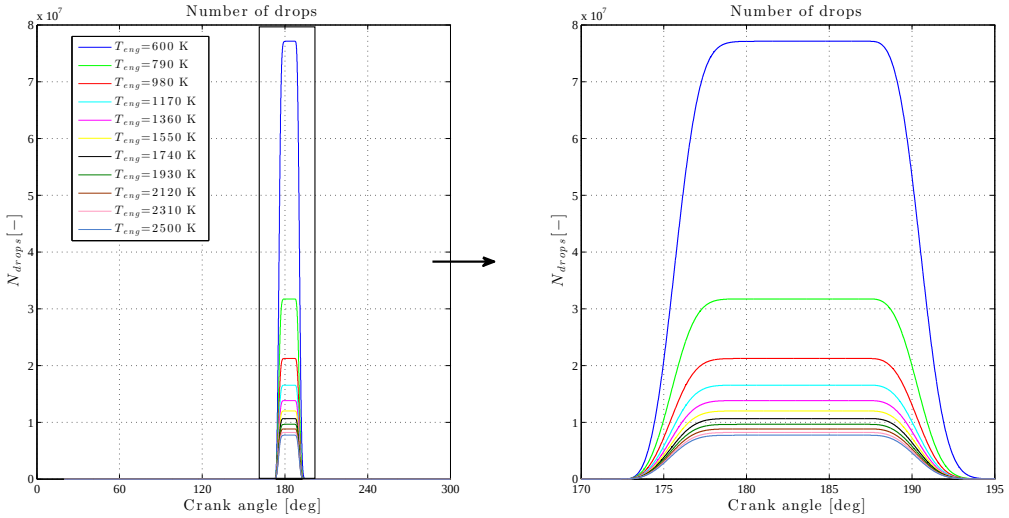

(b) Temperature variation

Figure 3-8: Number of fuel droplets CR

Evaporation Block

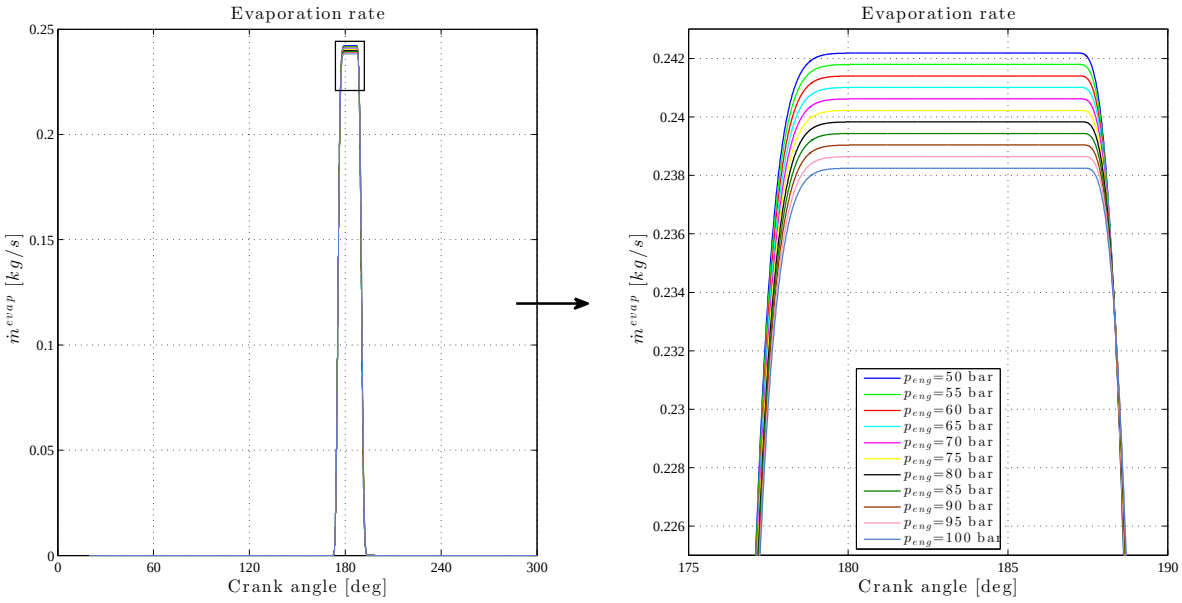

(a) Pressure variation

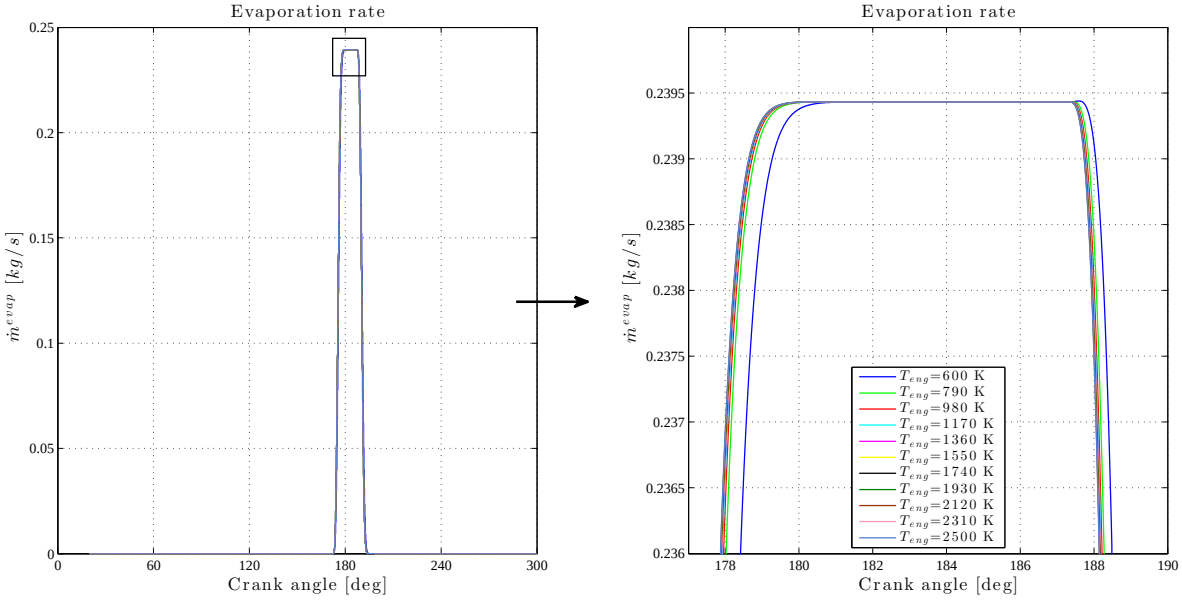

(b) Temperature variation

Figure 3-9: Evaporation rate CR

The evaporation rate is presented in figure 3-9 and heat transferred to the liquid is depicted in figure 3-10. Both flows are reduced as the gas pressure is increased (figs. 3-9a and 3-10a). This can be associated with the drop velocity reduction and drop diameter that ultimately will affect the heat and mass transfer processes negatively. From fig. 3-9b it can be observed that the evaporation rate is delayed with lower gas temperatures. Figure 3-10b presents the heat flow from the gas to the liquid fuel. The heat flow is higher for higher gas temperatures,

mainly related to the temperature difference between the gas and the liquid.

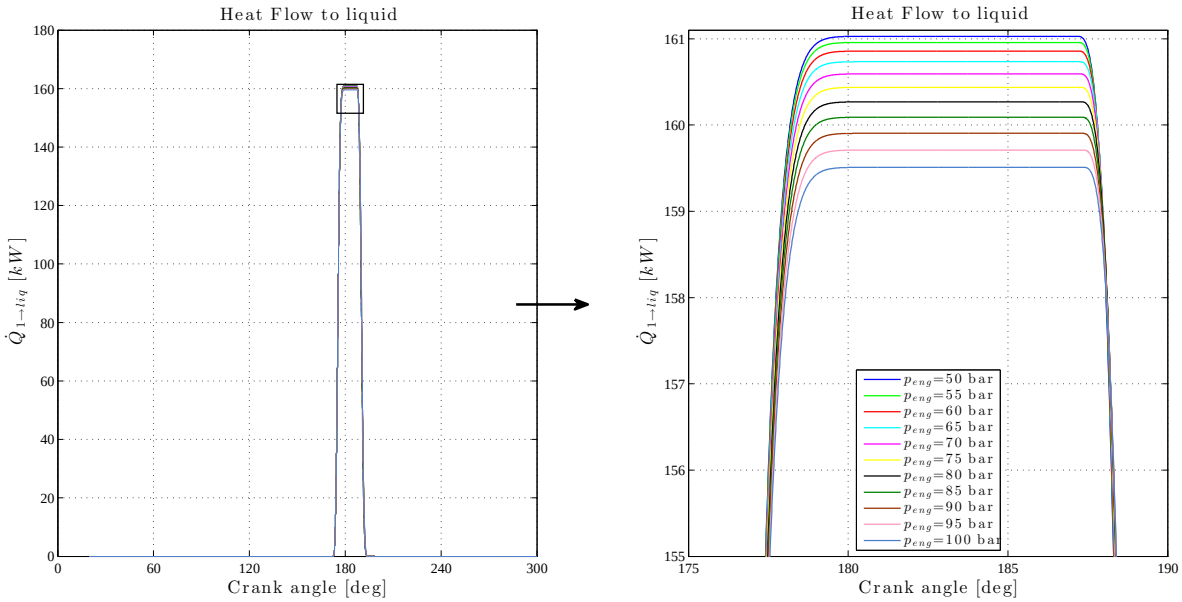

(a) Pressure variation

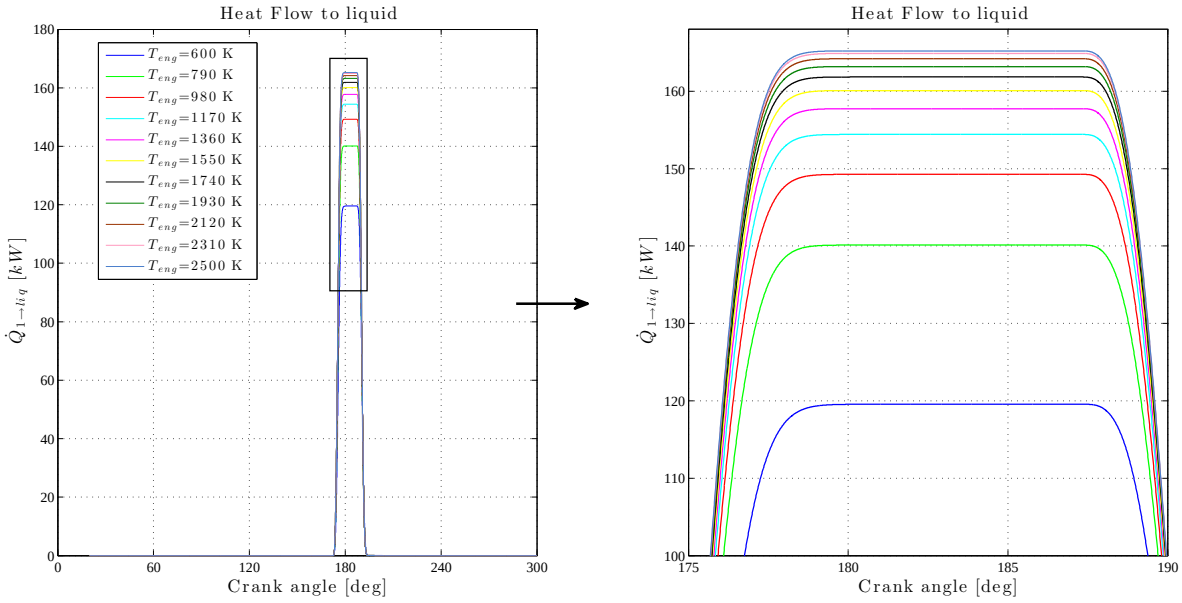

(b) Temperature variation

Figure 3-10: Heat flow to liquid zone CR

In figure 3-11 the heat transfer coefficient between the fuel droplet and the surrounding gas is presented. The value of the heat transfer coefficient is reduced as the gas pressure is increased (fig. 3-11a) and it is increased as the gas temperature increases (fig. 3-11b). It is important to note that the value of the heat transfer coefficient is around 100 000 $W/m^2/K$ which is within the typical values of the convection heat transfer coefficient as presented in [51].

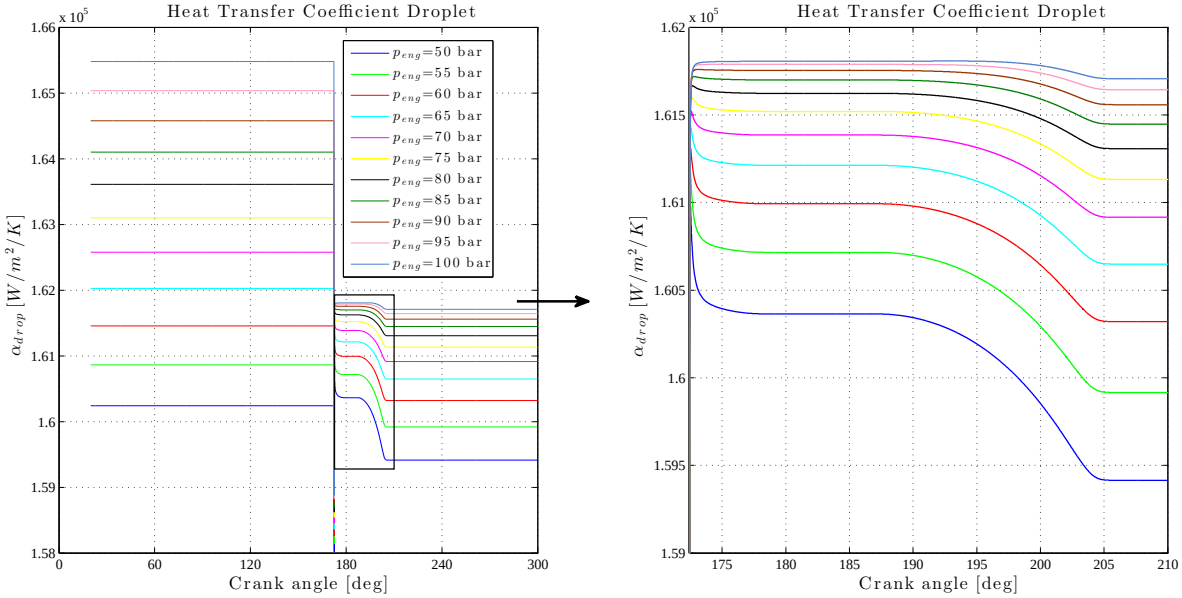

(a) Pressure variation

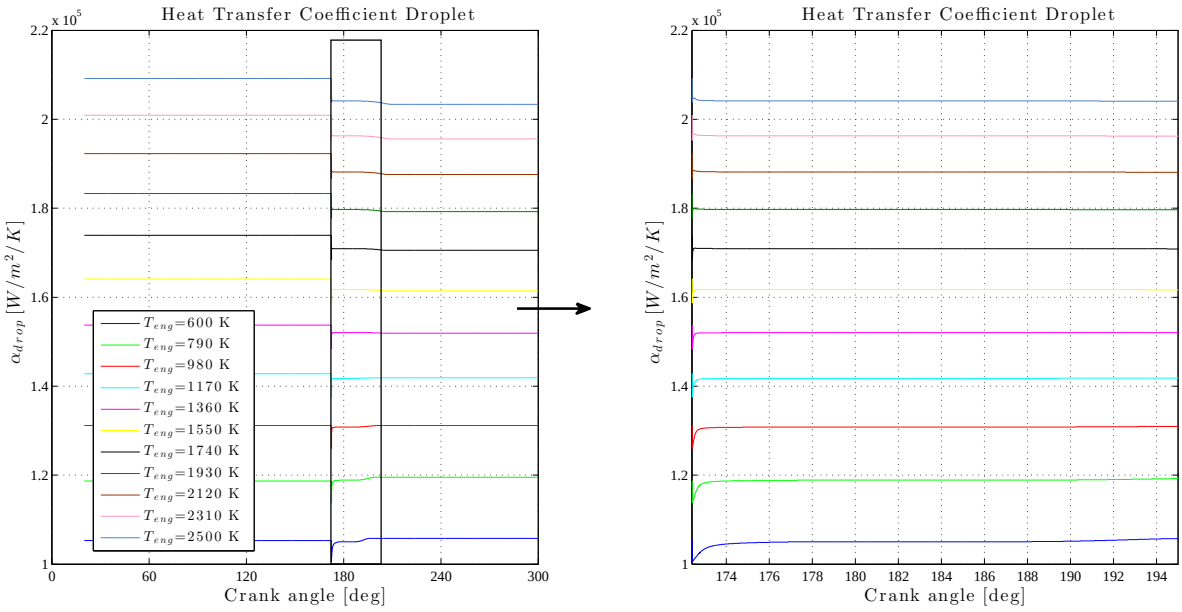

(b) Temperature variation

Figure 3-11: Heat transfer coefficient droplet evaporation CR

Liquid Zone state variables

Figures 3-12–3-14 present the state variables of the liquid zone (m_{liq}, T_{liq}, V_{liq}) respectively.

Figure 3-12 depicts the instantaneous mass of the liquid zone. The difference could be attributed to the difference between the injection rate and evaporation rate, and secondarily to the small difference in fuel injected in each case. For the temperature variation (fig. 3-12b) the mass of the liquid zone is greater with lower gas temperatures as a result of the delayed

evaporation rate which allows to accumulate more liquid fuel.

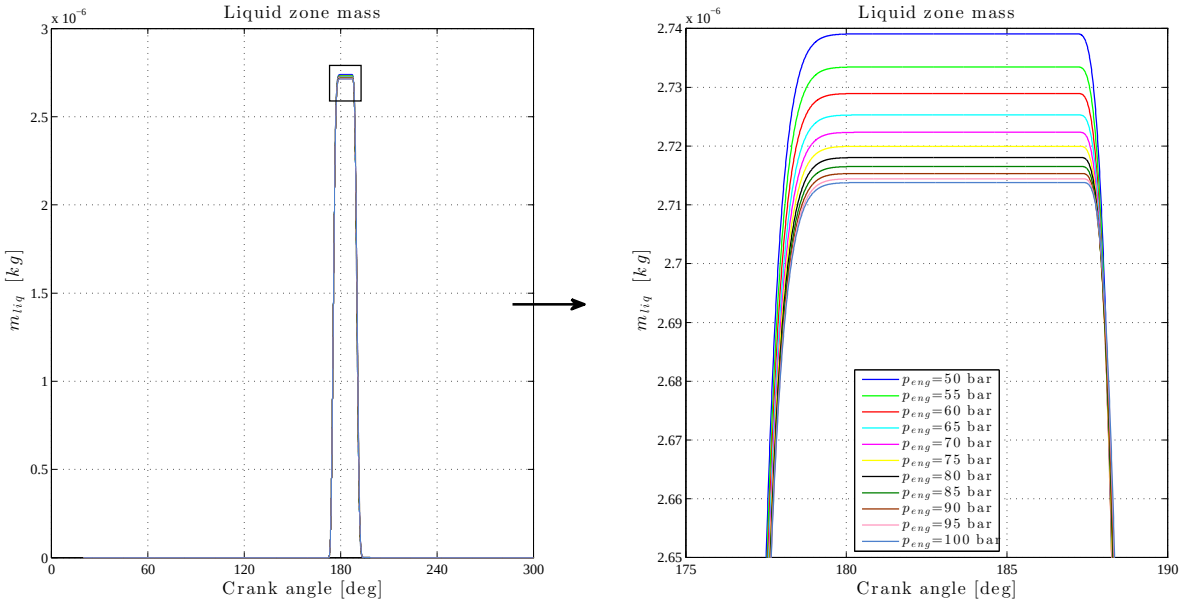

(a) Pressure variation

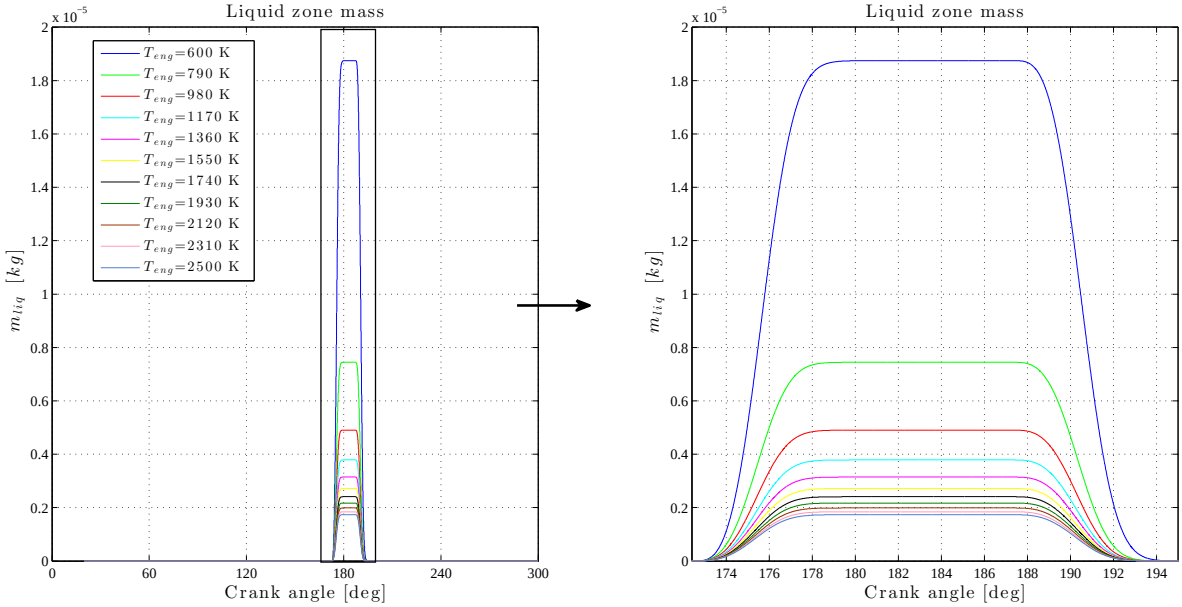

(b) Temperature variation

Figure 3-12: Liquid zone mass CR

The figure 3-13 shows that the temperature of the liquid zone is lower either with lower gas pressures or gas temperature.

The effect of the gas pressure over the liquid zone volume is less apparent since it depends on the instantaneous mass of the liquid zone and the fuel density at the instantaneous temperature of the liquid fuel (fig. 3-14a). The effect of temperature variation is much more marked as seen in fig. 3-14b. The variation is mainly attributed to the instantaneous mass of the

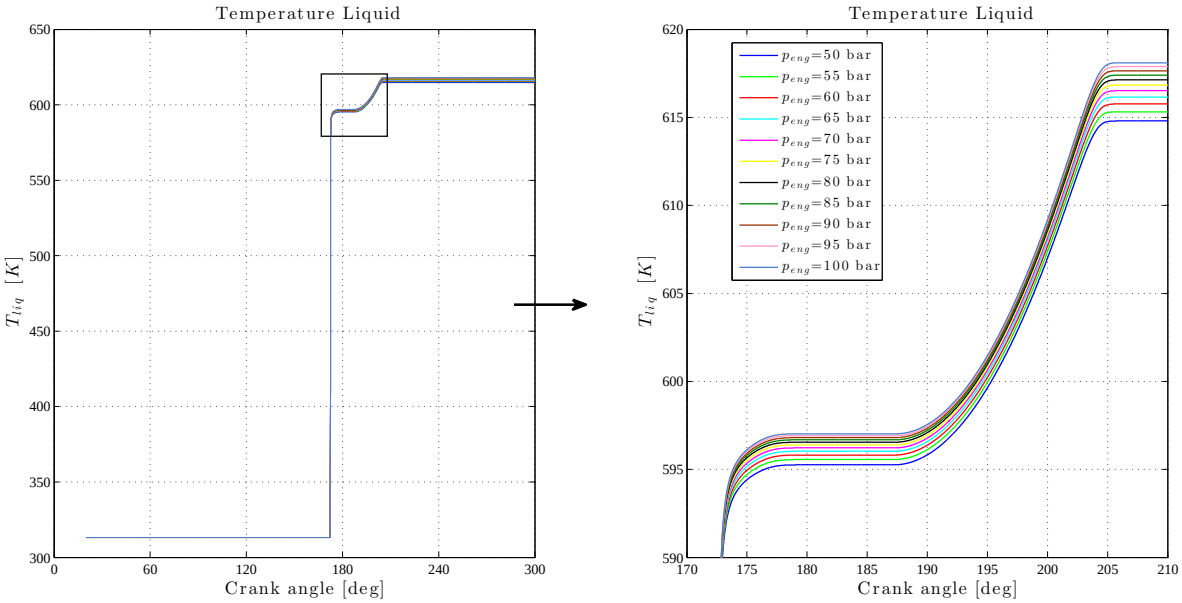

(a) Pressure variation

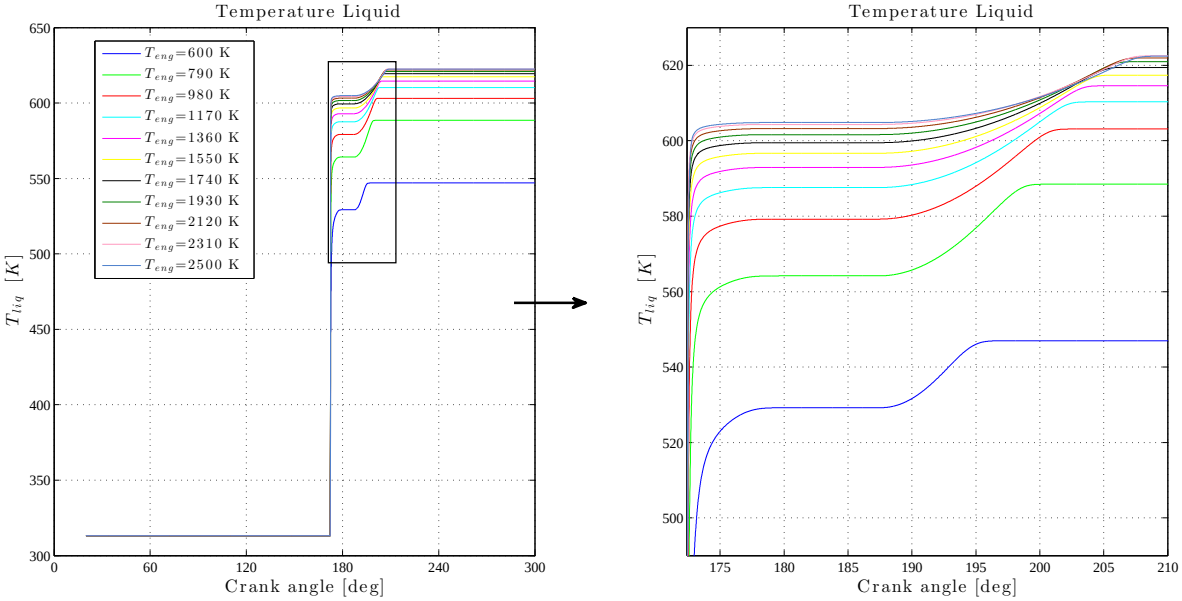

(b) Temperature variation

Figure 3-13: Liquid zone temperature CR

liquid zone.

3-4-2 Plunger Analysis

The plunger systems behaviour depends mainly on the shape of the cam pushing the plunger represented in this model by h' and the engine speed since it will affect the speed at which the plunger will be pushed and ultimately the liquid fuel. In this simulation the normalized plunger displacement is selected to produce reasonable maximum injection pressures and

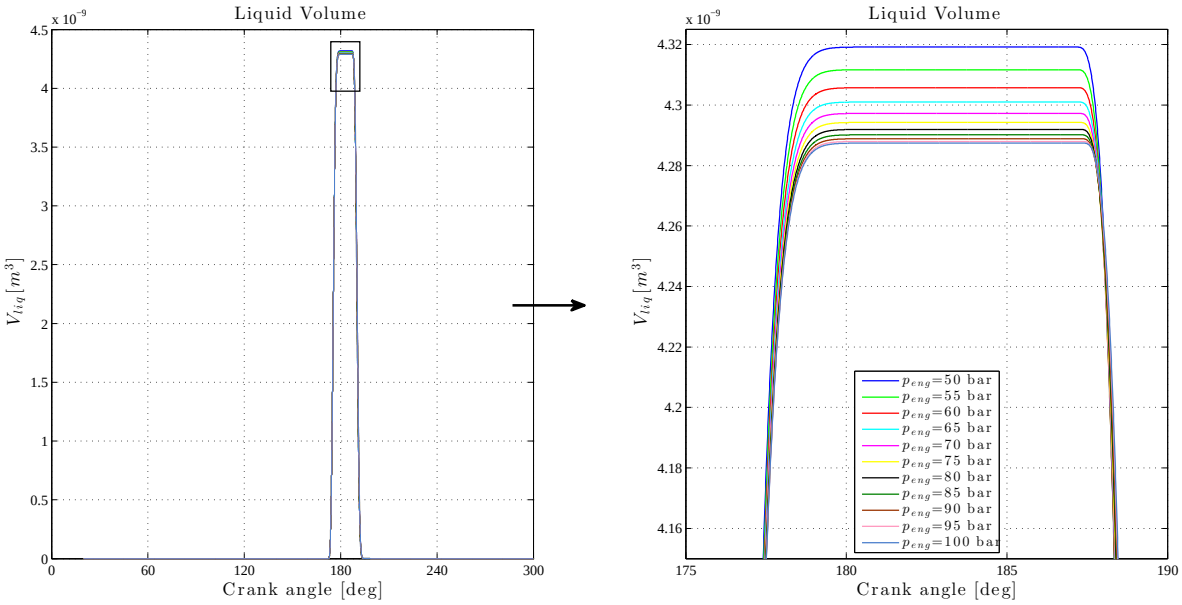

(a) Pressure variation

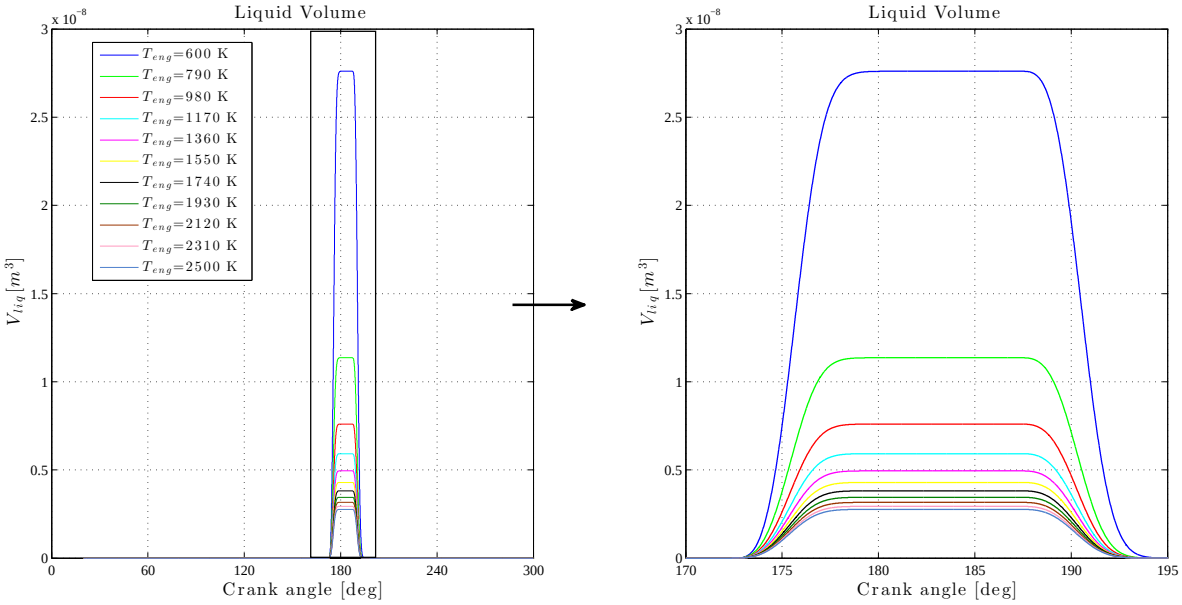

(b) Temperature variation

Figure 3-14: Liquid zone Volume CR

velocities.

Inputs

The figures presented below show the main parameters of the injection block, which can be seen as the driving inputs of the model. The pressure of the air is varied to see the influence on the fuel injection. Figure 3-15 presents the normalized displacement of the plunger. The figure 3-16 shows the injection velocity; here all curves are the same since the injection velocity

depends in this case on the plunger displacement. Figure 3-17 shows the injection pressure and as it can be seen the injection pressure is higher for higher gas pressures.

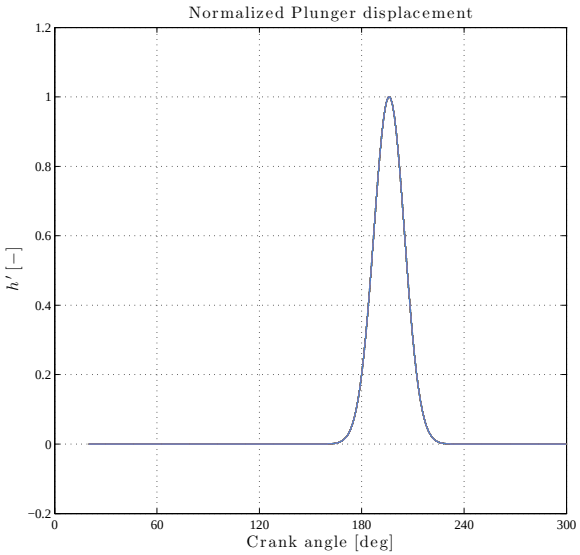

Figure 3-15: Plunger displacement

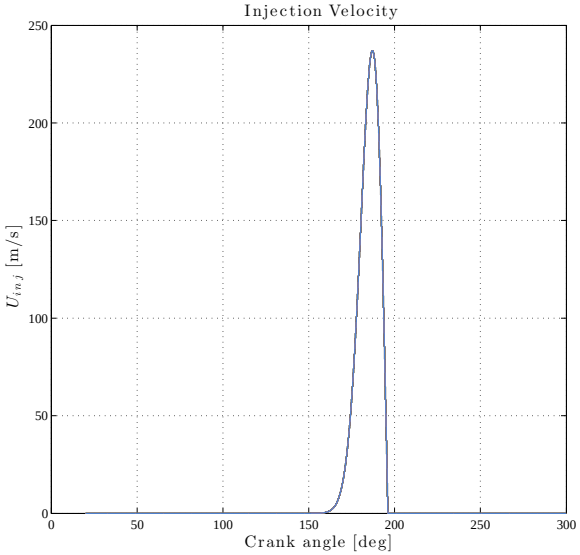

Figure 3-16: Injection Velocity PL

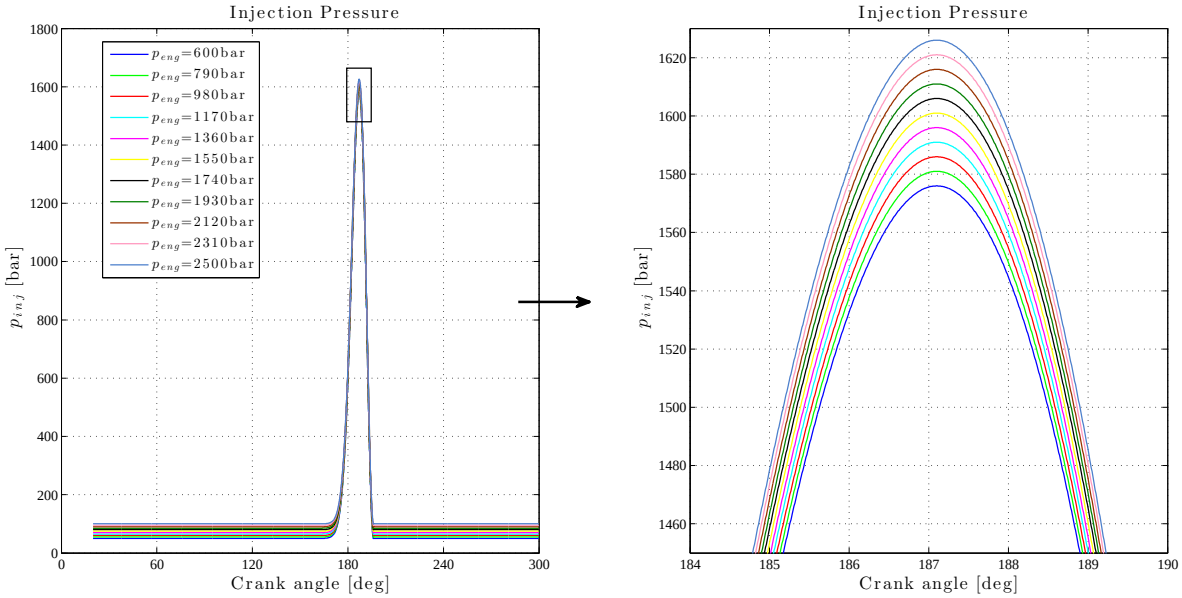

Figure 3-17: Injection Pressure PL

Figures 3-18 and 3-19 show the fuel injection rate and the injected fuel respectively. Here no variation is observed given that the injection rate comes as result of the plunger displacement only.

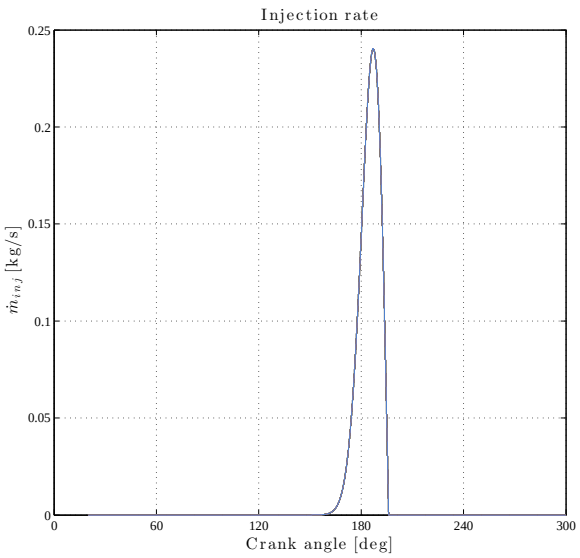

Figure 3-18: Injection Rate PL

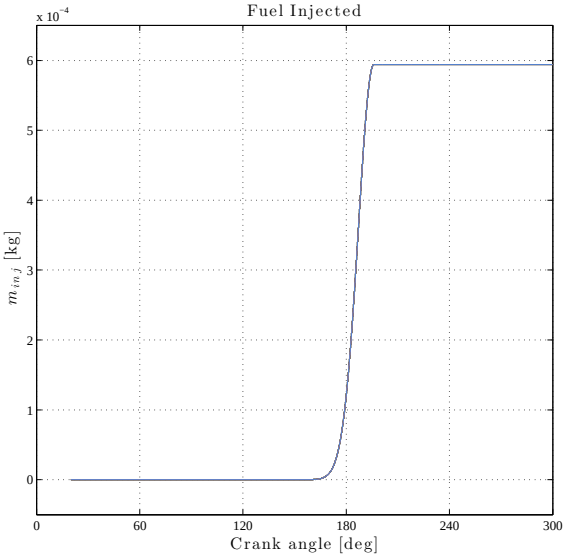

Figure 3-19: Fuel injected PL

Atomization Block

The primary outputs of the atomization block are presented in fig. 3-20 and fig. 3-21. In figure 3-20 the SMD is presented. The figure depicts a period with constant droplet diameter, this stage belongs to period where the injection velocity is low then a factor of the nozzle diameter is selected; once the pressure drop across the nozzle increases the injection velocity is increased producing smaller droplet diameters. Here is evidence of the problems that arise from computing the drop diameter from an empirical formula and not from droplet mass balance. Another problem with the use of such expressions to compute the SMD is that all of them cannot be used in the absence of injection therefore the discontinuity of the computed droplet diameter at the end of injection.

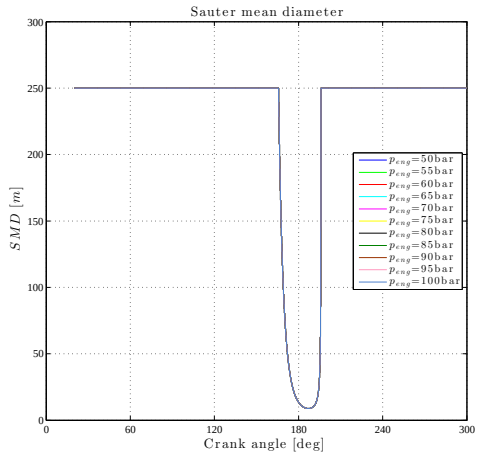

Figure 3-20: Drop diameter PL

Figure 3-21 shows the number of droplets in the cylinder computed as the quotient of the mass of liquid in the cylinder and the droplet mass. Figure 3-21a presents the variation of

the number of droplets for different gas pressures. Figure 3-21b shows the variation of the number of droplets with gas temperature changes. It can be observed that there are fewer droplets for higher gas temperatures. As in the common rail case this is a result of the faster response of the evaporation rate at high temperatures then less liquid fuel is present in the Liquid zone.

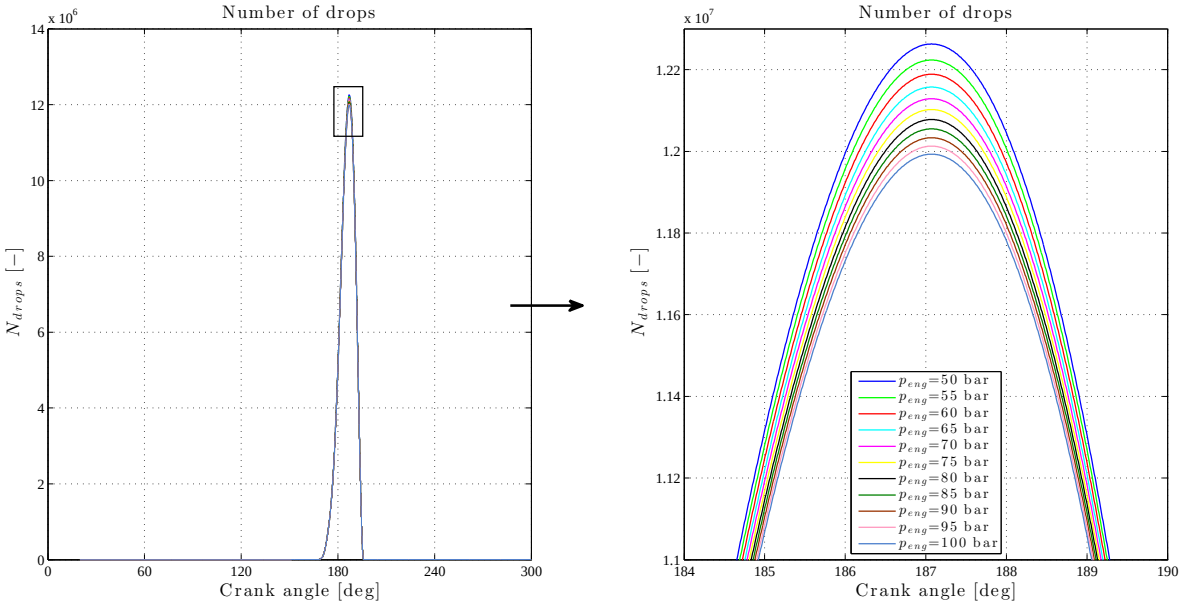

(a) Pressure variation

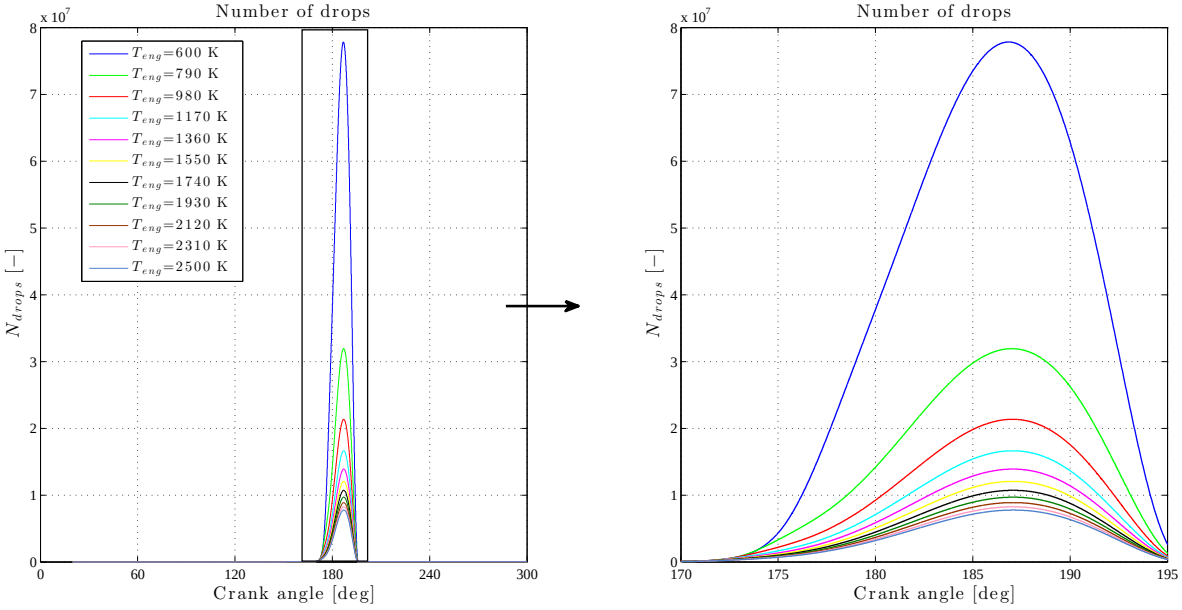

(b) Temperature variation

Figure 3-21: Number of fuel droplets PL

Evaporation Block

The main outputs of the liquid zone and their variation with gas pressure and gas temperature are presented in figs. 3-22 and 3-23 and the heat transfer coefficient in fig. 3-24.

As observed from figs. 3-22a and 3-22b the evaporation rate is affected mainly by the gas temperature. The main effect is that the delay of the evaporation rate is reduced as the temperature increases. With longer delay more liquid fuel is accumulated this allows for a sharp increase of the evaporation rate in a first stage; then as time elapses and the amount of fuel accumulated is evaporated the vaporous fuel production is controlled by rate at which the fuel is injected.

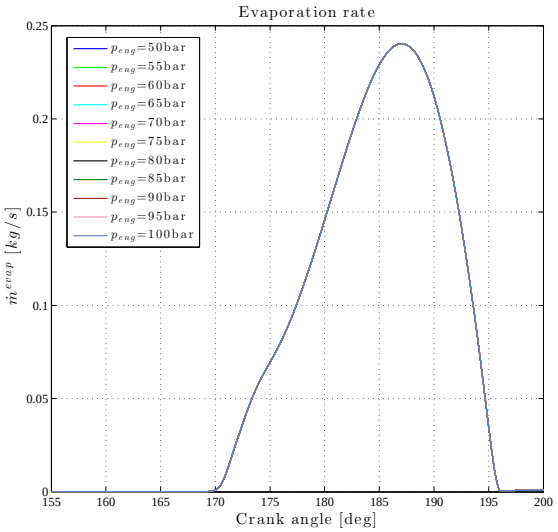

(a) Pressure variation

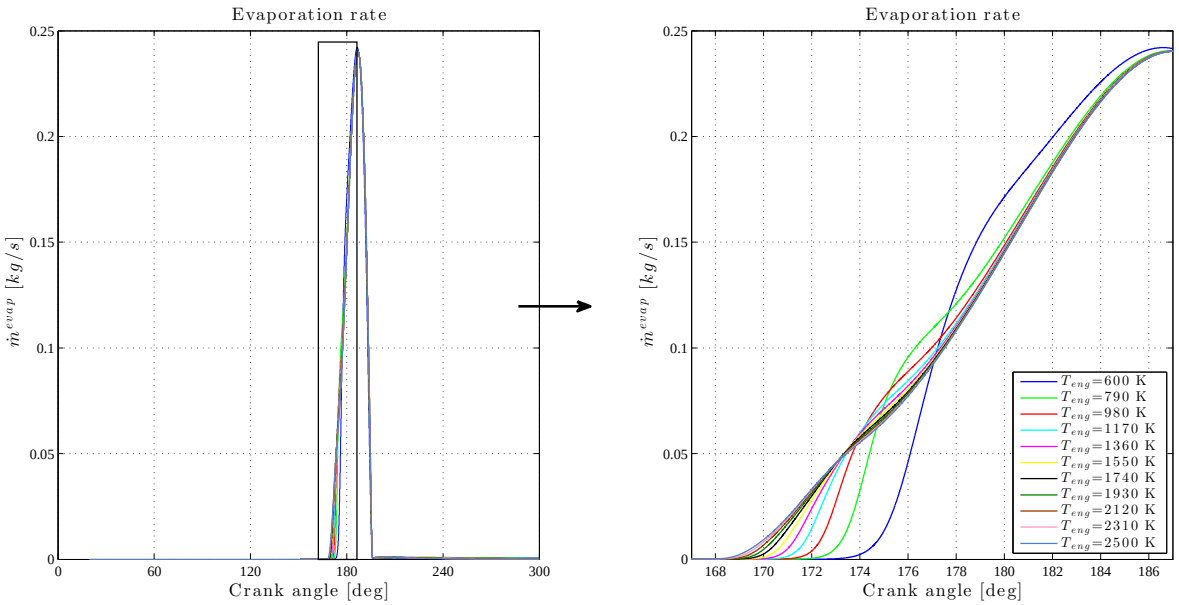

(b) Temperature variation

Figure 3-22: Evaporation rate PL

As in the common rail the change in the heat flow to the liquid zone is mainly affected by the variation of the gas temperature. The heat flow is increased with higher gas temperatures as a result of a greater temperature difference of the liquid zone and the surrounding gas (fig. 3-23b). The effect of pressure variation is very little and is mainly observed by changing the concentration at which the evaporation layer is computed (fig. 3-23a).

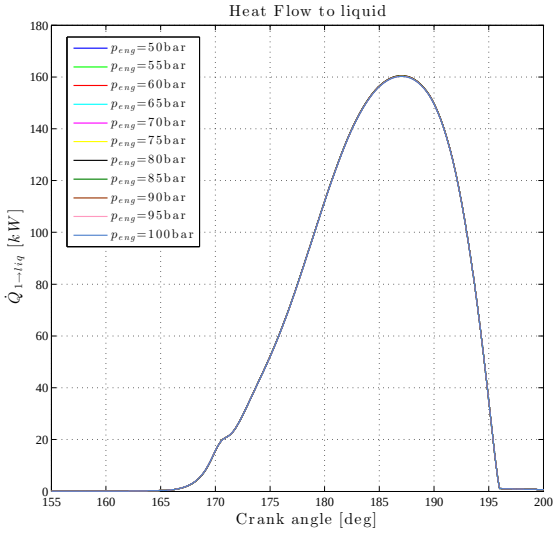

(a) Pressure variation

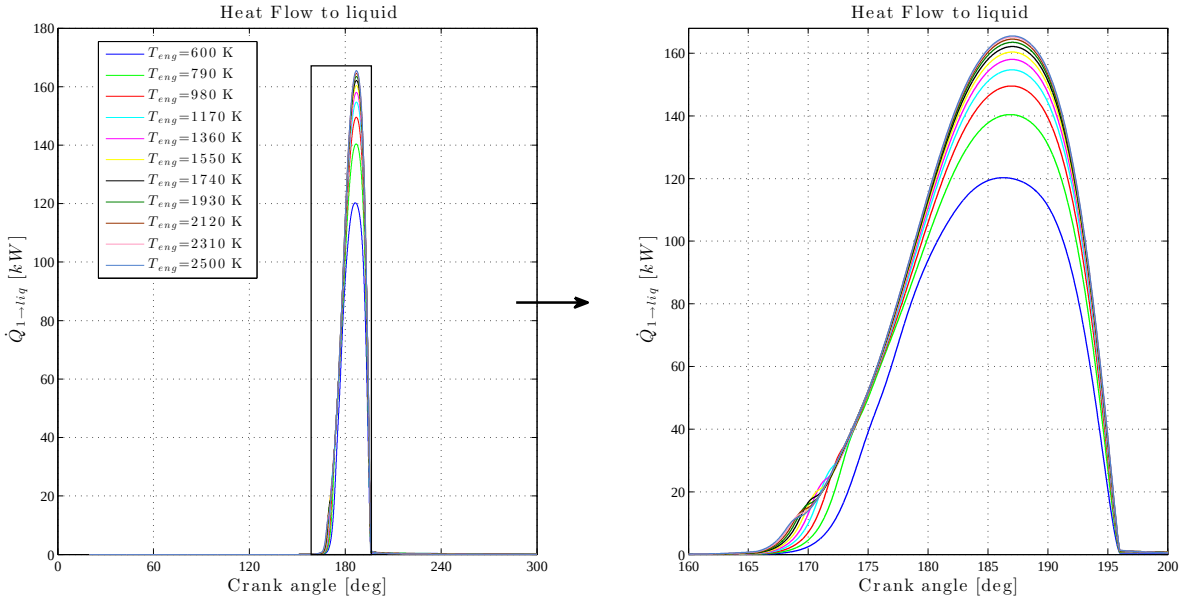

(b) Temperature variation

Figure 3-23: Heat flow to liquid zone PL

The heat transfer coefficient is shown in fig. 3-24. Again the temperature has a greater effect as the properties of the mixing layer have a stronger dependence on temperature than pressure. Additionally the values are on the high side as compared to the typical values presented by Incropera [51] but still in same range of magnitude.

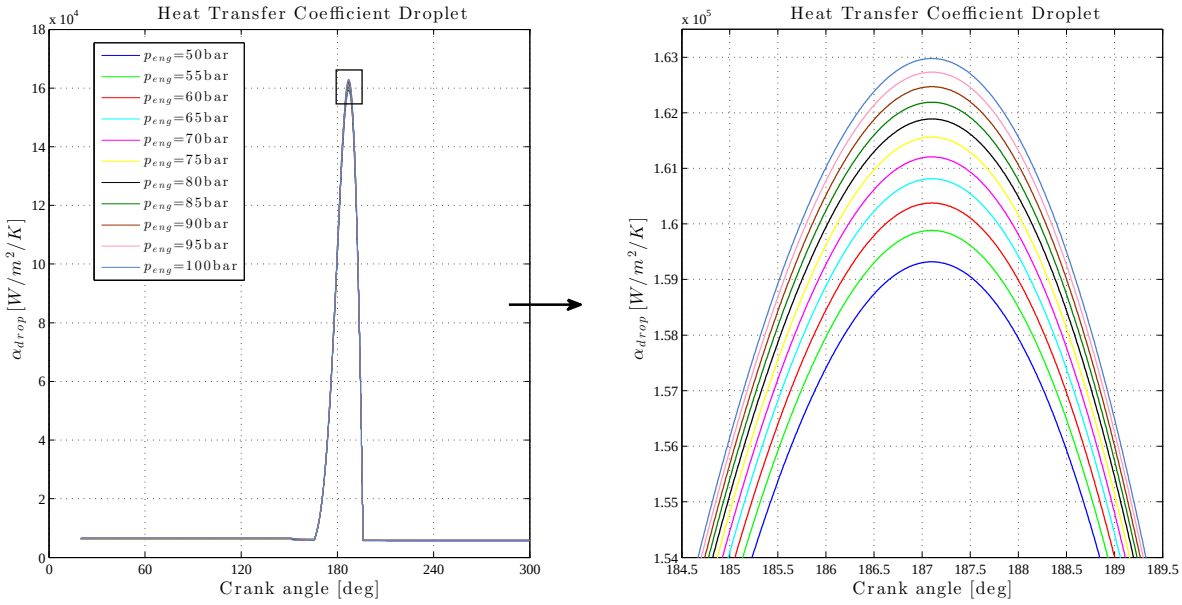

(a) Pressure variation

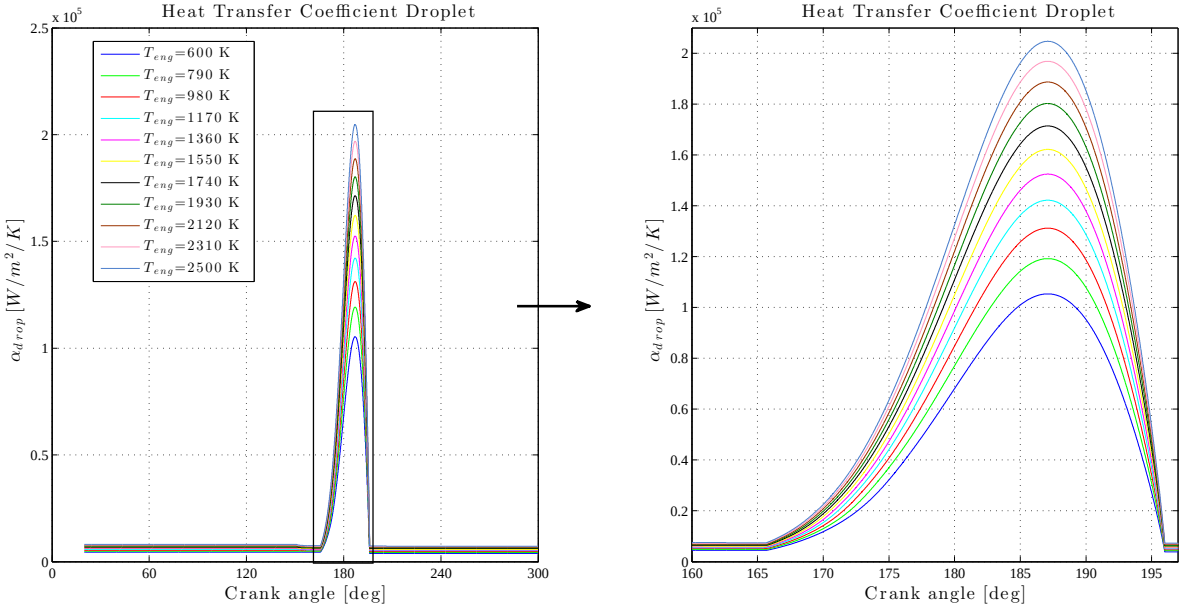

(b) Temperature variation

Figure 3-24: Heat transfer coefficient droplet evaporation PL

Liquid Zone state variables

Figures 3-25–3-27 show the variables m_{liq} T_{liq} and V_{liq} respectively and the influence of the gas variation on them.

From 3-25 it is evident that the influence of the gas temperature is greater than the gas pressure. Again the mass of the liquid zone is greater with lower gas temperatures as a result of the delayed evaporation rate which allows to accumulate more liquid fuel (fig. 3-25b). The

gas pressure variation in fig. 3-25a has very little influence and it is due to the variation of the evaporation rate since the injection rate is the same for different gas pressures.

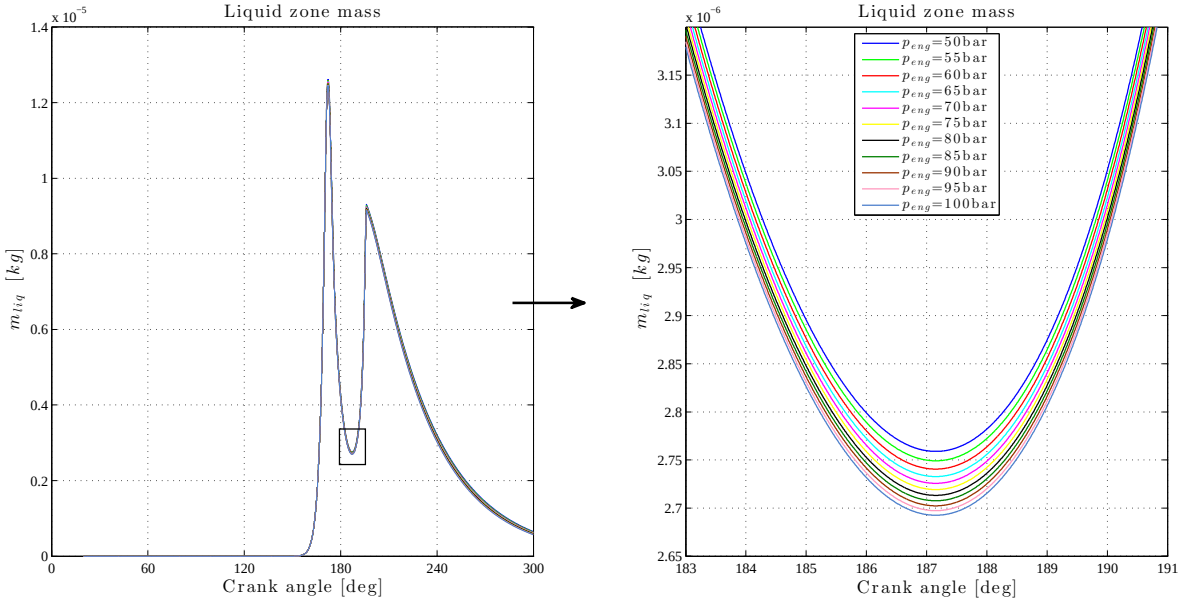

(a) Pressure variation

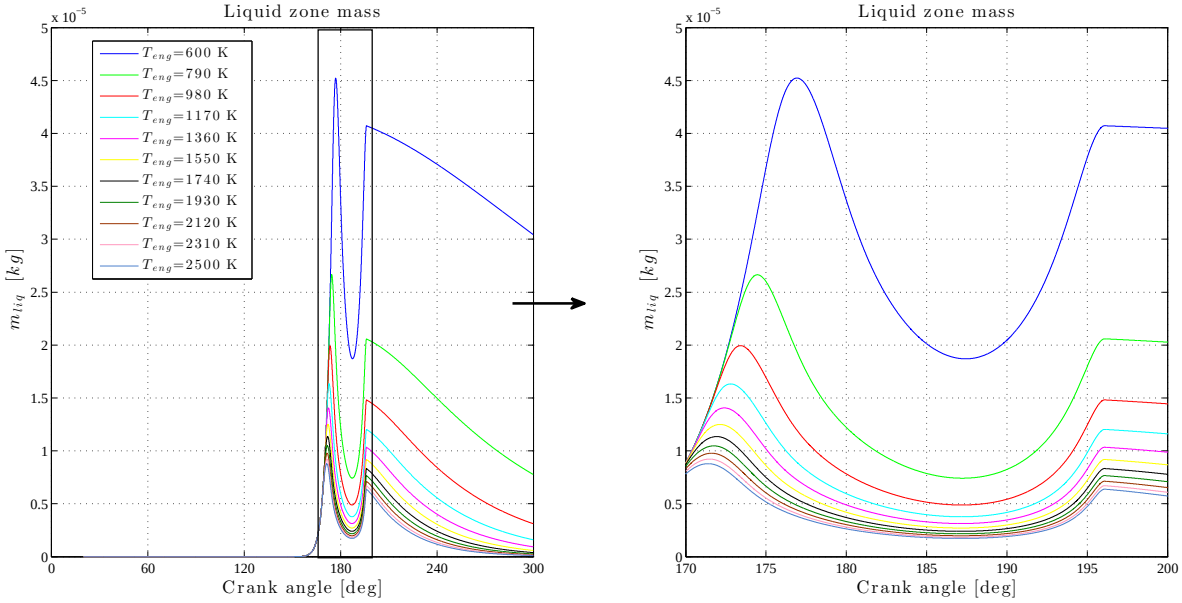

(b) Temperature variation

Figure 3-25: Liquid zone mass PL

In the fig. 3-26 the temperature of the liquid zone is presented. The variation of the liquid temperature with changes in gas pressure is small. However, in the detail it can be seen that the greater the gas pressure the higher the liquid zone temperature, this in accordance with the concept that at higher surrounding pressures the higher the boiling point of the liquid (fig. 3-26a). The influence of the gas temperature variation (fig. 3-26b) is much more notorious

than the gas pressure variation, here with higher gas temperatures the rise in temperature of the liquid is faster. The effect of the gas temperature on the liquid fuel temperature can be explained by the increased heat flow from the gases since the delta in temperature is bigger.

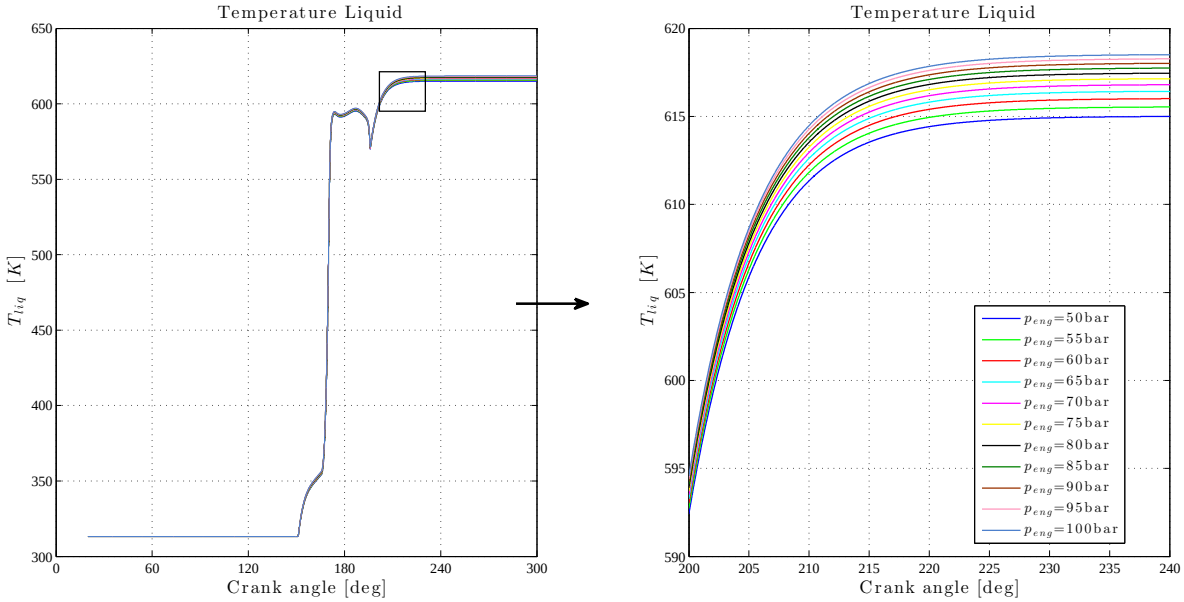

(a) Pressure variation

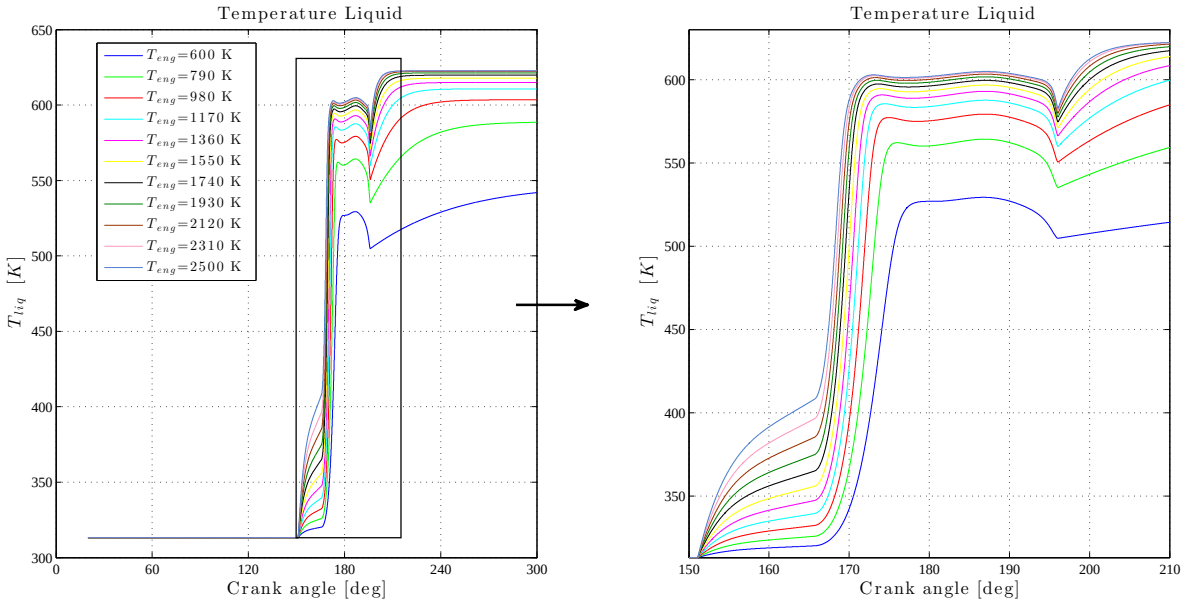

(b) Temperature variation

Figure 3-26: Liquid zone temperature PL

The liquid zone volume is presented in fig. 3-27. Figure 3-27a shows the volume of the liquid zone with different pressures for the surrounding gas. Figure 3-27b presents the volume of the liquid zone at different gas temperatures. The influence of these variations on the liquid volume follows the same patterns as the liquid mass. Additionally, with higher gas

temperatures the liquid zone temperature is higher and the liquid fuel density reduces then accentuating further the liquid volume difference.

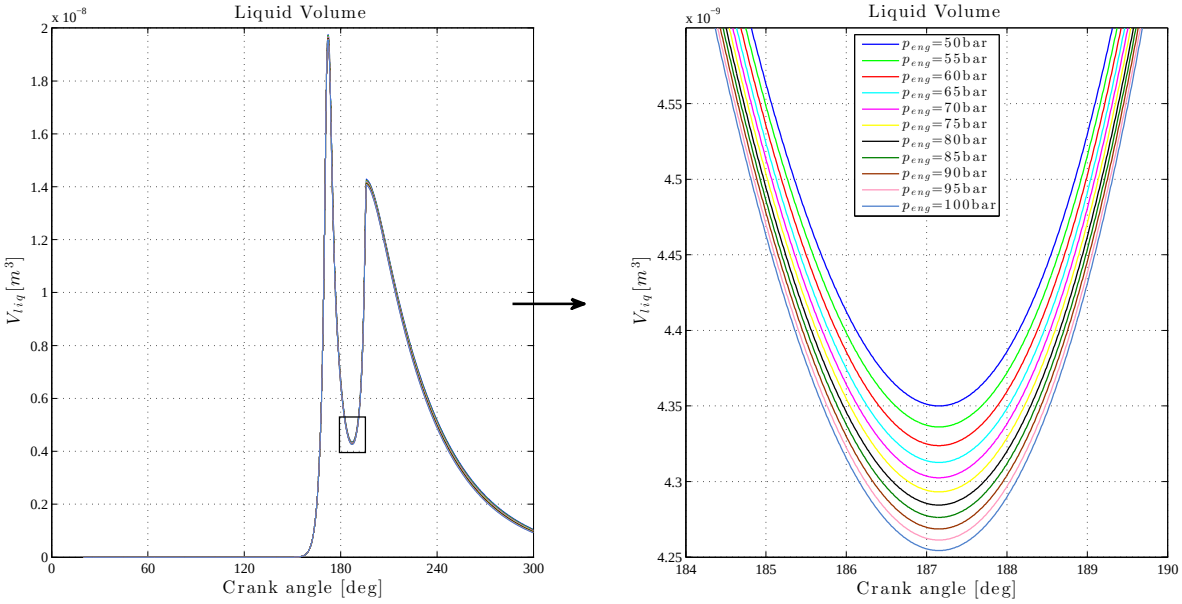

(a) Pressure variation

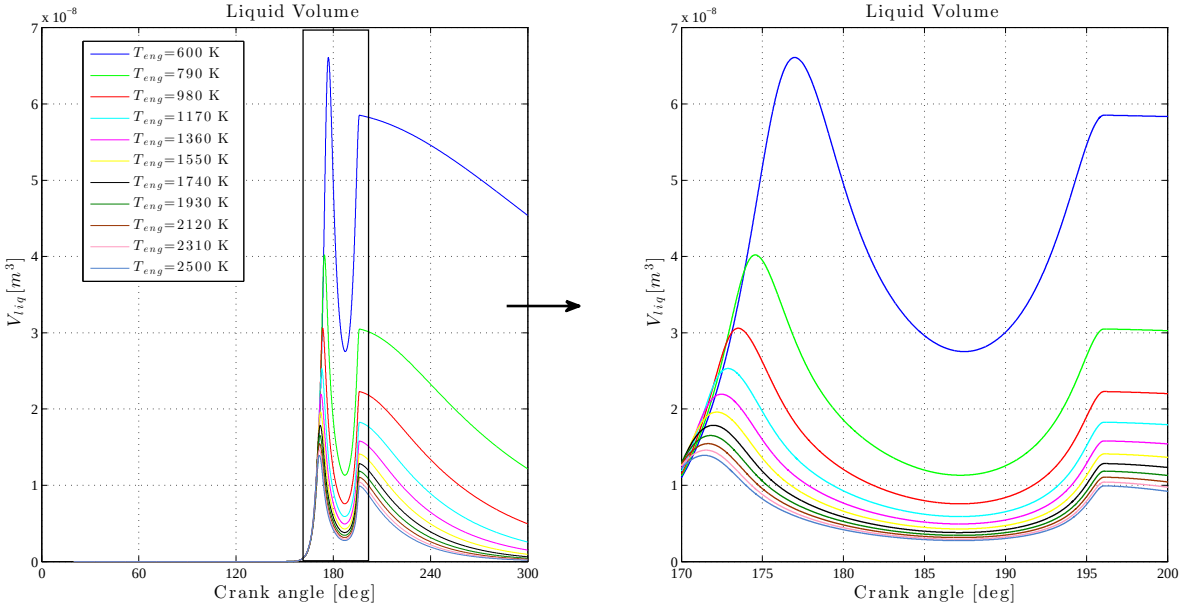

(b) Temperature variation

Figure 3-27: Liquid zone Volume PL

3-5 Discussion

The liquid block of the model has been described and implemented in this chapter. The injection models proposed to simulate the common rail system and the plunger provide useful information and allow to study the behaviour of the cylinder process under different injection

schemes. However the simulation of the injection system still is open to improvement to have a more realistic injection rate, injection velocity and pressure drop across the injection nozzle. The assumption that the average drop diameter can be estimated based on empirical formulas present some difficulties given the characteristics of the formulas used but proves to be a simple approach. The most important observation from the model and analysis is that in general the evaporation rates are very fast and ultimately the evaporation rate is controlled by the injection rate. This supports the assumption in the single zone model that the injection rate and evaporation rate are equal [52].

Chapter 4

Gas Phase - Two Zone Model

In this chapter the gas phase of the cylinder will be simulated, to do so the liquid zone is not present in the cylinder, and the driving mass flow is the evaporation flow. This in conjunction with a series of assumptions and simplifications that allow to solve the mass balances and energy balances of the Bulk zone and the Flame zone. The introduction of three parameters will be defined in order to describe the mass transport terms present in this set of equations. Finally, the heat transfer between each zone and the walls will be explained as well.

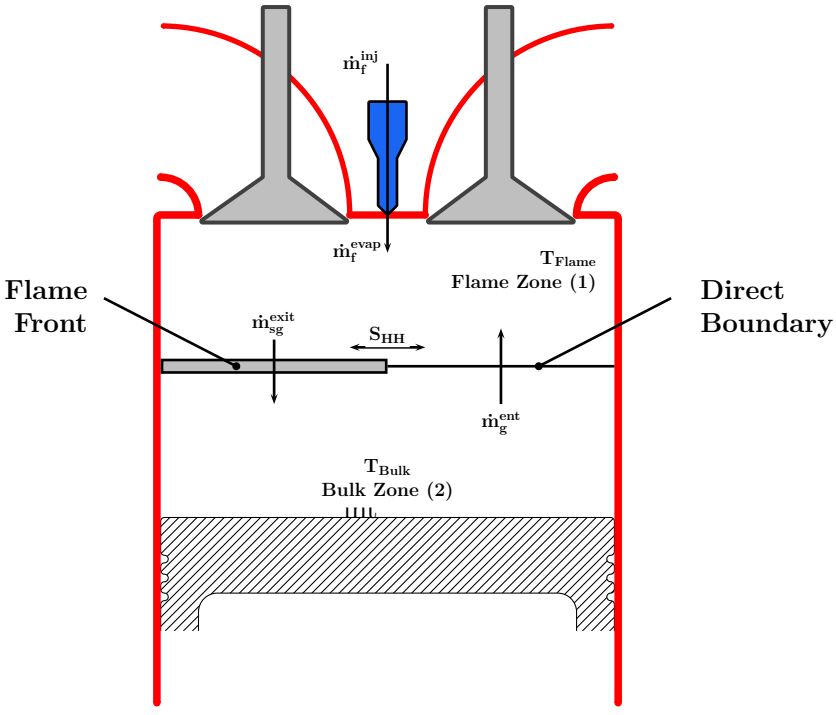

Figure 4-1: Two Zone Model

In this model one of the major assumptions is that pressure is homogeneous inside the cylinder. As a result of the homogeneity of the pressure inside the cylinder, an algebraic loop is generated when trying to solve the Volume balance eq.(2-40). Since it is an essential loop it cannot be disregarded and later in this chapter its treatment will be described .

The equations used to simulate the gas phase where developed in chapter 2. For the Flame Zone the equations used are (2-16, 2-17 and 2-26)

$$\frac{dm_{f,1}}{dt} = \dot{m}_f^{evap} - \xi$$

$$\frac{dm_{a,1}}{dt} = \dot{m}_a^{ent} - \sigma \cdot \xi$$

$$\frac{dm_{sg,1}}{dt} = \dot{m}_{sg}^{ent} - \dot{m}_{sg}^{exit} + (1+\sigma) \cdot \xi$$

$$\frac{dm_1}{dt} = \dot{m}_f^{evap} + \underbrace{\dot{m}_a^{ent} + \dot{m}_{sg}^{ent}}_{\dot{m}_g^{ent}} - \dot{m}_{sg}^{exit}$$

and

$$m_1 c_{v,1} \frac{dT_1}{dt} = \dot{m}_f^{evap}\left(h_{f,g}^{evap} - u_{f,1}\right) + \dot{m}_a^{ent}\left(h_a^{ent} - u_{a,I}\right) + \dot{m}_{sg}^{ent}\left(h_{sg}^{ent} - u_{sg,1}\right) - \dot{m}_{sg}^{exit}\left(h_{sg}^{exit} - u_{sg,1}\right) - \langle (1+\sigma)\, u_{sg,1} - \sigma \cdot u_{a,1} - u_{f,1} \rangle\, \xi - \dot{Q}_{1\to liq} - \dot{Q}_{1\to wall} - p \cdot \frac{dV_1}{dt}$$

and for the Bulk Zone the equations used are (2-27, 2-28 and 2-37).

$$\frac{dm_{a,2}}{dt} = -\dot{m}_a^{ent}$$

$$\frac{dm_{sg,2}}{dt} = -\dot{m}_{sg}^{ent} + \dot{m}_{sg}^{exit}$$

$$\frac{dm_2}{dt} = -\underbrace{\left(\dot{m}_a^{ent} + \dot{m}_{sg}^{ent}\right)}_{\dot{m}_g^{ent}} + \dot{m}_{sg}^{exit}$$

and

$$m_2 c_{v,2} \frac{dT_2}{dt} = -\dot{m}_a^{ent}\left(h_a^{ent} - u_{a,2}\right) - \dot{m}_{sg}^{ent}\left(h_{sg}^{ent} - u_{sg,2}\right) + \dot{m}_{sg}^{exit}\left(h_{sg}^{exit} - u_{sg,2}\right) - \dot{Q}_{2\to wall} - p \cdot \frac{dV_2}{dt}$$

As mentioned before, in order to solve this system of equations it is necessary to determine the mass flows, heat flows and the volumes of the two zones. To do so it is necessary to introduce models or expressions able to reproduce these flows. The mass flows to be determined in this equations are $\dot{m}_f^{evap}$, $\dot{m}_g^{ent}$and $\dot{m}_{sg}^{exit}$.

4-1 Injection, Evaporation and Combustion rate

The evaporation rate in this model is assumed to be very fast and follows the injection rate. Furthermore, in this chapter the shape of the evaporation rate is the same as the combustion reaction rate (CRR). In addition, it is assumed that the fuel evaporates immediately after injection and combustion also proceeds instantly, this idea is derived from the single zone model in the work of Ding Ju [52], thus the injection rate, evaporation rate and combustion rate are equal.

$$\begin{aligned} \dot{m}_f^{evap} &= \dot{m}_f^{inj} \\ &= \xi \end{aligned} \tag{4-1}$$

4-1-1 Introduction Vibe heat release model

The Vibe function is based on the first principle of chain reactions [4], where the formation of radicals is proportional to the amount of fuel and the increase of radicals is proportional to the decrease of fuel:

$$\frac{dm_f^+}{dt} = k \cdot m_f \quad \text{and} \quad dm_f^+ = -\mu \cdot dm_f \tag{4-2}$$

and thus the reaction rate:

$$\xi = \frac{dm_f}{dt} = -\frac{k}{\mu} \cdot m_f \tag{4-3}$$

The normalized rate of combustion Z, which is linked to the normalized reaction rate X, can be defined as:

$$Z = \frac{dX}{d\tau} = \xi \cdot \frac{t_{comb}}{m_{f,0}} \quad \text{and} \quad X = \frac{m_f}{m_{f,0}} \tag{4-4}$$

where τ is normalized time:

$$\tau = \frac{t}{t_{comb}} \tag{4-5}$$

Vibe proposed a model assuming a nonlinear time dependency of the reaction constant in equation (4-3),

$$k \propto t^m \tag{4-6}$$

The normalized reaction rate and reaction coordinate then can be shown to be:

$$Z = a \cdot (m+1) \cdot \tau^m \cdot e^{-a \cdot \tau^{m+1}} \quad \text{and} \quad X = 1 - e^{-a \cdot \tau^{m+1}} \tag{4-7}$$

If the duration of combustion time and the total injected fuel are given, the CRR can be acquired after selecting parameters m and a.

To make the model more suitable for real combustion processes and make a division between the premix and diffusive combustion stages, a double Vibe model is often used:

$$Z = b_1 \cdot a \cdot (m_1+1) \cdot \tau^{m_1} \cdot e^{-a \cdot \tau^{m_1+1}} + b_2 \cdot a \cdot (m_2+1) \cdot \tau^{m_2} \cdot e^{-a \cdot \tau^{m_2+1}} \tag{4-8a}$$

$$X = b_1 \cdot \left(1 - e^{-a \cdot \tau^{m_1+1}}\right) + b_2 \cdot \left(1 - e^{-a \cdot \tau^{m_2+1}}\right) \tag{4-8b}$$

Here b_1 and b_2 are the weighting factor for premix and diffusive combustion, which must obey:

$$b_1 + b_2 = 1 \tag{4-9}$$

The parameter a is taken equal for both Vibe functions and then can easily be linked to the combustion efficiency:

$$1 - e^{-a} = \eta_{comb} \tag{4-10}$$

A series progression of Vibe functions was proposed by Knobbe [53]:

$$X = \sum_{k=1}^{n} b_k \cdot X_k = \sum_{k=1}^{n} b_k \cdot \left(1 - e^{-a \cdot \tau^{m_k+1}}\right) \tag{4-11}$$

The Vibe function is considered a wavelet from which a series expansion is formed. Each single Vibe function has its own form factor m_k and weight factor b_k but they share the same a and the same duration of combustion.

4-2 Entrainment rate

The entrainment rate in literature is related to the momentum conservation of the jet, based on expressions of the spray penetration S. Since in this model the individual history of the droplet or group of droplets is not followed, as a first approach the entrainment rate $\dot{m}_g^{ent}$ is fixed by the stoichiometry of the fuel and the evaporation rate.

$$\dot{m}_*^{ent} = \sigma \cdot \dot{m}_f^{evap} \tag{4-12}$$

where σ is the stoichiometric ratio.

A first parameter is introduced to account for the fact that the composition of the bulk zone is not pure fresh air and the possibility that entrained air could be more than or less than the stoichiometric amount. This first parameter defined as:

$$\lambda_{ent} \stackrel{\text{def}}{=} \frac{\dot{m}_g^{ent}}{\dot{m}_*^{ent}} \tag{4-13}$$

then the entrained gas rate is:

$$\dot{m}_g^{ent} = \lambda_{ent} \cdot \sigma \cdot \dot{m}_f^{evap} \tag{4-14}$$

4-3 Stoichiometric gas flow $\dot{\mathbf{m}}_{\mathbf{sg}}^{\mathbf{exit}}$

The $\dot{m}_{sg}^{exit}$ is the term that allows for the stoichiometric gas produced in the Flame to leave to the Bulk zone. Thus this term represents the further mixing that the stoichiometric gas undertake in the cylinder.

The mass flow of stoichiometric gas leaving the flame zone is related to the rate at which is produced in the zone. Referring to the literature, on the one hand in the work of Holhbaum [2] all the produced gas leaves the zone where the mixture of air and fuel is present, and on the other hand in the Heider model[2] the produced stoichiometric gas stays in the zone where the air-fuel mixture is present. Therefore, a second factor S_{HH} is introduced to allow for a

more general case. It is defined as the quotient between the stoichiometric gas flow leaving the flame zone and the stoichiometric gas production rate. Then flow of stoichiometric gas leaving the flame zone is:

$$\dot{m}_{sg}^{exit} = S_{HH} \cdot (1 + \sigma) \cdot \xi \tag{4-15}$$

where S_{HH} will be referred as to the Heider-Holhbaum factor.

4-4 Heat Transfer to walls

Given that the two volumes that represent the gas phase are in contact with the walls of the cylinder (head, crown and wall) then both lose heat to the walls. The heat transfer is expressed by means of convective heat transfer.

$$\dot{Q}_{i \to wall} = \alpha \cdot A_{wall,i} \cdot (T_i - T_{wall}) \tag{4-16}$$

with $i = \{1, 2\}$.

The wall temperature represents the average temperature of the walls, but it is allowed different temperatures for the piston crown, cylinder head and cylinder wall (T_{crown}, T_{Head}, T_{wall}). Furthermore the temperature of the walls is considered constant in time.

The area for heat transfer is computed based on the geometry of the cylinder. Additionally, since the cylinder is divided in two volumes then from figure 4-1 the Flame zone looses heat to the cylinder head and cylinder walls, and the Bulk zone to the piston crown and cylinder walls. The cylinder wall area split is done with the calculated volume of each zone.

$$A_{head} = A_{crown} = \frac{\pi}{4} \cdot D_B^2 \tag{4-17a}$$

$$A_{wall,T} = \pi \cdot L_p \cdot D_B$$

$$A_{wall,2} = S_{HL} \cdot A_{wall,T} \tag{4-17b}$$

$$A_{wall,1} = (1 - S_{HL}) \cdot A_{wall,T} \tag{4-17c}$$

where L_p is computed with eq.(2-42), D_B is the cylinder bore. S_{HL} is the split factor and it is defined as the quotient of the volume of the Bulk Zone and the cylinder volume.

$$S_{HL} = \frac{V_{Bulk}}{V_{cyl}} = \frac{\cancel{A_{crown}} \cdot L_{Bulk}}{\cancel{A_{crown}} \cdot L_p} \tag{4-18}$$

The heat transfer coefficient is calculated using the expression proposed by Woschni.

$$\alpha_i = C_2 \cdot D_B^{m-1} \cdot p_{cyl}^{m} \cdot T_i^{p-(1+q)\cdot m} \cdot \left(C_3 \cdot c_m + C_4 \cdot \frac{p_{cyl} - p_{nof}}{p_{EC}} \frac{V_s}{V_1} * T_{EC} \right)^m \tag{4-19}$$

with

$$m = 0.786$$
$$p = 0.75$$
$$q = 0.62$$
$$\frac{w_t}{c_m} = 5$$
$$C_2 = 220$$
$$C_3 = 2.28 + 0.308 \cdot \frac{w_t}{c_m}$$
$$C_4 = 0.00324 \left[\frac{m}{s\,K}\right]$$

It is important to note that the units of the pressure used in this formula are in bar. w_t is the swirl velocity. For a complete description of this formula refer to Stapersma [54].

Now the heat transfer from the Flame Zone (1) is,

$$\dot{Q}_{1\rightarrow wall} = \alpha_1 \cdot [A_{wall,1} \cdot (T_1 - T_{wall}) + A_{head} \cdot (T_1 - T_{head})] \tag{4-20}$$

and the heat transfer from the Bulk Zone (2) is ,

$$\dot{Q}_{2\rightarrow wall} = \alpha_2 \cdot [A_{wall,2} \cdot (T_2 - T_{wall}) + A_{crown} \cdot (T_2 - T_{crown})] \tag{4-21}$$

4-5 Volume Balance

The volume balance is an important element to consider in order to compute the cylinder pressure and the volume of the two zones.

In order to solve this balance, the Ideal Gas law and the geometry of the engine are used.

$$V_{gas} = A_B \cdot L_s \tag{4-22a}$$
$$V_2 = \frac{\int \dot{m}_2 dt \cdot R_2 \cdot T_2}{p_{cyl}} \tag{4-22b}$$
$$V_1 = V_{gas} - V_2 \tag{4-22c}$$
$$p_{cyl} = \frac{\int \dot{m}_1 dt \cdot R_1 \cdot T_1}{V_1} \tag{4-22d}$$

As can be seen in figure 4-2 the assumption that the pressure is homogeneous in the cylinder introduces an algebraic loop. This loop is broken by computing each of the volumes and the pressure individually by introducing the term ϕ_V which is the quotient of terms $(mRT)_1$ and $(mRT)_2$.

$$\phi_V \stackrel{\text{def}}{=} \frac{(mRT)_1}{(mRT)_2} \tag{4-23}$$

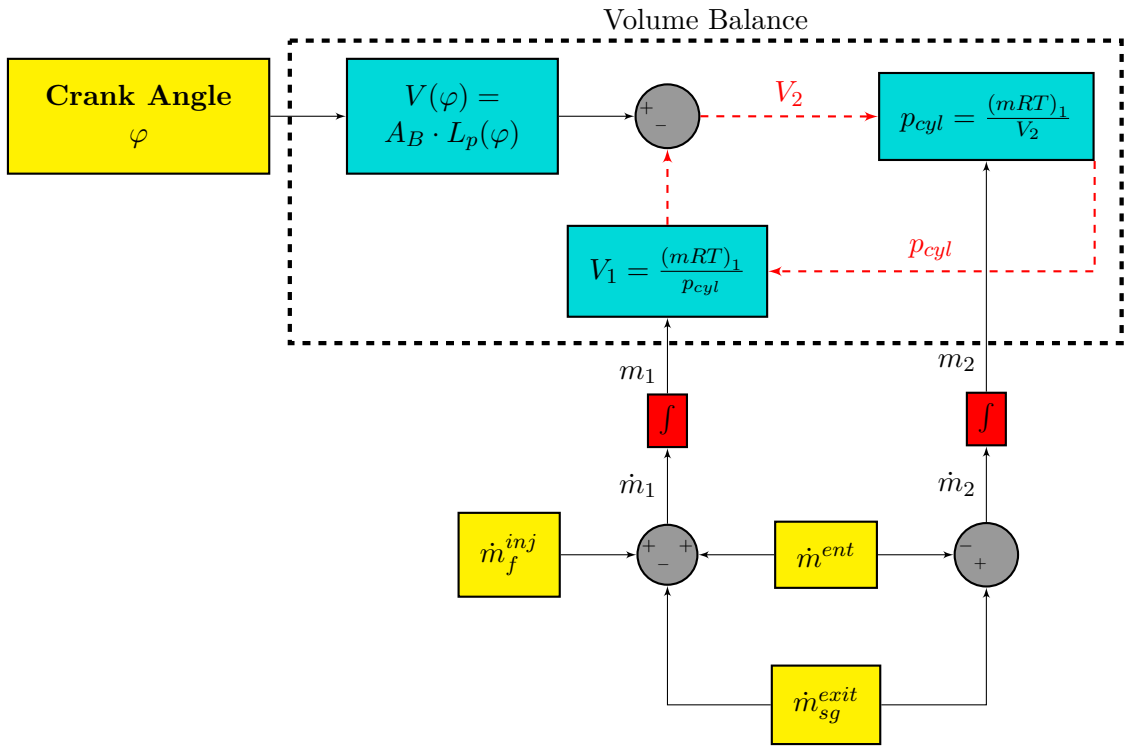

Figure 4-2: Volume Balance

then

$$p_{cyl} = \frac{\phi_V + 1}{\phi_V} \cdot \frac{(mRT)_1}{V_{gas}} \tag{4-24}$$

$$V_1 = \frac{\phi_V}{\phi_V + 1} \cdot V_{gas} \tag{4-25}$$

$$V_2 = \frac{1}{\phi_V + 1} \cdot V_{gas} \tag{4-26}$$

Once these values are computed the derivatives of the volumes are calculated numerically to obtain the work terms in the energy balances.

4-6 Initial Conditions

A final element to be considered is the initial conditions related to the Flame and Bulk zones. Both zones exist from the beginning of the simulation, then first it is needed to define the gas composition and temperature at IC. Additionally the initial mass of the two zones must be determined; this is done by introducing a third factor (S_{mass}) defined as the ratio between the initial mass of the flame zone and the trapped mass at inlet valve closed.

Then the initial conditions for the cylinder are:

$$T_{cyl,0} = T_{cyl}\,(@\text{IC}) \tag{4-27a}$$

$$m_{cyl,0} = m_{cyl}\,(@\text{IC}) \tag{4-27b}$$

$$x_{air\,cyl,0} = x_{a,cyl}\,(@\text{IC}) \tag{4-27c}$$

The mass factor S_{mass} is:

$$S_{mass} \stackrel{\text{def}}{=} \frac{m_{flame,0}}{m_{cyl,0}} \tag{4-28}$$

The initial conditions for the Flame zone are:

$$T_{flame,0} = T_{cyl,0} \tag{4-29a}$$

$$m_{flame,0} = S_{mass} \cdot m_{cyl,0} \tag{4-29b}$$

The initial conditions for the Bulk zone are:

$$T_{bulk,0} = T_{cyl,0} \tag{4-30a}$$

$$m_{bulk,0} = (1 - S_{mass}) \cdot m_{cyl,0} \tag{4-30b}$$

Finally, with the mass and heat flows modelled the gas phase can be implemented in Matlab/Simulink.

4-7 Analysis

To test the model a basic study case is used. For this study case the engine used and initial conditions are taken from the work of Ding Yu [52]. The engine geometry, initial conditions and the different constants are presented in table 4-1.

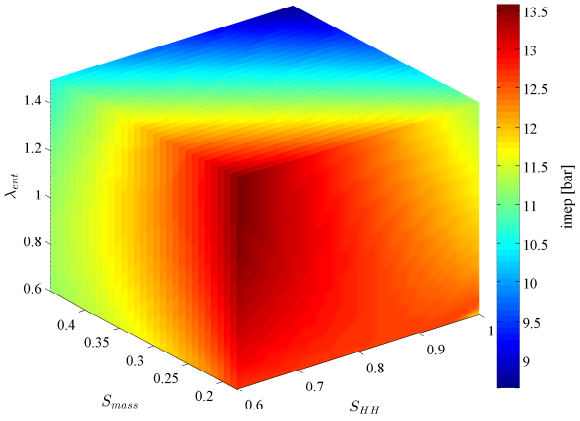

Figure 4-3: imep space

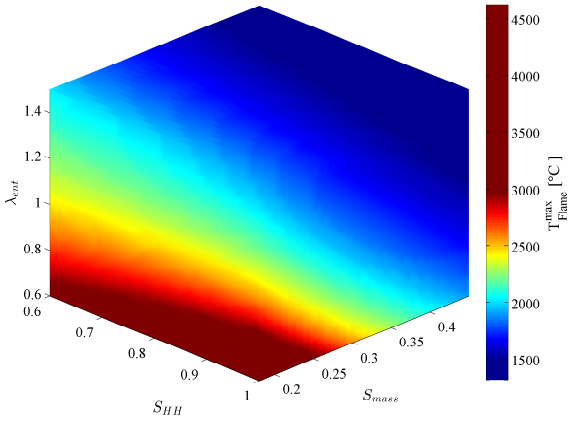

Figure 4-4: T^{max}_{flame} space

After the code was implemented in Matlab/Simulink and verified, some simulations were performed with different values for the three parameters S_{HH}, λ_{ent} and S_{mass}. The results obtained showed solutions where the state variables for the flame zone vary significantly.

In order to stablish the range of validity for the three parameters mentioned, the simulation must achieve the same indicated mean effective pressure (imep) as the single zone model used by Ding Yu, described in [4, 52]. After running the simulation with the single zone cylinder process code, the computed imep value was 11.21 bar.

Table 4-1: Parameters used for simulation Two-Zone

Engine geometry	
Nominal engine speed	1000 rpm
EO	300° after BDC
IC	20° after BDC
SOI	3° before TDC
L_s	0.270 m
D_b	0.200 m
L_{CR}	0.600 m
ϵ	13.4
Trapped condition	
T_{cyl} (@IC)	360 K
p_{cyl} (@IC)	2.12 bar
m_{cyl} (@IC)	0.0183 kg
x_{cyl} (@IC)	0.95
Cylinder wall temperatures	
$T_{cyl-wall}$	400 K
$T_{piston-crown}$	600 K
$T_{cyl-head}$	580 K
Heat loss parameters	
swirl factor (w_t/c_m)	5
C_{hl}	220
Fuel injection conditions	
T_f^{inj}	$40°C$
p_f^{inj}	800 bar
Air excess ratio (λ)	2
Vibe shape and weight factors	
m_1	0.3
m_2	10
$\eta_{comb,1}$	99.9%
$\eta_{comb,2}$	99.9%
b_1	0.98
$b_2 = 1 - b_1$	0.02

Once the constraint value for the imep was computed, the two zone model was run varying each of the parameters within a range of values presented in table 4-2 to map the solution space of the model.

Figures 4-3 and 4-4 present the values of imep and maximum temperature in the flame zone, with each of the three parameters in one axis.

It can be observed from fig. 4-3 that there is a significant variation of the indicated mean effective pressure. It can be noted that the S_{HH} factor can take values from 0 to 1 but for values around 0.6 the computed imep is already too high. Thus what could be called as the Heider limit $S_{HH} = 0$ is not suitable in this model.

The max flame zone temperature is presented in the same way as the imep (fig. 4-4). The

Table 4-2: Parameters range simulation Two-Zone

Parameter	
S_{HH}	0.6 - 1
S_{mass}	0.18 - 0.45
λ_{ent}	0.6 - 1.5

reason to present this value is to use it as a second restriction since the thermal NOx formation occurs in the regions with gas temperatures well above $2000K$ [12].

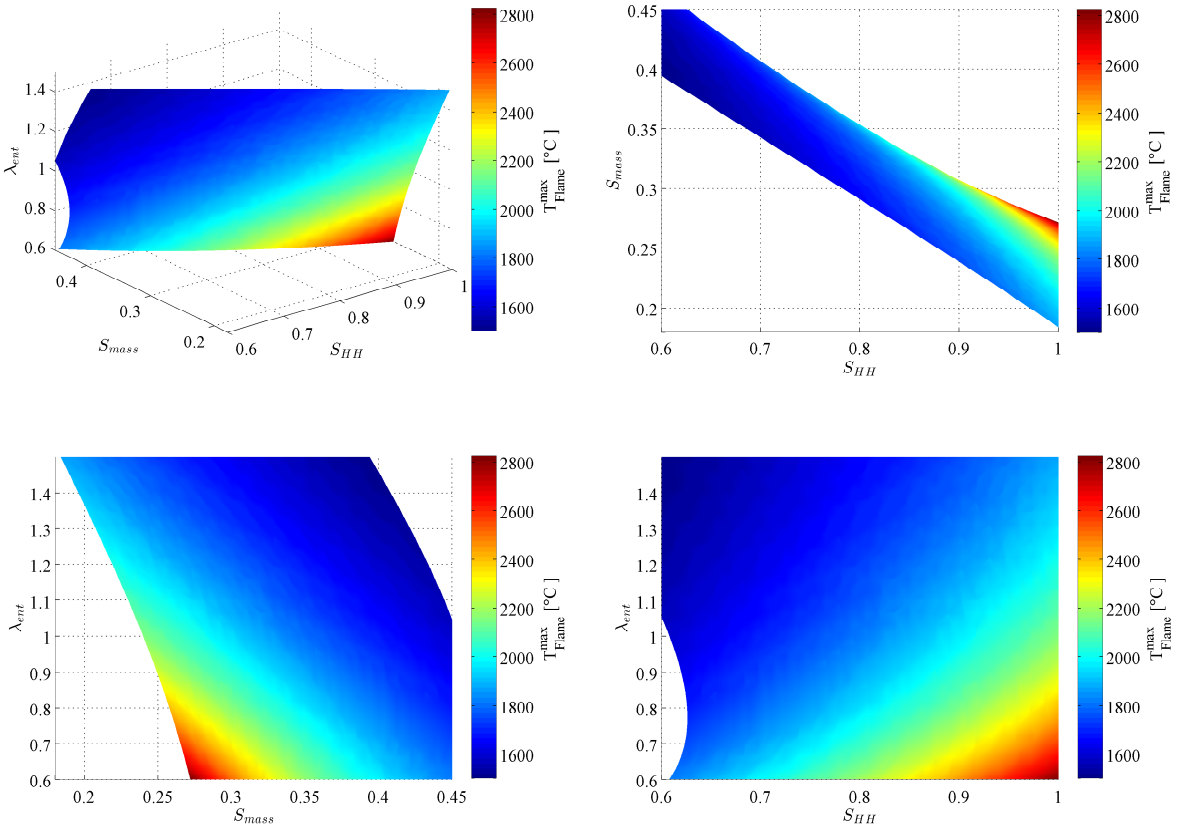

Figure 4-5: imep=11.21 iso-surface with T^{max}_{flame} on surface

Figure 4-5 shows an iso-surface where the imep value is 11.21 bar. The surface is coloured with the corresponding maximum flame temperature. From the figure it can be observed that in general for high entrainment rates, represented by λ_{ent}, the flame temperature is low. Additionally, it can be seen that for small initial flame masses together with high S_{HH} values, the max temperature tend to be higher mainly as a result of the small mass of the flame zone throughout the simulation.

Figures 4-6 to 4-26 present the state variables together with the composition of the two zones for some selection of the three parameters (S_{mass}, S_{HH}, λ_{ent}). The values were selected in order to study the influence of each of the parameters. In this selection at least one value for each factor variation achieve imep equal 11.21 bar. Table 4-3 summarises the values of the

three parameters selected along with computed imep, η_i, maximum pressure and maximum temperature.

Table 4-3: Summary study cases Two-Zone

λ_{ent} variation							
Case	S_{mass}	S_{HH}	λ_{ent}	imep [bar]	η_{ind}	p_{max} [bar]	T_{max} [K]
1	0.300	0.910	0.8	11.21	0.3743	90.809	2438.4
2	0.300	0.910	0.9	11.16	0.3730	90.829	2316.5
3	0.300	0.910	1.0	11.11	0.3710	90.840	2214.8
4	0.300	0.910	1.1	11.03	0.3684	90.844	2128.1
S_{HH} variation							
Case	S_{mass}	S_{HH}	λ_{ent}	imep [bar]	η_{ind}	p_{max} [bar]	T_{max} [K]
1	0.260	0.780	1.0	11.92	0.3982	91.863	2361.5
2	0.260	0.840	1.0	11.70	0.3908	91.503	2361.2
3	0.260	0.900	1.0	11.46	0.3830	91.132	2359.4
4	0.260	0.960	1.0	11.21	0.3747	90.750	2355.4
S_{mass} variation							
Case	S_{mass}	S_{HH}	λ_{ent}	imep [bar]	η_{ind}	p_{max} [bar]	T_{max} [K]
1	0.251	0.900	1.0	11.54	0.3857	91.194	2395.7
2	0.291	0.900	1.0	11.21	0.3746	90.946	2245.6
3	0.331	0.900	1.0	10.93	0.3650	90.743	2120.2
4	0.371	0.900	1.0	10.66	0.3563	90.562	2013.3

4-7-1 Entrainment factor

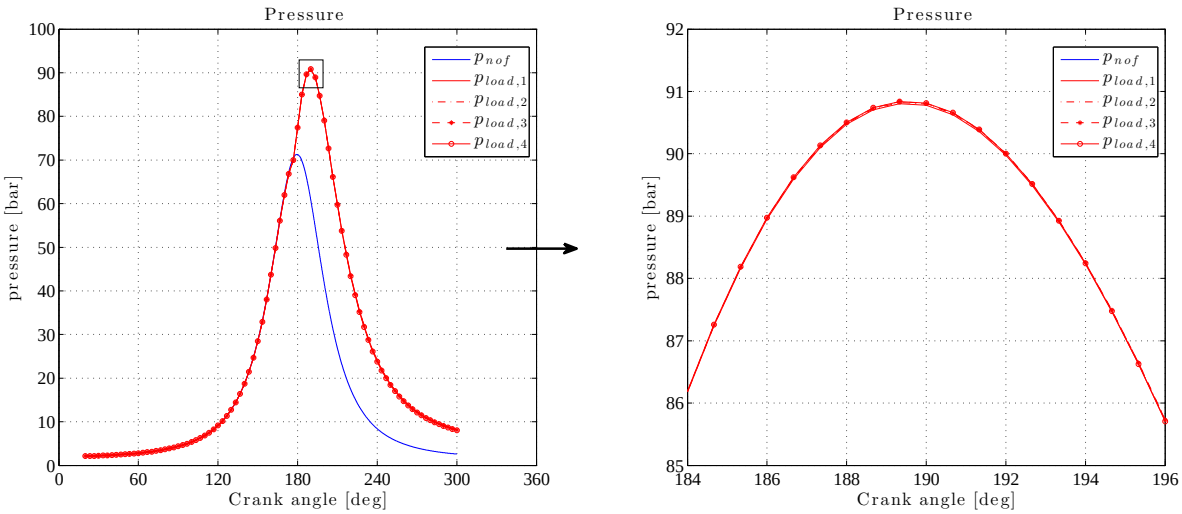

Figure 4-6: Cylinder Pressure

The entrainment factor affects particularly the temperature of the flame zone. As the entrainment factor is increased the temperature in the flame volume is reduced with maximum temperature decrease around 100 degrees with each increment of the entrainment factor (Figure 4-7). It can be seen from fig. 4-9 that the final mass of the flame zone increases as the

entrainment is enhanced. This is expected as the other mass flows are kept equal. The effect on the volumes of the zones is similar to the effect on the masses of the zones but less marked (Figure 4-8). The change in the entrainment factor has little impact on the pressure trace and the imep (Figure 4-6).

Figures 4-10–4-12 show the composition of the zones. The influence of the entrainment factor on the composition of the bulk zone is small given that the air excess ratio in the engine is 2 (Figure 4-11). The small changes in composition in the Bulk zone along with the smaller flame zone mass as the entrainment factor is reduced results in lower air fraction in the flame zone (Figure 4-12). Figure 4-10 serves as a verification of the code since as it can be seen the air fraction of the cylinder is equal for all the cases.

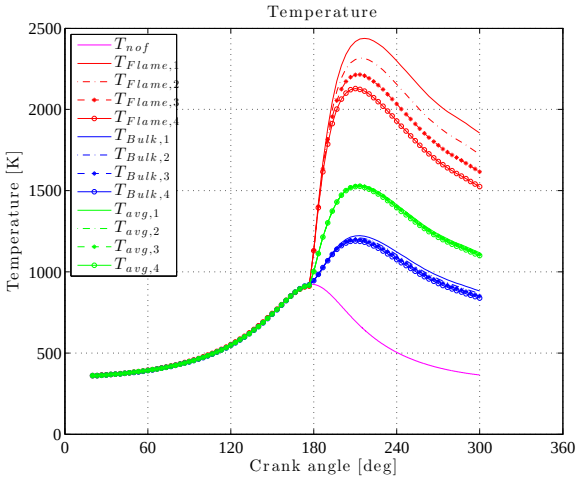

Figure 4-7: Zone Temperatures

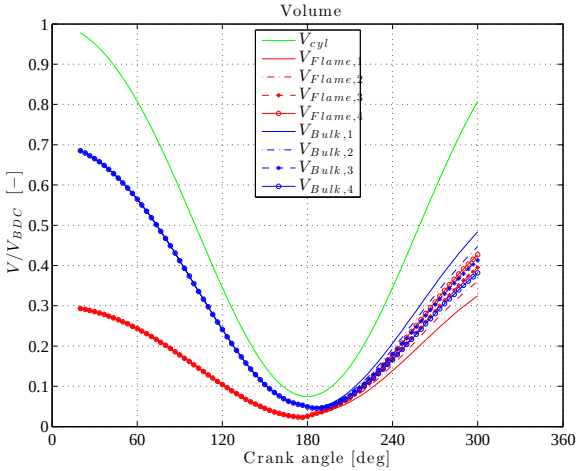

Figure 4-8: Zone Volumes

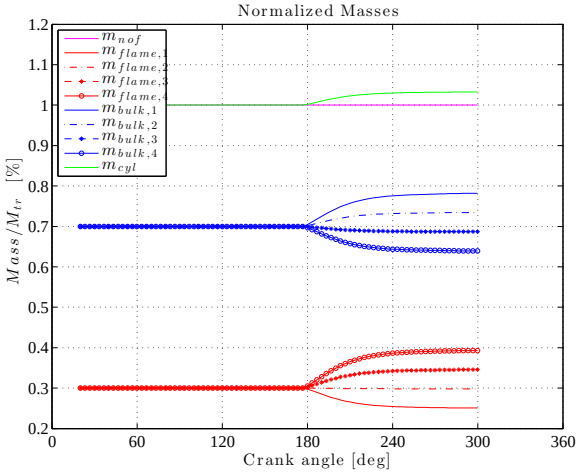

Figure 4-9: Zone masses

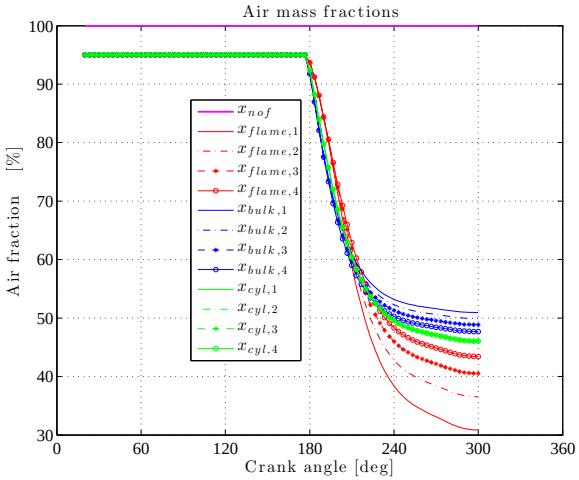

Figure 4-10: Zone air fractions

4-7-2 Heider Holhbaum factor S_{HH}

The effects of the Heider-Holhbaum factor are less apparent from figs. 4-13–4-19. In general with an increase of the factor the imep is reduced. Zooming in the pressure trace (Figure 4-13) it becomes more evident that with smaller values of S_{HH} the pressure is higher as combustion

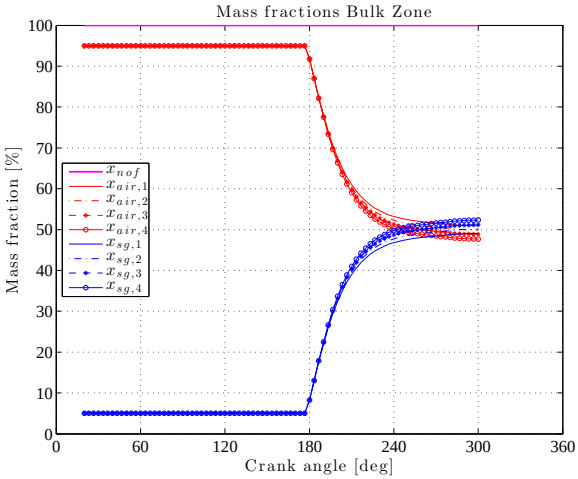

Figure 4-11: Mass fractions Bulk zone

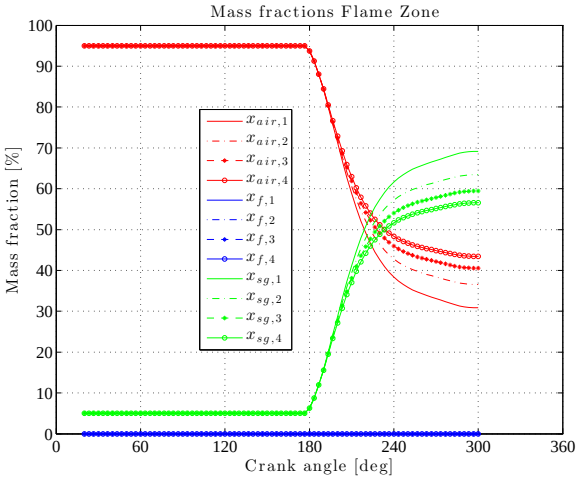

Figure 4-12: Mass fractions Flame zone

proceeds.The temperature of the flame zone changes little with the Heider-Hohlbaum factor but the cylinder average temperature is higher for smaller factor values which ultimately translates into higher indicated efficiencies. As it is expected the mass of the Flame zone is higher with smaller S_{HH} because less amount of the stoichiometric gas produced in the flame front is flowing to the Bulk Zone.

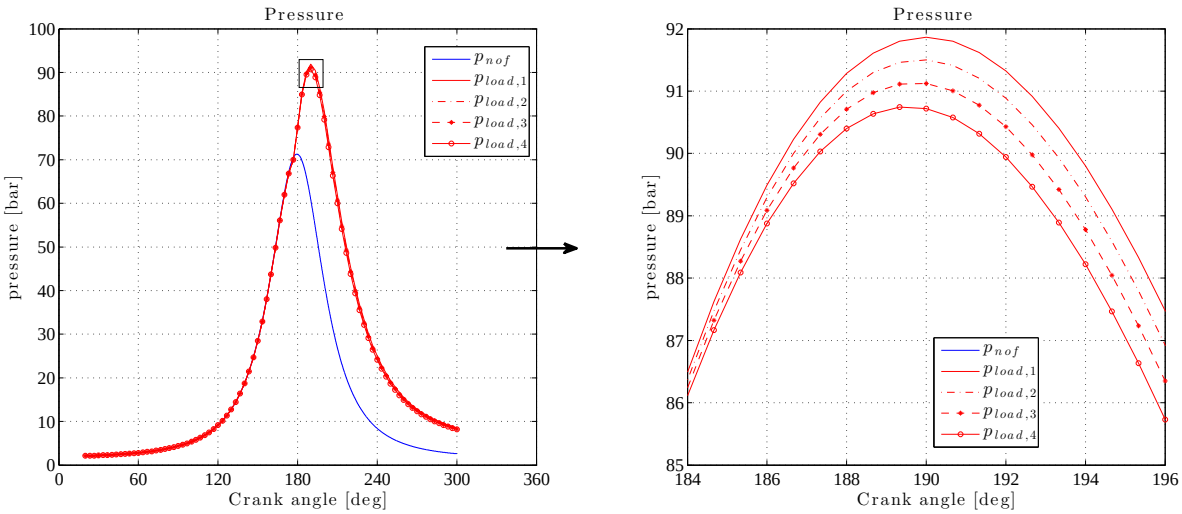

Figure 4-13: Cylinder Pressure

The air fraction in the flame zone is smaller and the air content in the bulk zone is higher as combustion proceeds for smaller values of the Heider_Holhbaum factor (Figures 4-16 and 4-17). This opposed effect on the air fraction in the two zones is expected because as the flow of produced stoichiometric gas going into the bulk zone is increased, the produced stoichiometric gas that stays the flame zone must reduce in the same amount. Figure 4-17 proves that independently of the values used for the three factors the air fraction of the cylinder is the same.

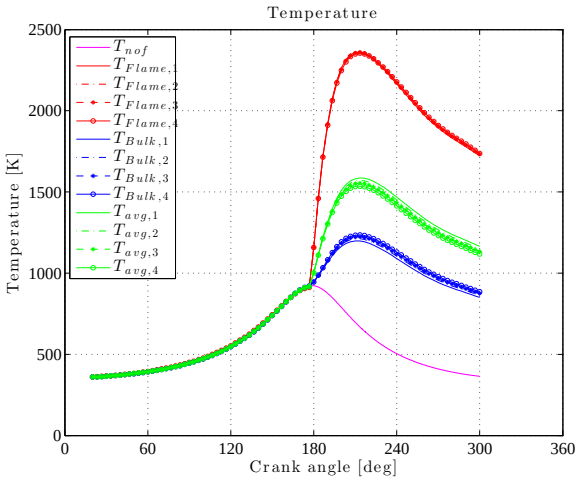

Figure 4-14: Zone Temperatures

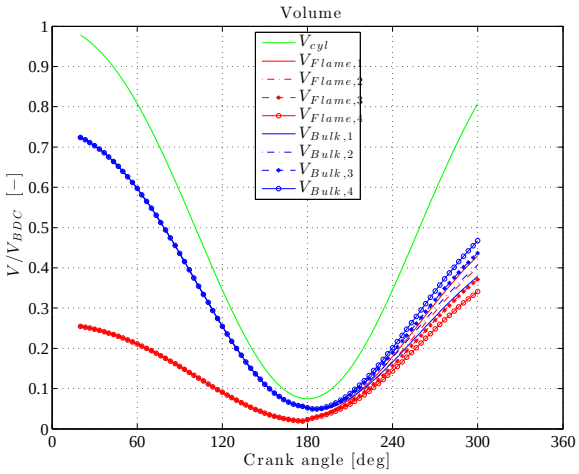

Figure 4-15: Zone Volumes

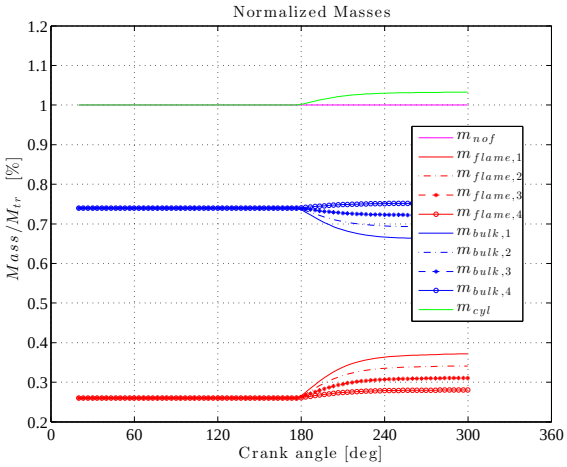

Figure 4-16: Zone masses

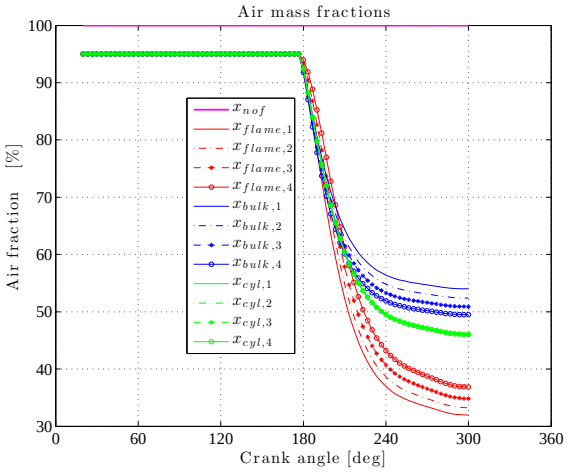

Figure 4-17: Zone air fractions

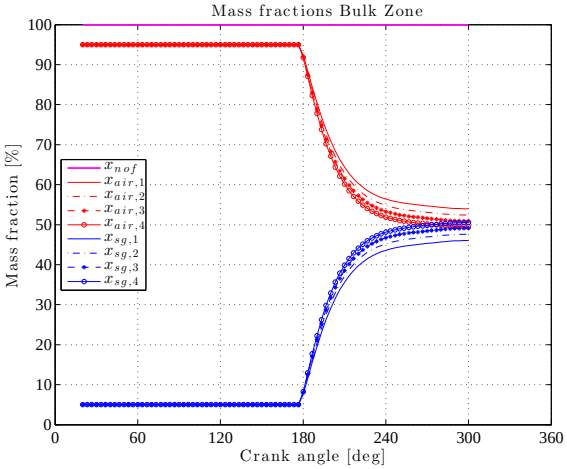

Figure 4-18: Mass fractions Bulk zone

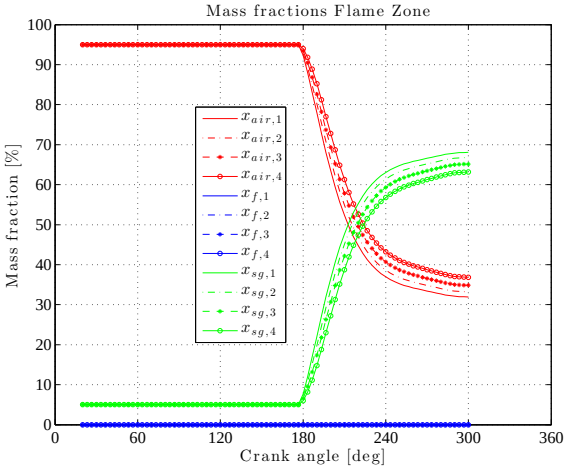

Figure 4-19: Mass fractions Flame zone

4-7-3 Mass factor S_{mass}

The mass factor indicates the normalized initial mass of the Flame zone, as it is expected if the masses flowing in and out of this zone are kept equal, the normalized mass is just shifted up as S_{mass} is increased (Figure 4-23). With smaller initial mass the heat capacity of the zone is reduced then the stronger is the initial rise of temperature and ultimately the maximum temperature is higher as well (Figure 4-21). The variation of pressure trace with S_{mass} is presented in fig. 4-20. The Volumes of the two zones can be seen in fig. 4-22, here the smaller the mass factor the smaller the flame zone and consequently the bulk zone volume is higher.

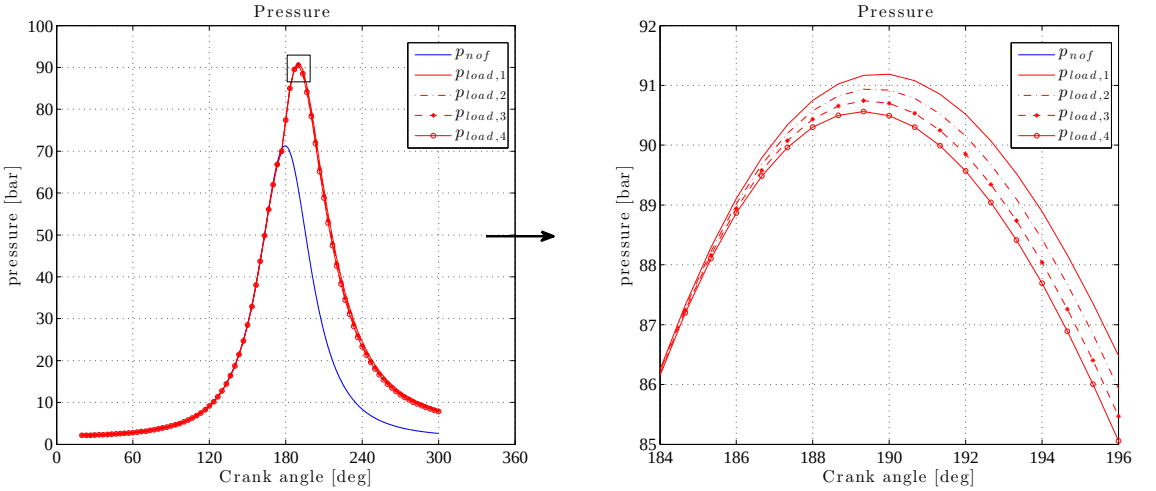

Figure 4-20: Cylinder Pressure

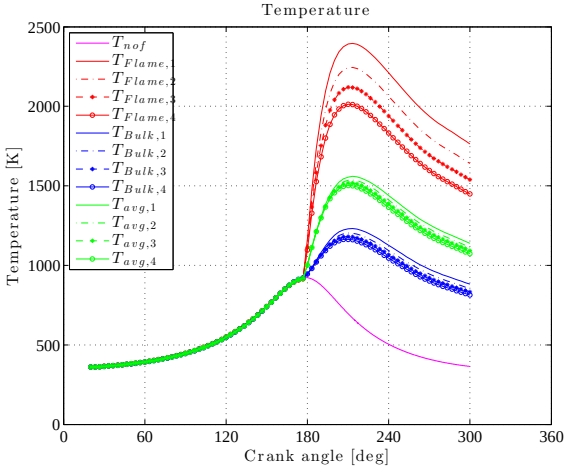

Figure 4-21: Zone Temperatures

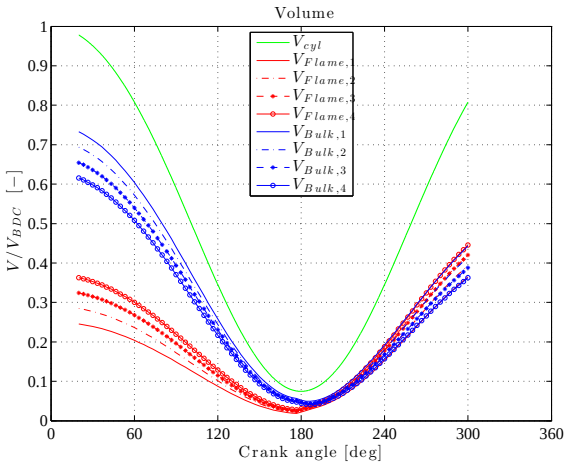

Figure 4-22: Zone Volumes

Since the initial mass of the Flame zone is reduced as the mass factor is decreased, and the amount of stoichiometric gas produced is the same then the stoichiometric gas mass fraction is higher for smaller S_{mass} factors (Figure 4-26). The effect on the mass fractions of the bulk Zone is the opposite to the Flame Zone which is expected because as the mass factor is decreased the initial mass of the bulk zone is increased (Figure 4-25). Figure 4-24 serves again to show that invariantly of the selection of the three factors the air fraction of the cylinder is

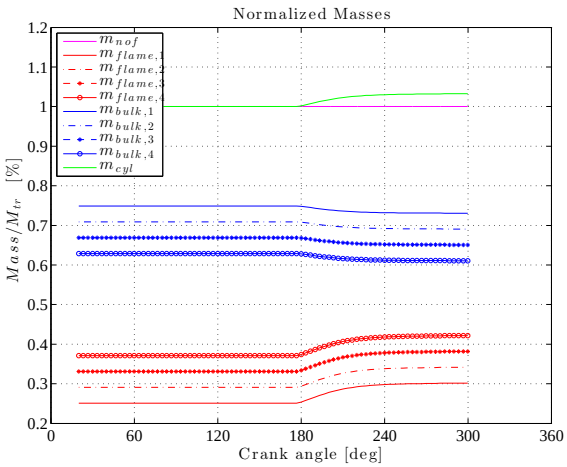

Figure 4-23: Zone masses

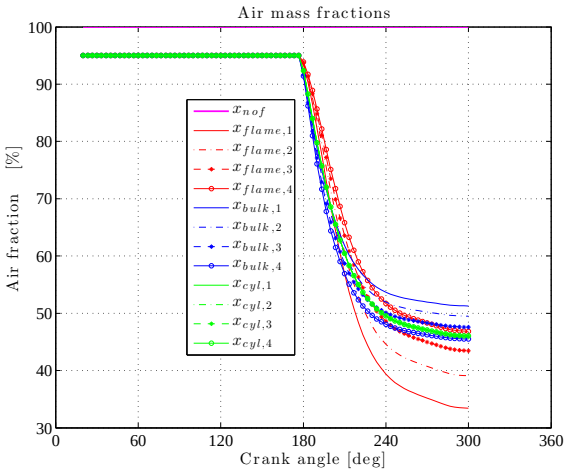

Figure 4-24: Zone air fractions

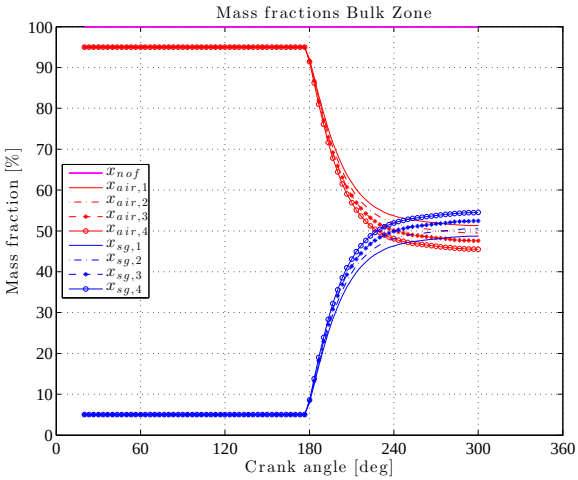

Figure 4-25: Mass fractions Bulk zone

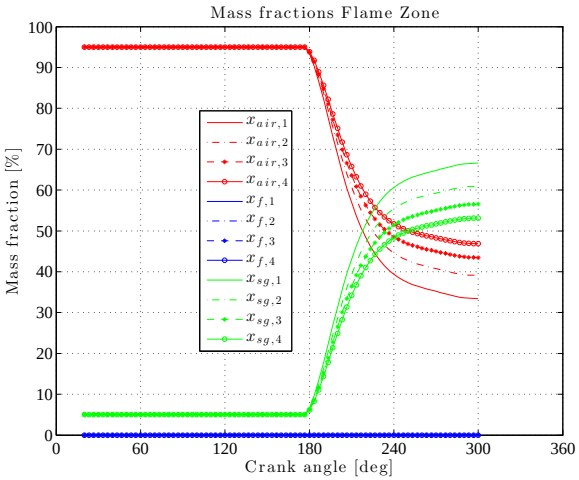

Figure 4-26: Mass fractions Flame zone

the same.

4-8 Discussion

The model proves to be fit to simulate the in-cylinder process with the assumptions added. However, it is important to note that it is required to use the single zone model in order to calibrate the three factors (λ_{ent}, S_{HH} and S_{mass}) which is a drawback of the model. Furthermore, the calibration of the model only with imep is not sufficient because under this restriction a wide range of flame zone temperatures are obtained. For these reasons it is considered that the calibration of the model must be done adding a second restriction as the NOx emissions.

The analysis of the entrainment factor shows that higher entrainment rate is desirable because it does not affect significantly the pressure trace but reduces the flame zone temperature which is an important factor in the NOx formation. The exchange of combustion products represented by the Heider-Holhbaum factor plays an important role; this can be particularly noted in the Heider limit ($S_{HH} \approx 0$) where solutions are far from the single zone model imep.

The mass factor plays an important role in the flame zone temperature thus it affects the thermal NOx formation. Additionally, the S_{mass} factor could be regarded as a consequence of the ignition delay, in this period of time an amount of fuel is evaporated and mixed with air and this mixture will sustain the premixed phase of combustion.

Chapter 5

3-Zone Model

In this chapter the complete model will be analysed after separate simulation and analysis of the two phases in the previous two chapters. Here the model will be assembled in Matlab/Simulink and tested. The simulations made in this chapter will cover one simulation with common rail system and one for the plunger system. The two injection systems are used but it must be noted that the model engine used for this engine has a plunger system, thus it is more fit to use a plunger injection system in order to simulate the process. The results presented will be limited to the main variables of the simulation, in a similar fashion to chapters 3 and 4.

In addition, in this chapter the ignition delay concept is implemented since the assumptions regarding the shape and timing of the injection rate, evaporation rate and reaction rate (ξ) do not hold. Moreover, the ignition delay helps to address difficulties that arise from the simulation of the combustion rate by means of the Vibe function, which is a blindfold actor regarding the availability of fuel and air in the flame zone.

Finally the formation of NO by means of the basic Zeldovich mechanism will be presented and coupled with the three zone model to compute NO emissions.

5-1 Ignition Delay

Ignition delay in direct injection diesel engines has great importance because of its direct impact on the intensity of heat release immediately following autoignition.

There are multiple definitions of the ignition delay. Hiroyasu [19] presents the two most used definitions. The first is the pressure rise delay defined as the point at which pressure rise caused by combustion is detected on a cylinder pressure time record. The second definition is the illumination delay. Here the delay is marked by emission of visible radiation due to chemiluminescence or thermal radiation.

In addition, the pre-ignition process may be divided into physical and chemical processes. In the physical delay period the fuel is atomized, vaporized, mixed with air and raised in

temperature. In the chemical delay, reaction starts slowly and then accelerates until ignition takes place.

Assanis [55] and Hiroyasu [19] present in their work a summary of different ignition delay correlations. These correlations are the result of studies under different conditions and different measuring methods. Generally the type of expression used for the ignition delay is of the following form:

$$\tau_{id} = A \cdot p^{-n} \cdot \phi^{-k} \cdot \exp\left(\frac{E}{R_u \cdot T}\right) \tag{5-1}$$

where p, ϕ and T are pressure, equivalence ratio and temperature respectively, E is activation energy, R_u is the universal gas constant, and A, n and k are adjustable constants.

As a condition for ignition the following expression is used [22]:

$$\int_0^t \frac{1}{\tau_{id}} \cdot dt \geq 1 \tag{5-2}$$

The use of this equation accounts for the effects that a variable volume combustion chamber will have on state properties over the ignition delay interval [55].

In this work the expression used by Hiroyasu [3] is adopted to estimate the ignition delay. The values of the constants in his equation are:

Table 5-1: Constants ignition delay Hiroyasu

Constant	Value
A	$4 \cdot 10^{-3}$
n	2.5
k	1.04
E/R_u	4000

5-2 NO formation

This section describes the mechanism by which the thermal NO is formed. The description follows the presentation of Stapersma in [56] that provides the fundamentals of his Matlab/Simulink model. This Simulink model is integrated to the three zone model in this project and applied to the gas phase of the model to compute NO emissions in the cylinder.

The formation of NO from nitrogen and oxygen is described by the so-called Zeldovich mechanism. The Basic mechanism contains the following two equilibrium reactions:

$$\mathrm{O} + \mathrm{N_2} \rightleftharpoons \mathrm{NO} + \mathrm{N} \tag{5-3a}$$

$$\mathrm{N} + \mathrm{O_2} \rightleftharpoons \mathrm{NO} + \mathrm{O} \tag{5-3b}$$

A third reaction involving OH was added, together they lead to the so-called extended Zeldovich mechanism.

$$\mathrm{N} + \mathrm{OH} \rightleftharpoons \mathrm{NO} + \mathrm{H} \tag{5-4}$$

5-2-1 Equilibrium

Sum the two reactions to get the overall reaction:

$$\begin{aligned} &\mathrm{O} + \mathrm{N_2} \rightleftharpoons \mathrm{NO} + \mathrm{N} \\ &\underline{\mathrm{N} + \mathrm{O_2} \rightleftharpoons \mathrm{NO} + \mathrm{O}} \quad + \\ &\mathrm{N_2} + \mathrm{O_2} \rightleftharpoons 2 \cdot \mathrm{NO} \end{aligned} \tag{5-5}$$

Equilibrium of the two reactions between forward and reverse reaction:

$$k_1^+ \cdot [\mathrm{O}]_\mathrm{e} \cdot [\mathrm{N_2}]_\mathrm{e} - k_1^- \cdot [\mathrm{NO}]_\mathrm{e} \cdot [\mathrm{N}]_\mathrm{e} = 0 \Rightarrow \quad \frac{k_1^+}{k_1^-} = \frac{[\mathrm{O}]_\mathrm{e} \cdot [\mathrm{N_2}]_\mathrm{e}}{[\mathrm{NO}]_\mathrm{e} \cdot [\mathrm{N}]_\mathrm{e}} \tag{5-6a}$$

$$k_2^+ \cdot [\mathrm{N}]_\mathrm{e} \cdot [\mathrm{O_2}]_\mathrm{e} - k_2^- \cdot [\mathrm{NO}]_\mathrm{e} \cdot [\mathrm{O}]_\mathrm{e} = 0 \Rightarrow \quad \frac{k_2^+}{k_2^-} = \frac{[\mathrm{NO}]_\mathrm{e} \cdot [\mathrm{O}]_\mathrm{e}}{[\mathrm{N}]_\mathrm{e} \cdot [\mathrm{O_2}]_\mathrm{e}} \tag{5-6b}$$

Then the equilibrium constant of the overall reaction:

$$\mathrm{K_{NO}} = \frac{k_1^+}{k_1^-} \cdot \frac{k_2^+}{k_2^-} = \frac{[\mathrm{NO}]_\mathrm{e}^2}{[\mathrm{N_2}]_\mathrm{e} \cdot [\mathrm{O_2}]_\mathrm{e}} \tag{5-7}$$

Finally the equilibrium constant can be computed from the reaction constants in table 5-2.

5-2-2 Reaction kinetics

The rate of formation of NO via the reactions of the basic Zeldovich mechanism is is given by:

$$\frac{d[\mathrm{NO}]}{dt} = k_1^+ \cdot [\mathrm{O}] \cdot [\mathrm{N_2}] - k_1^- \cdot [\mathrm{NO}] \cdot [\mathrm{N}] + k_2^+ \cdot [\mathrm{N}] \cdot [\mathrm{O_2}] - k_2^- \cdot [\mathrm{NO}] \cdot [\mathrm{H}] \tag{5-8}$$

Similarly the rate of formation of N is given by:

$$\frac{d[\mathrm{N}]}{dt} = k_1^+ \cdot [\mathrm{O}] \cdot [\mathrm{N_2}] - k_1^- \cdot [\mathrm{NO}] \cdot [\mathrm{N}] - k_2^+ \cdot [\mathrm{N}] \cdot [\mathrm{O_2}] + k_2^- \cdot [\mathrm{NO}] \cdot [\mathrm{H}] \tag{5-9}$$

where the reaction constants are in general:

$$k = A \cdot T^m \cdot \exp\left(\frac{-E}{R_u \cdot T}\right) \tag{5-10}$$

Assuming N equilibrium:

$$\frac{d[\mathrm{N}]}{dt} = k_1^+ \cdot [\mathrm{O}] \cdot [\mathrm{N_2}] - k_1^- \cdot [\mathrm{NO}] \cdot [\mathrm{N}] - k_2^+ \cdot [\mathrm{N}] \cdot [\mathrm{O_2}] + k_2^- \cdot [\mathrm{NO}] \cdot [\mathrm{H}] = 0 \tag{5-11}$$

Summation of eq. (5-8) and eq. (5-11) produces

$$\frac{d[\mathrm{NO}]}{dt} = 2 \cdot \left(k_1^+ \cdot [\mathrm{O}] \cdot [\mathrm{N_2}] - k_1^- \cdot [\mathrm{NO}] \cdot [\mathrm{N}]\right) \tag{5-12}$$

The unknown concentration of nitrogen radical is computed from eq. (5-11) solving for [N].

Table 5-2: Reaction Constants [5]

	A $[cm^3/mol/s]$	m	E/R_u
k_1^+	7.6×10^{13}	0	38,000
k_1^-	6.0×10^{13}	0	0
k_2^+	6.4×10^9	1	3,150
k_2^-	1.5×10^9	1	19,500

5-2-3 Solution of reaction kinetics

In order to compute the NO formation the concentrations of N_2, O_2 and O are needed.

Following Heywood [5] the equilibrium concentrations are used. The nitrogen and oxygen concentration follow from the gas composition.

$$[\mathrm{N_2}] = [\mathrm{N_2}]_\mathrm{e} \tag{5-13a}$$

$$[\mathrm{O_2}] = [\mathrm{O_2}]_\mathrm{e} \tag{5-13b}$$

$$[\mathrm{O}] = [\mathrm{O}]_\mathrm{e} \tag{5-13c}$$

Additionally, the equilibrium of the oxygen radical follows from the reaction

$$\frac{1}{2}\mathrm{O_2} = \mathrm{O} \tag{5-14}$$

With the equilibrium constant definition, applied to the O reaction it follows:

$$\mathrm{K_O} = \frac{y_{O,e}}{y_{O_2,e}^{1/2}} \cdot \left(\frac{p}{p_{ref}}\right)^{1-1/2} \tag{5-15}$$

where y denotes mole fraction.

This equation combined with the ideal gas law and the definition of mole fraction, can be re-written in terms of concentrations as follows:

$$\mathrm{K_O} = \frac{c_{O,e}}{c_{O_2,e}^{1/2}} \cdot \left(\frac{R_u \cdot T}{p_{ref}}\right)^{1/2} \tag{5-16}$$

Solving for O concentration and using an alternative notation and unit (mol per cm^3 instead of mol per $m3$), then the O radical is:

$$[\mathrm{O}]_\mathrm{e} = \frac{\mathrm{K_O}}{1000} \cdot \left(\frac{p_{ref}}{R_u \cdot T}\right)^{1/2} \cdot [\mathrm{O_2}]_\mathrm{e}{}^{1/2} \tag{5-17}$$

where $c_j = [\mathrm{j}] \cdot 10^6$.

In general K is temperature dependent. Assume:

$$\mathrm{K_O} = \mathrm{K_{ref}} \cdot \exp\left(-\frac{E}{R_u \cdot T}\right) \tag{5-18}$$

So finally:

$$[\mathrm{O}]_\mathrm{e} = \frac{\mathrm{K_{ref}}}{1000} \cdot \left(\frac{p_{ref}}{R_u \cdot T}\right)^{1/2} \cdot \exp\left(-\frac{E_O}{R_u \cdot T}\right) \cdot [\mathrm{O_2}]_\mathrm{e}{}^{1/2} \tag{5-19}$$

From Heywood [5]

$$\mathrm{K_{ref}} \cdot \left(\frac{p_{ref}}{10^5}\right)^{1/2} = 3.6 \times 10^3 \tag{5-20}$$

and

$$\frac{E_O}{R_u} = 31090 \tag{5-21}$$

Stapersma [56] mentions the difficulties that arise if freezing is considered from concentrations

$$\frac{d[\mathrm{NO}]}{dt} = 0 \tag{5-22}$$

since it would mean that for a varying volume the number of moles would change which does not seem logical.

In turn he proposes to consider freezing from the mole rate of change,

$$\frac{d\mathrm{n_{NO}}}{dt} = 0 \tag{5-23}$$

so the number of moles will remain constant. If the volume would change the concentration of course would change as well.

Then the formation rates are computed under the assumption that the rate of change of NO can be expressed as follows

$$\frac{d[\mathrm{NO}]}{dt} = \frac{1}{V} \cdot \frac{d[\mathrm{NO}] \cdot V}{dt} \tag{5-24}$$

and this expression holds for varying volume.

5-3 Analysis

As stated earlier in this chapter the complete model is implemented and simulations were performed with a base engine model as in chapter 4 and its characteristics can be found in table 4-1. In this chapter the assumptions that injection rate, evaporation rate and combustion rate are equal and the dwelling time between these rates is zero, are discarded in view of the fact that injection rate and evaporation rate are computed in the liquid block.

It is also important to mention that in the 3-zone analysis in the volume balance (Section 4-5) the gas volume is not instantaneous the cylinder volume computed from the geometry of the engine but this geometric value minus the instantaneous volume of the liquid zone.

$$V_{gas} = V_{cyl} - V_{liq} \tag{5-25}$$

Table 5-3 presents a summary of the study cases done in this chapter, it includes the values selected for the three parameters (S_{HH}, S_{mass} and λ_{ent}), along with the type of injection system and timing. It is also included the computed maximum values for temperature and pressure, imep and η_{ind} similarly to table 4-3. The presented start of injection angle (SOI) is selected to have start of combustion between 175 and 180 degrees after bottom dead center.

Table 5-3: Summary study cases Three-Zone

Injection	SOI [deg]	S_{mass}	S_{HH}	λ_{ent}	imep [bar]	η_{ind}	p_{max} [bar]	T_{max} [K]	SOC [deg]
CR	172.4	0.045	0.490	1.020	11.21	0.3743	92.187	2434.3	177
PL	160	0.045	0.775	1.170	11.21	0.3742	91.366	2449.4	177

CR: common rail; PL: plunger

In this analysis red coloured lines are used to present the results for the common rail system case and blue lines for the plunger case.

Inputs

The injection rate together with the injection pressure are presented in figs. 5-1 and 5-2. The injection rate was adjusted to reach reasonable values of the injection pressure and initial response to have start of combustion around 177 degrees after bottom dead center.

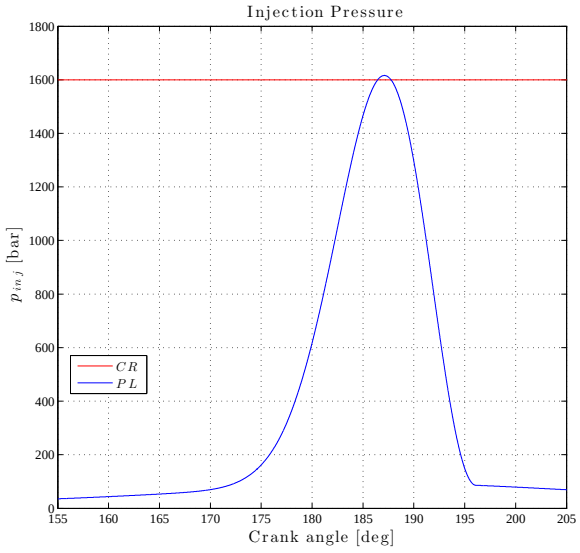

Figure 5-1: Injection pressure

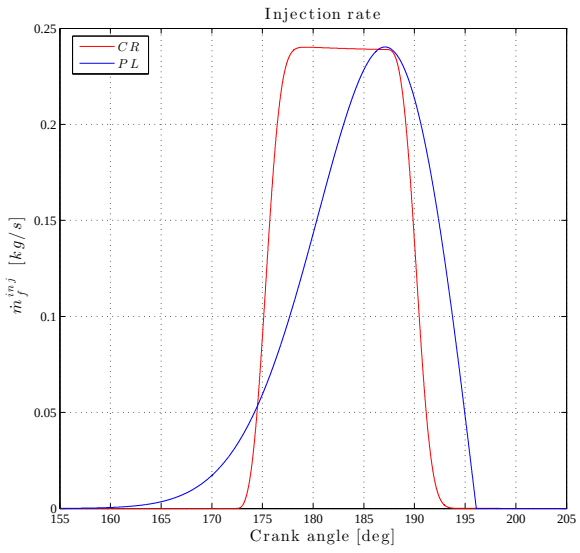

Figure 5-2: Injection rate

As it can be seen the high constant pressure of the common rail system allows to start injection later than the plunger system. Additionally, the injection time for the common rail system

is shorter than the injection time for the plunger which is another advantage of the common rail system.

Mass flows

Figure 5-3 presents the mass flows related to the fuel. It can be observed that the injection rate is followed closely by the evaporation rate. At start of combustion the evaporation rate is enhanced as the temperature of the flame zone increases. As in chapter three, the evaporation rate exhibits a delay with respect to the injection rate, which is larger for the plunger system than the common rail system given the low initial velocity for the plunger. The combustion rate is almost equal for both cases which obvious because the combustion rate is computed from Vibe function using the same parameters except for the combustion time that is slightly different.

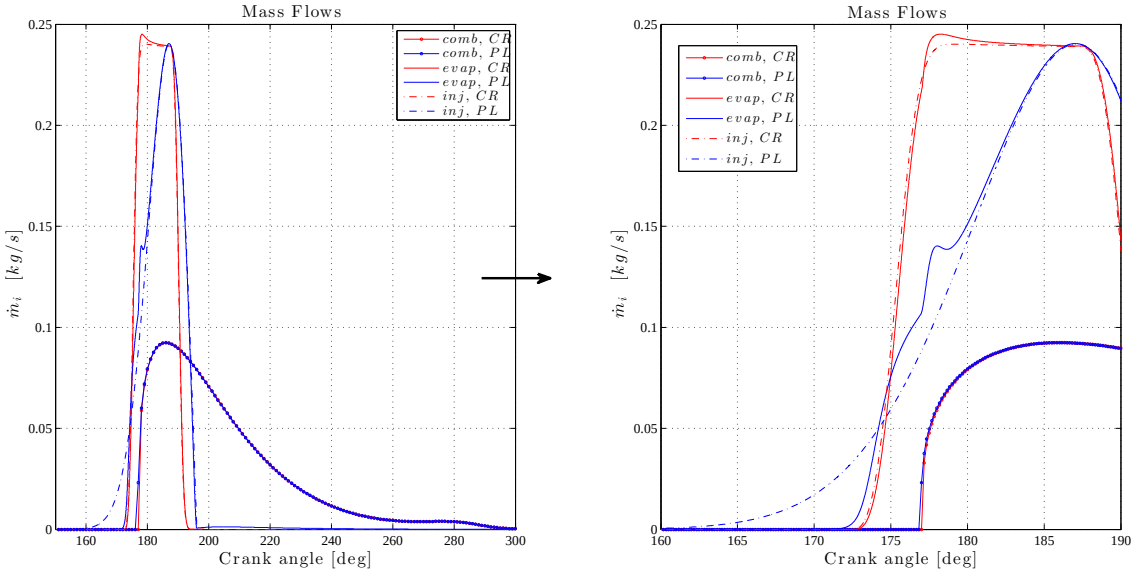

Figure 5-3: Fuel mass flows

The normalized progress of the variables representing the fuel in the cylinder for both cases can be seen in fig. 5-4. Again the evaporation follows closely the injection process. In the plunger system, the last part of evaporation is affected as the input of fuel is reduced which results in less energy input and less effective atomization.

Heat Flows flows

The heat flows are presented in figs. 5-5–5-7. Similar to the evaporation rate, the heat flow from gas to the liquid fuel follows the shape of the injection rate (Figure 5-5) but the duration is slightly longer than injection rate because by the end of injection not all fuel has been evaporated. Figure 5-6 shows the heat loss to the walls by each zone computed with Woschni's model. In the first part of the process the heat loss is lower for the Flame zone given the smaller volume of the zone that ultimately relates to the heat transfer area. For the second part of the process heat losses in the flame increases rapidly overtaking the heat loss in the bulk zone, this as a result of the steep increase in temperature of the flame zone. The difference in heat losses can be explained by looking at the state variables of each

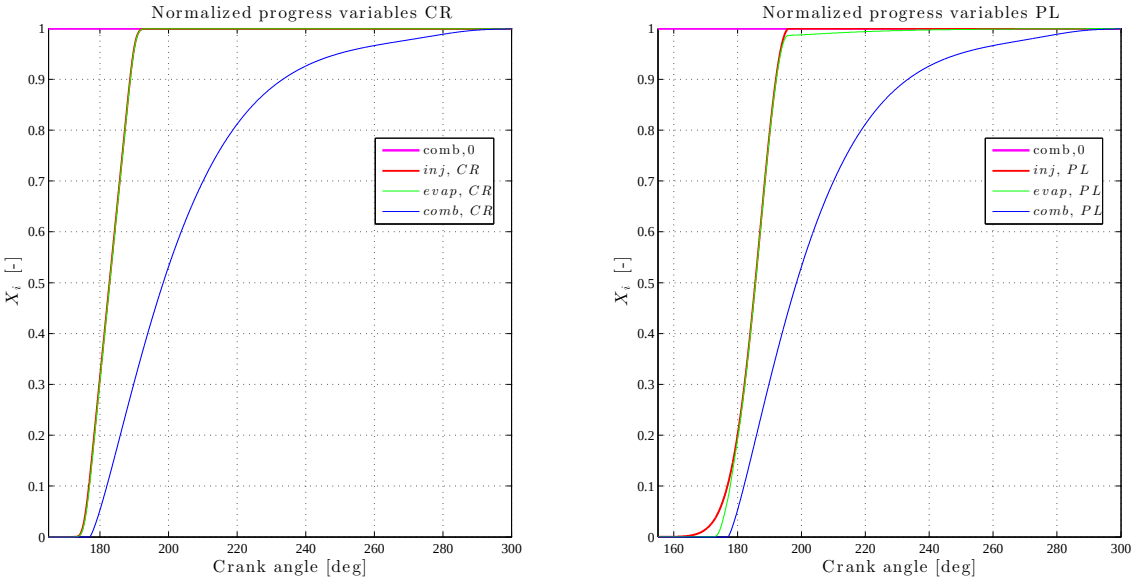

Figure 5-4: Normalized progress

zone. Although the temperatures of the zones for the plunger system are higher than the temperatures for the common rail system, the volume of the flame zone for the common rail case is larger than the plunger case thus larger heat transfer area.

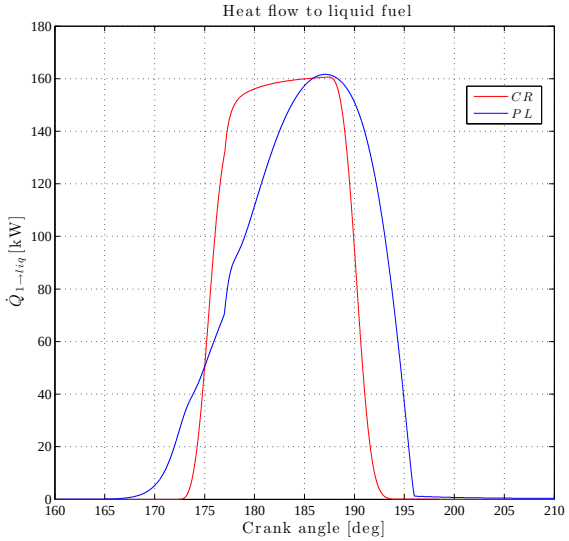

Figure 5-5: Heat flow to liquid

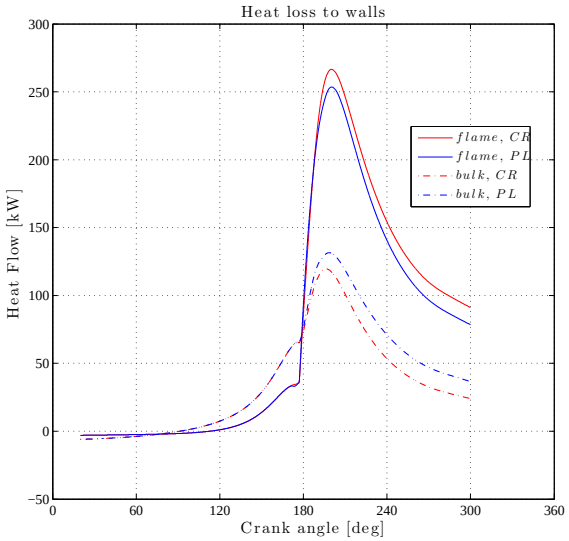

Figure 5-6: Heat loss flow

The Combustion heat flow can be observed in fig. 5-7 alongside the net heat flow. The net heat flow computed as the difference of the combustion heat flow minus the heat loss flow to the walls and heat flow to the liquid fuel. The combustion heat flow is almost identical for both cases since the combustion rate is almost identical and the small differences can be attributed to variable heat of combustion. The detail of the figure shows the effect of heating and evaporating the liquid fuel before combustion starts.

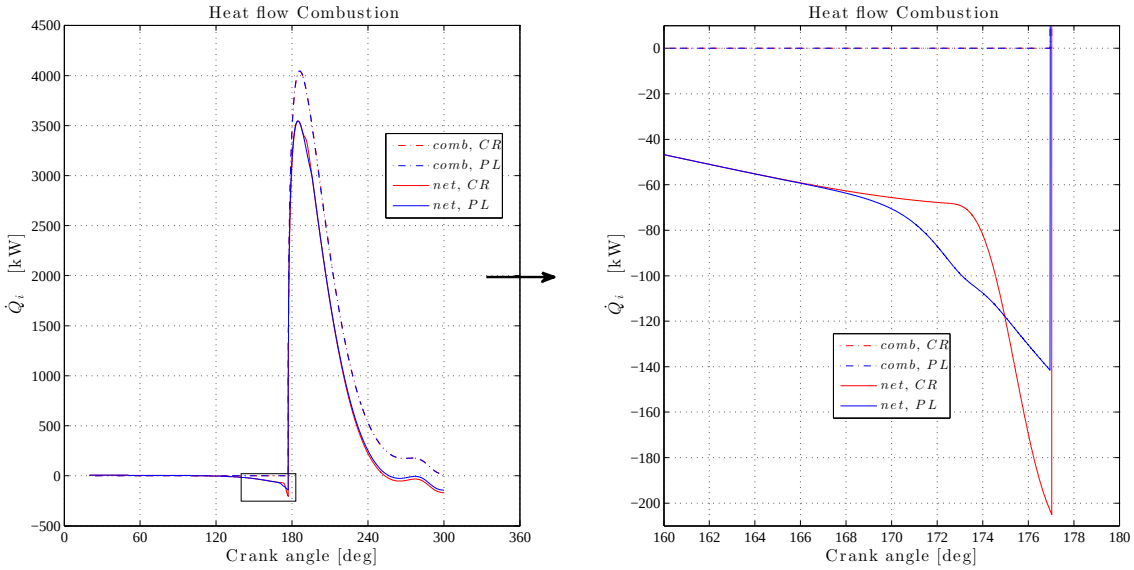

Figure 5-7: Heat flow combustion

Gas State variables

The gas state of the zones is shown in figs. 5-8–5-11. The in-cylinder pressures for the two study cases are presented in fig. 5-8 and it can be seen that the pressure for the common rail case is higher than for the plunger case but the difference is small. This small difference was expected since the computed imep is the same for the two cases.

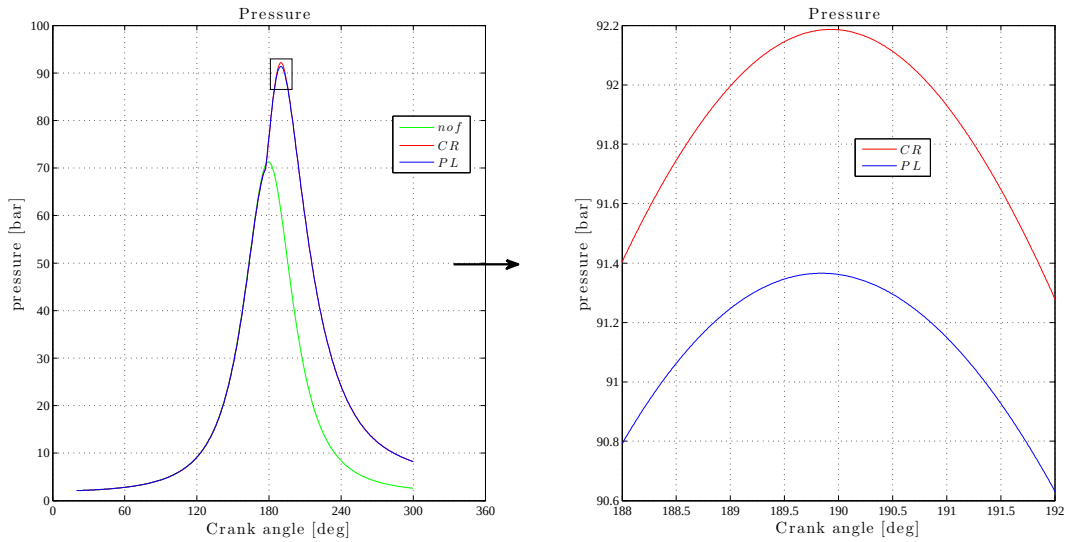

Figure 5-8: Cylinder Pressure

The temperatures of the different zones can be seen in fig. 5-9. Although the max temperature for the two cases is very close, the temperature throughout the process of the flame zone for the plunger system is higher that for the common rail system which is important when computing NO emissions. In both cases the flame zone temperature goes down once injection starts until

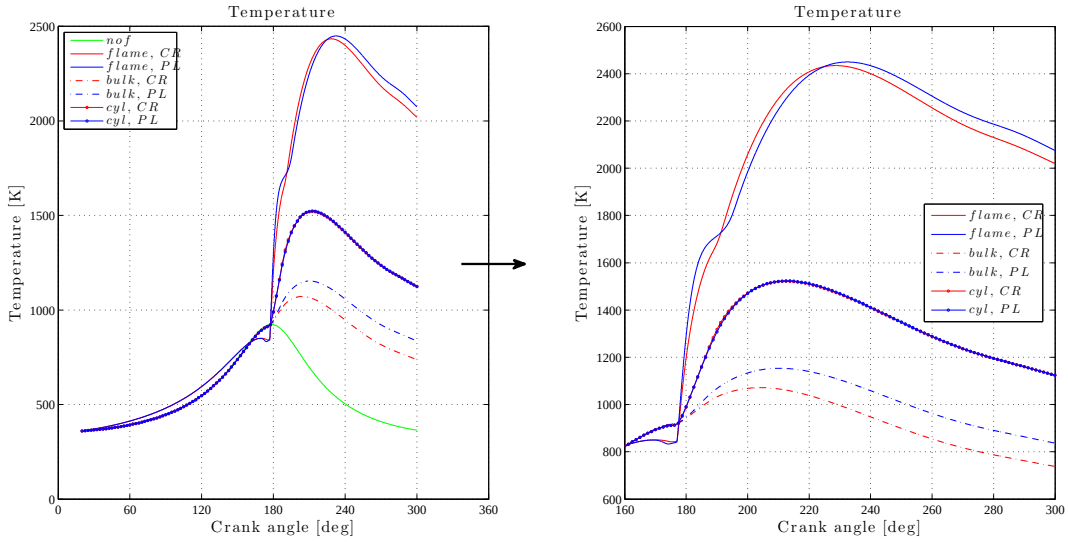

Figure 5-9: Zone Temperatures

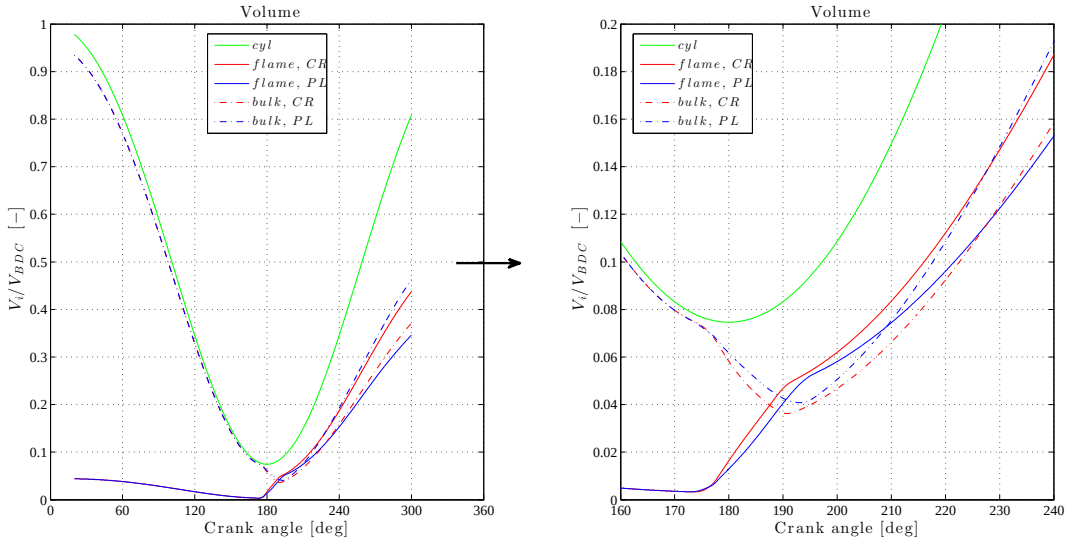

Figure 5-10: Zone Volumes

combustion starts after this point the temperature rises steeply.

In figs. 5-8 and 5-9, the in-cylinder pressure and temperature for no fuel injection are presented because these two values are used to calculate the heat transfer coefficient to the walls.

The volume versus crank angle is given in fig. 5-10, the volume of the flame zone surpasses the bulk volume after combustion starts as a consequence of the increase in mass and temperature of the flame zone.

The mass in the cylinder (Figure 5-11) increases from the start of injection, and the masses of the gas phase start to change once evaporation and entrainment starts. The change in masses for the common rail case are steeper initially than for the plunger case, this as a result of the steeper evaporation rate and associated entrainment rate for the common rail case. The mass of the flame zone is larger for the rest of the process for the common rail case than for

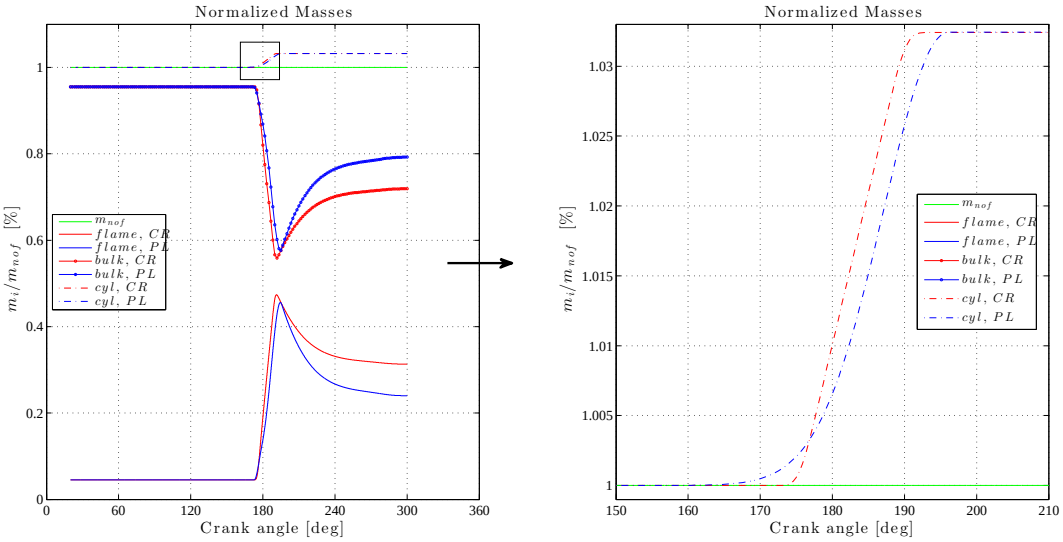

Figure 5-11: Zone masses

the plunger case since the S_{HH} factor is smaller for the common rail. In the detail, the total cylinder mass is shown. Here the injection progress variable can be seen indirectly, and again it can be noted how the injection process is shortened in the common rail system by using high constant injection pressure.

Gas Composition

Figure 5-12 illustrates the fresh air fraction in the cylinder. The shapes are very similar and the major difference is before the start of combustion where the air fraction change is dominated by the evaporation rate, which is different for each study case.

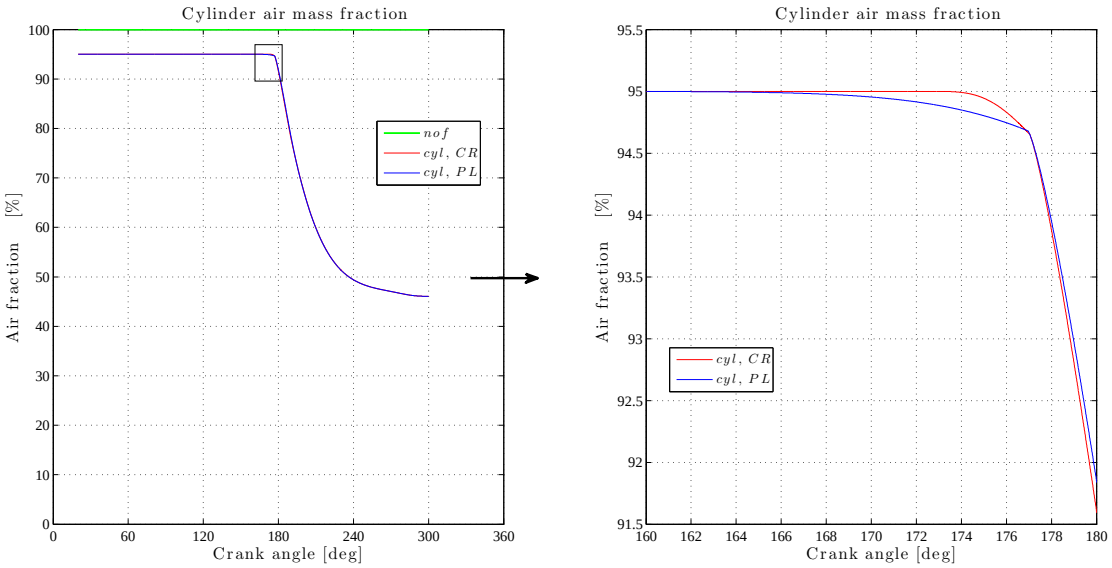

Figure 5-12: cylinder air fractions

In fig. 5-13 can be seen that the composition of the bulk zone is constant until combustion

starts and $\dot{m}_{sg}^{exit}$ is activated thus introducing stoichiometric gas to the zone. For the plunger system the air fraction is lower than the plunger system from that point until the end of the simulation since more stoichiometric gas is leaving the flame zone as a consequence of the higher S_{HH} factor used.

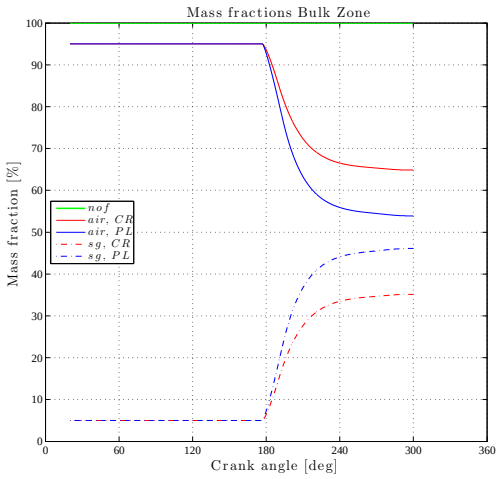

Figure 5-13: Mass fractions Bulk zone

The composition of the flame starts to change with evaporation and the corresponding entrained gas (Figure 5-14). The change of the flame zone composition is more marked once combustion starts. The difference in stoichiometric gas fraction between the two cases is a result of the S_{HH} factor given that the combustion rate is almost the same for either of the study cases. Contrary to the results in chapter 4 the amount of fuel in the flame zone is not zero because the evaporation rate and combustion rate are not equal and they do not start at the same time.

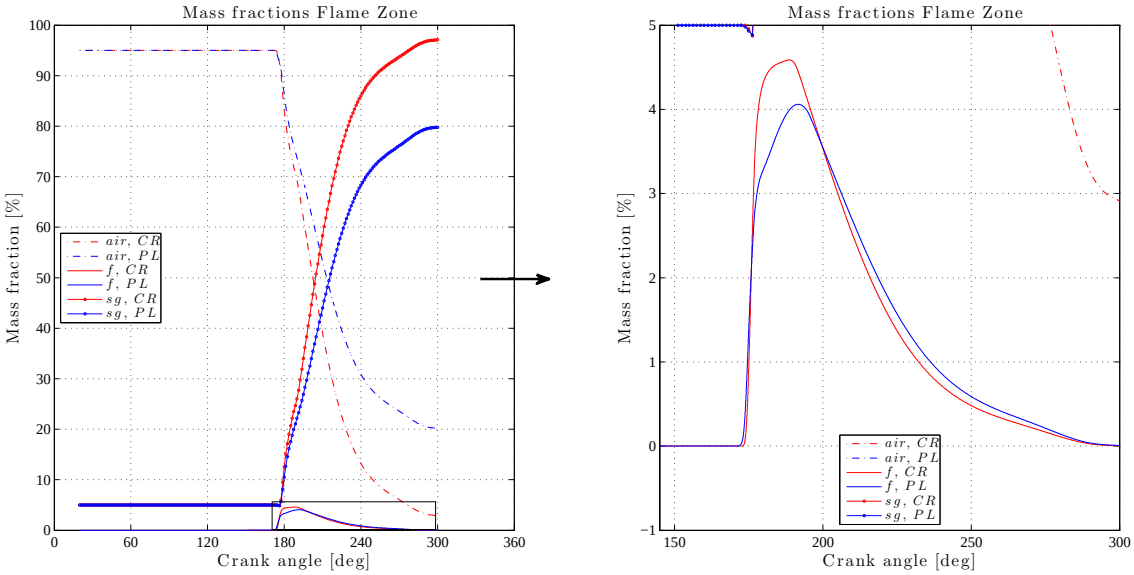

Figure 5-14: Mass fractions Flame zone

NOx emissions

In this section the results for the computed NO formation using the basic Zeldovich mechanism are presented. Although, the mechanism gas was implemented in the flame zone and the bulk zone, the results of the bulk zone are omitted because the formed NO in this zone is almost zero.

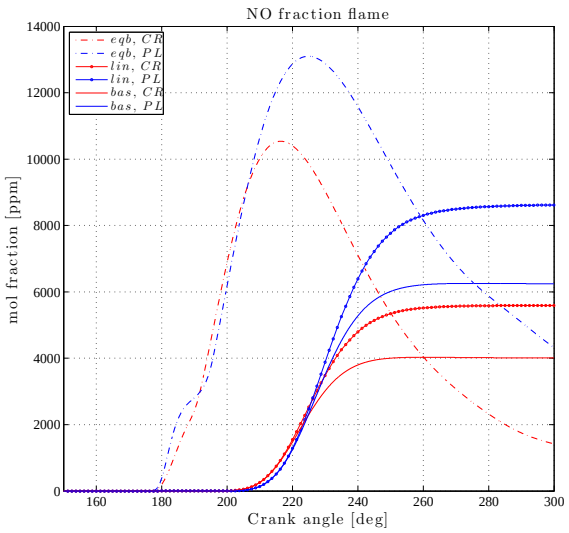

Figure 5-15: NOx fraction flame

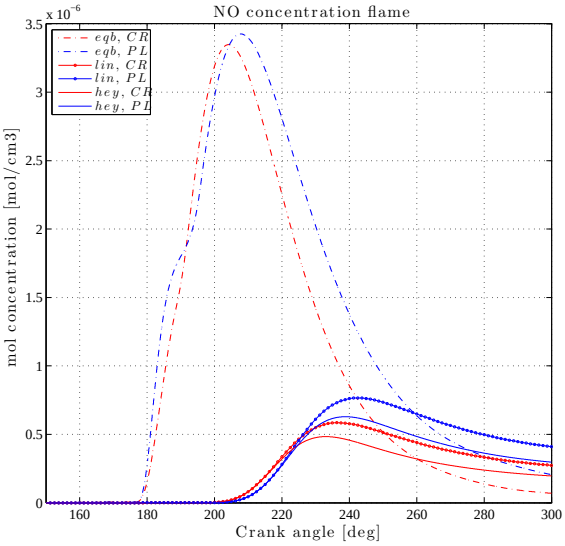

Figure 5-16: NOx concentration flame

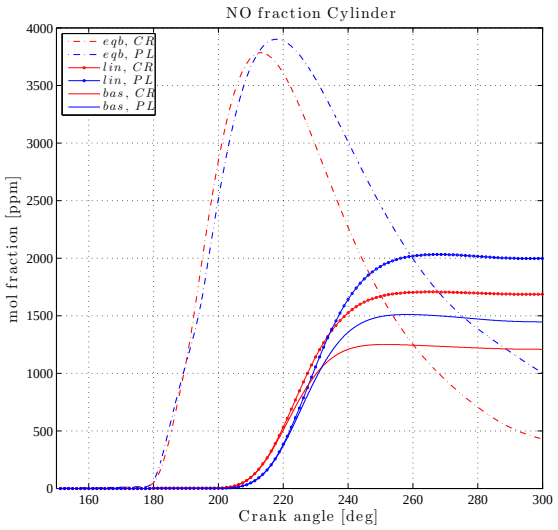

Figure 5-17: NOx fraction cyl

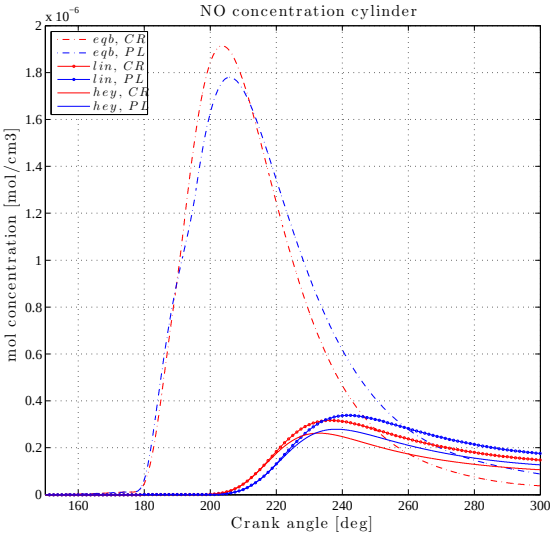

Figure 5-18: NOx concentration cyl

Figures 5-15–5-18 illustrate the NO formation. The figures present the computed values of NO using the basic Zeldovich mechanism along with the equilibrium values and the initially NO formed. The initially NO formed is the NO produced when $[NO]/[NO]_e \ll 1$.

First the computed NO fraction and concentration in the flame zone are shown in figs. 5-15 and 5-16. The values of NO are higher with the plunger injection system than with the common rail injection system, which was the expected result given the higher temperatures

of the flame zone for the plunger case. In the second set (figs. 5-17 and 5-18) the NO fraction and concentration are presented as the NO formed in the flame after being mixed with the rest of the gases in the cylinder and the values follow the same trends of the flame zone NO. The NO fractions of the flame zone are higher since there are less moles in the flame zone than in the cylinder. Same happens with the concentration because the cylinder volume is larger than the flame volume.

It can be seen from flame or cylinder values that NO formation is slow and does not reach the equilibrium values, and by the end of the closed in-cylinder process the equilibrium values are lower than the chemical kinetics values.

5-4 Discussion

The simulation of the complete model was discussed in this chapter. The ignition delay and NO formation were implemented in the model and results presented. From the results obtained it is clear that the model is capable to model the closed in-cylinder process. Apart from the already mentioned difficulties for the liquid block in chapter 3, the evaporation model responds well to the changing conditions of the engine. Even though the evaporation rate is distorted once combustion starts, in general terms the evaporation rate follows the shape of the injection rate. In addition, the model provides information on the differences of the two injection systems and the advantages of common rail injection.

The capability of the model to work with the mass flows having a different shape is presented and it was shown that suitable values for the three factors (S_{HH}, S_{mass} and λ_{ent}) can be selected to reproduce the imep and get reasonable values of NO emissions. It is important to note that the combustion rate used in this chapter is the same for the two cases which ultimately is unrealistic.

Difficulties arise from the use of Vibe reaction rate because it does not take into account the availability of fuel or fresh air in the flame zone. For this reason careful selection of the three parameters must be done to avoid complete depletion of fuel or fresh air in the flame zone before EO.

As a final remark, it can be said that the model in its current state can reproduce NO emissions results for a given engine but its prediction capabilities are rather limited. This because there are multiple combinations of factors for which the imep is reproduced with very different flame zone temperature traces.

Chapter 6

Conclusions and Recommendations

In this chapter, the key-points of the previously discussed topics are brought together in the conclusions section. This is then followed by a set of recommendations for future work to model the closed in-cylinder process.

6-1 Conclusions

In this work, modelling of the closed in-cylinder process for DI diesel engines is addressed. Different approaches where revised initially, covering single, few and multi-zone models. A three-zone model was proposed based on the basic concept devised in the work of Stapersma [4] and using some concepts of the models revised in chapter 1. The Model proposed in this work has one liquid zone and two gas zones that together form the cylinder volume. This approach was taken in order to have a simple model where computational times are short and to study how much can be studied with a minimal number of zones. The model was implemented in Matlab/Simulink using fundamental blocks and property libraries inherited from the single zone in-cylinder model developed in the SDPO group in TU Delft. Extension of the gas properties was made to allow for the existence of vaporous fuel in the flame zone. Libraries for the physical properties of the fuel were introduced and can be used in future work.

The basic concept and division of the cylinder volume is presented in chapter 2 accompanied with the basic equations derivation based on first principles (mass and energy conservation) providing a strong foundation and supporting the adequacy of the model. From the interaction between the different zones and the cylinder boundary, mass and heat flows arise in the conservation equations and modelling of the flows is needed. Basic models for these flows are introduced in chapters 3 and 4 trying to keep the simplicity of the model.

In order to implement the model, it was split; in chapter 3 the liquid phase is modelled and tested, and the same is done for the gas phase (flame zone and bulk zone) in chapter 4. This approach was chosen because it helped the programming and debugging of the Matlab/Simulink code and it also allowed to study the sub-models proposed before putting all together.

In Chapter 3 a single droplet approach together with the expressions proposed by Borman [49] is used to describe the evaporation process and from the analysis it can be concluded that it is adequate to simulate the evaporation process in the engine. Additionally, the injection rate is modelled for two injection systems. The proposed modelling of the injection is not reached by simulating the dynamics of the injector but the fundamentals of each injection scheme are captured while keeping the model simple. The calculation of the drop diameter from SMD empirical expressions to determine the drop diameter every time step rather than from droplet mass balance causes some difficulties, producing some non-physical results. Despite the fact that this approach for the fuel drop diameter is fundamentally wrong, it proves to be a simple approach and helps to avoid the need to follow the history of individual fuel packets.

In Chapter 4 the gas phase is modelled neglecting the existence of liquid fuel assuming that evaporation is infinitely fast and dwelling time between injection and start of combustion is zero. Furthermore the injection rate follows the same shape as the combustion rate. The modelling of the combustion rate is inherited from the single zone model using a double Vibe function. The entrainment rate is modelled by the concept that entrainment is linked to evaporation rate that ultimately is related to the injection rate, and combustion stoichiometry. In a similar thinking the flow of stoichiometric gas from the flame zone to the bulk zone is linked to the production rate of stoichiometric gas. In this way the simplicity of the overall in-cylinder process model is preserved. In the analysis of chapter 4 it was shown that the model is able to simulate the in-cylinder process but the lack of extra modelling of the mixing process ($\dot{m}_g^{ent}$, $\dot{m}_{sg}^{exit}$) limits the prediction abilities of the model, because the single zone in-cylinder process is needed to calibrate the model by matching the imep.

The complete model is assembled and tested in Chapter 5. In this chapter the timing of the combustion rate is introduced by means of ignition delay. Moreover, the mechanism of NO formation is coupled with the model to compute emissions, which is the ultimate reason to model the in-cylinder process using more than one zone. The analysis of the complete model shows the capacity of the model to simulate the process with the existence of liquid and gaseous fuel in the cylinder; this permits to grasp details of the complexities of the mixing process in the cylinder that in a single zone cannot be extracted. With appropriate selection of the three factors (S_{mass}, S_{HH} and λ_{ent}) the model can be calibrated to match imep and compute NO emission at reasonable values. The capacity of the model to predict emissions is then limited because for different selection of factors very different conditions in the flame zone can be achieved.

All in all, the model proposed in this work is able to simulate the in-cylinder process, but extra modelling to incorporate more physics into the model particularly the mixing process is needed to improve the description of the process so that predictions can be made with the model.

6-2 Recommendations

The recommendations for further work following this graduation project are:

- As mentioned in chapter 3 and chapter 5 the evaporation rate follows closely the injection rate. Thus it is recommended to continue with a two zone model where no liquid fuel exists in the cylinder and connect the injection block directly to the flame zone.
- The main input for the model is the injection rate, then a more detailed modelling of the injector including the dynamics of the injector and possible control system will provide a more detailed injection rate and a more accurate simulation of the closed in-cylinder process.
- Modelling of the mixing process is of utmost importance to simulate the in-cylinder process. Therefore, more detailed models for the entrainment rate and exit of stoichiometric must be included. This modelling could be done based on turbulent mixing using turbulent time scales in a similar way as it is done in the work of Mehta [38].
- Given the limitations of the Vibe function to adapt to the conditions in the flame zone and once a more detailed model for the entrainment rate is implemented; a new model for the combustion rate that takes into account the availability of fuel and fresh air in the flame zone should be included. This can be done using one of the approaches presented in Chapter 1.

Appendix A

Thermodynamic properties

The in-cylinder gas consists of air, stoichiometric gas and vaporous fuel. The air is a mixture of Nitrogen (N2), Oxygen (O2), Argon (Ar) and Carbon dioxide (CO2); the stoichiometric gas is the mixture of of Nitrogen (N2), Argon (Ar), Carbon dioxide (CO2), Sulphur oxide (SO2) and Water (H2O). For each species in air and stoichiometric gas, they are considered to be ideal but non-perfect gases and then the mixture behaves as ideal but non-perfect as well. Therefore the specific heat, enthalpy, and internal energy of air and, stoichiometric gas are functions of only temperature and the mixture fractions. The latter is well defined for air and for stoichiometric gas it can be calculated based on fuel composition and a fuel reaction mass balance. Ultimately the properties of the gas phase are functions of only temperature and air fraction in the cylinder.

A power series of the (normalized) temperature is used to fit these property data for all the species in both air and stoichiometric gas and then the properties of air and stoichiometric gas can be known on the basis of ideal mixture. Finally the composition of each zone is used to calculate the in-cylinder gas property data.

The specific heat at constant pressure is:

$$c_p = a_1 + a_2 \cdot \theta + a_3 \cdot \theta^2 \ldots + a_k \cdot \theta^{k-1} \ldots a_m \cdot \theta^{m-1} \tag{A-1}$$

where $\theta = \frac{T - T_{shift}}{T_{norm}}$.

If the Kelvin temperature scale is used the shift temperature is zero Kelvin and the normalized temperature is 1000 K.

$$T_{shift} = 0K \tag{A-2}$$

$$T_{norm} = 1000K \tag{A-3}$$

The specific heat at constant volume is computed from ideal gas consideration as follows:

$$c_{v,j} = c_{p,j} - R_j = \sum_{k=1}^{m} a_{k,j}\theta^{k-1} - R_j \tag{A-4}$$

Additionally, for an ideal gas

$$dh_j \overset{\text{ideal}}{=} c_{p,j} \cdot dT \qquad \Longrightarrow \Delta h_j = h_j - h_j^{ref} = \int_{T_{ref}}^{T} c_{p,j} \cdot dT \tag{A-5}$$

In terms of the normalized temperature (θ)

$$\begin{aligned} \Delta h_j = h_j - h_j^{ref} &= T_{norm} \cdot \int_{\theta_{ref}}^{\theta} c_{p,j} \cdot d\theta \\ &= \sum_{k=1}^{m} \frac{a_{k,j}}{k} \cdot T_{norm} \cdot \theta^k - \sum_{k=1}^{m} \frac{a_{k,j}}{k} \cdot T_{norm} \cdot \theta_{ref}^k \end{aligned} \tag{A-6}$$

where:

- θ_{ref} is the normalised reference temperature.

- h_j^{ref} is enthalpy at reference condition (temperature).

The internal energy is obtained from ideal gas.

$$u_j = \Delta u_j + u_j^{ref} = h_j - R_j \cdot T \tag{A-7}$$

Then the properties of air can be calculated summing the properties of each species weighted by the mass fractions of the species. The expressions for the stoichiometric gas are the same as for air, the index "sg" (stoichiometric gas) taking the place of index "a" (air) in the next set of equations

$$c_{v,a} = c_{p,a} - R_a = \sum_j x_j^a \cdot c_{p,j} - \sum_j x_j^a \cdot R_j \tag{A-8}$$

$$h_a = \sum_j x_j^a \cdot h_j \tag{A-9}$$

$$u_a = \sum_j x_j^a \cdot u_j \tag{A-10}$$

In the dry air, the species considered are N_2, O_2, Ar and CO_2; in the stoichiometric gas the species are N_2, Ar, CO_2 H_2O and CO_2.

In the work of Ding Yu [52], the diesel fuel is assumed to consist of an alkane ($C_{13}H_{28}$) and a benzene ($C_{13}H_{28}$), the idea being that the chosen species are typical for all alkanes and aromatics and that the specific heat of alkanes and aromatics differ both at reference temperature and in their temperature dependence. The fraction of $C_{13}H_{28}$ and $C_{13}H_{28}$ is calculated from the carbon percentage of the fuel, which is known when the fuel type is determined.

Finally, the gas properties in each zone are computed from the respective composition.

$$c_{v,i} = x_{a,i} \cdot c_{v,a,i} + x_{f,i} \cdot c_{v,f,i} + (1 - x_{a,i} - x_{f,i}) \cdot c_{v,sg,i} \tag{A-11}$$

$$h_i = x_{a,i} \cdot h_{a,i} + x_{f,i} \cdot h_{f,i} + (1 - x_{a,i} - x_{f,i}) \cdot h_{sg,i} \tag{A-12}$$

$$u_i = x_{a,i} \cdot u_{a,i} + x_{f,i} \cdot u_{f,i} + (1 - x_{a,i} - x_{f,i}) \cdot u_{sg,i} \tag{A-13}$$

The sub index "i" in these equation refers to the zones (flame and bulk).

The calculation of the properties of liquid fuel is somewhat different from the gaseous fuel. The enthalpy of the liquid fuel is based on the definition:

$$h_{f,liq} = u_{f,liq} + \frac{p}{\rho_{f,liq}} \tag{A-14}$$

The internal energy of liquid fuel is:

$$u_{f,liq} = u_f^{ref} + c_{v,f,liq} \cdot (T - T_{ref}) \tag{A-15}$$

The reference value u_f^{ref} equals h_f^{ref} minus the volume work (p_{ref}/ρ_f^{ref}) at the same reference temperature. The reference enthalpy h_f^{ref} of the fuel was used to match the effective heat of combustion. The evaporation heat of the two typical fuel constituents at reference condition can be estimated based on [57].

The density of liquid fuel can be taken according to [4]

$$\rho_{f,liq} = \rho_f^{15} - 0.68 \cdot (T - 15) \tag{A-16}$$

With ρ_f^{15} the fuel liquid density at $15°C$, and T is in $°C$.

Table A-1: Coefficients for the polynomial to calculate c_p

	a_1	a_2	a_3	a_4	a_5	a_6
N_2	3.5463	-0.5773	1.8224	-1.1149	0.2731	-0.0239
O_2	3.0845	1.8622	-1.0049	0.2817	-0.0320	0.0007
Ar	2.500	0.000	0.000	0.000	0.000	0.000
CO_2	2.5468	8.0614	-5.9398	2.2908	-0.4380	0.0327
H_2O	3.9800	-0.4380	2.5797	-1.4469	0.3244	-0.0264
SO_2	2.7915	8.9226	-8.4591	4.1789	-1.0431	0.1038
$C_{13}H_{10}(g^*)$	-74.758	1018.70	-717.21	221.4	-20.28	0.000
$C_{13}H_{28}(g^*)$	110.40	533.21	739.84	1021.2	324.23	0.000
$C_{13}H_{10}(l^+)$	2210	0.000	0.000	0.000	0.000	0.000
$C_{13}H_{28}(l^+)$	1700	0.000	0.000	0.000	0.000	0.000

**(g): means gaseous fuel; $^+$ (l): means liquid fuel*

Table A-2: Evaporation heat of fuel composition at $p = 0.1\,MPa$, $T = 25°C$

	h_{ref} [kJ/kg]
$C_{13}H_{10}$	339
$C_{13}H_{28}$	246

Table A-3: Reference enthalpy at $p = 0.1\,MPa$, $T = 25°C$

	h_{ref} [kJ/mol]
N_2	0.00
O_2	0.00
Ar	0.00
CO_2	-393.51
H_2O	-241.83
SO_2	-296.8

Appendix B

Physical properties the fuel

The transport properties of the fuel required to compute the evaporation rate and sauter mean diameter (SMD) are presented in this appendix. These properties were taken from different sources because no individual source provided the complete set of properties needed for the computations in this model.

B-1 Liquid properties

The main physical properties which affect the atomization process are kinematic viscosity, surface tension and density.

The liquid properties of the diesel fuel are taken from the work of El-Kotb [46].

$$\nu_{f,l} = A \cdot (T + 30)^{-b} \cdot \exp(c \cdot F) \tag{B-1}$$

$$\sigma_{f,l} = \left(1 - 9 \times 10^{-4} \cdot T\right) \cdot (K + a \cdot F) \cdot 10^{-3} \tag{B-2}$$

where F represents the volume percentage of diesel if the fuel is a mixture of Diesel fuel and Light diesel fuel. The kinematic viscosity (nu) is meter squared per second $[m^2/s]$ and the surface tension in newton per meter $[N/m]$.

The coefficients for the formulas are presented in the next table.

Table B-1: Coefficients for liquid fuel properties

	Diesel fuel-light diesel fuel
A	5.55×10^{-4}
a	0.51
b	1.14
c	0.274
K	27.4

B-2 Gas properties

The gas thermal conductivity and the vapour pressure are taken from Lefebvre [58].

$$k_{f,g} = 10^{-6} \left[13.2 - 0.0313 \cdot (T_{bn} - 273)\right] \cdot \left(\frac{T}{273}\right)^{n} \tag{B-3}$$

where $n = 2 - 0.0372 \cdot \left(\frac{T}{T_{bn}}\right)^2$ and $T_{bn} = 536.4K$.

The vapour pressure is:

$$p_{vap,f} = 1000 \cdot \exp\left(15.5274 - \frac{5383.59}{T - 43}\right) \tag{B-4}$$

with T in K and $p_{vap,f}$ is in [Pa].

The fuel diffusivity in air and the dynamic viscosity are taken from Yaws [59] using n-Tetradecane to represent these properties as proposed by [22].

$$D_{fa} = (a + b \cdot T + c \cdot T^2) \cdot 10^{-4} \tag{B-5}$$

$$\mu_{f,g} = (a + b \cdot T + c \cdot T^2) \cdot 10^{7} \tag{B-6}$$

where the diffusivity is in $[m^2/s]$ and the dynamic viscosity is in $[\frac{kg}{m \cdot s}]$.

The coefficients for these two formulas are presented table B-2.

Table B-2: Coefficients for gaseous fuel properties

	a	b	c
D_{fa}	-0.02513	0.00013439	3.1511×10^{-7}
$\mu_{f,g}$	-10.397	0.157	1.0229×10^{-6}

Bibliography

[1] G. P. Merker, B. Hohlbaum, and M. Rauscher, "Two-zone model for calculation of nitrogen-oxide formation in direct-injection diesel engines," SAE Technical Paper 932454, SAE International, Warrendale, PA, Sept. 1993.

[2] G. Heider, G. Woschni, and K. Zeilinger, "Two-zone calculation model for the prediction of NO emissions from diesel engines.," (Interlaken), CIMAC, May 1995.

[3] H. Hiroyasu, T. Kadota, and M. Arai, "Development and use of a spray combustion modeling to predict diesel engine efficiency and pollutant emissions : Part 1 combustion modeling," vol. 26, no. 214, pp. 569–575, 1983.

[4] D. Stapersma, *Diesel Engines*, vol. 3: Combustion. The Netherlands: TU Delft / Royal Netherlands Naval College, 5th ed., 2009.

[5] J. B. Heywood, *Internal combustion engine fundamentals*. McGraw-Hill, 1988.

[6] G. P. Merker, "The two-zone cylinder model," in *Simulating Combustion: Simulation of Combustion and Pollutant Formation for Engine-development*, pp. 187–195, Springer, 2006.

[7] G. P. Merker, C. Schwarz, and R. Teichmann, *Combustion engines development mixture formation, combustion, emissions and simulation*. Berlin; New York: Springer, 2012.

[8] F. G. Chmela, G. H. Pirker, and A. Wimmer, "Zero-dimensional ROHR simulation for DI diesel engines a generic approach," *Energy Conversion and Management*, vol. 48, pp. 2942–2950, Nov. 2007.

[9] A. Jaipuria and P. A. Lakshminarayanan, "Prediction of the rate of heat release of mixing-controlled combustion in a common-rail engine with pilot and post injections," *Proceedings of the Institution of Mechanical Engineers, Part D: Journal of Automobile Engineering*, vol. 225, pp. 246–259, Feb. 2011.

[10] P. A. Lakshminarayanan, Y. V. Aghav, A. D. Dani, and P. S. Mehta, "Accurate prediction of the rate of heat release in a modern direct injection diesel engine," *Proceedings of*

the Institution of Mechanical Engineers, Part D: Journal of Automobile Engineering, vol. 216, pp. 663–675, Aug. 2002.

[11] P. A. Lakshminarayanan and Y. V. Aghav, "Phenomenology of diesel combustion and modelling," in *Modelling Diesel Combustion*, Mechanical Engineering Series, pp. 9–21, Springer Netherlands, Jan. 2010.

[12] G. Stiesch, *Modeling engine spray and combustion processes*. Berlin; New York: Springer, 2003.

[13] N. D. Whitehouse and R. Way, "Rate of heat release in diesel engines and its correlation with fuel injection data," *Proceedings of the Institution of Mechanical Engineers, Conference Proceedings*, vol. 184, pp. 17–27, Sept. 1969.

[14] A. E. W. Austen and W.-T. Lyn, "Relation between fuel injection and heat release in a direct-injection engine and the nature of the combustion processes," *Proceedings of the Institution of Mechanical Engineers: Automobile Division*, vol. 14, pp. 47–62, Jan. 1960.

[15] T. J. Williams and N. D. Whitehouse, "Investigation into some aspects of the computation of diesel engine combustion," *Proceedings of the Institution of Mechanical Engineers*, vol. 190, pp. 467–475, June 1976.

[16] C. Rakopoulos, D. Rakopoulos, E. Giakoumis, and D. Kyritsis, "Validation and sensitivity analysis of a two zone diesel engine model for combustion and emissions prediction," vol. 45, pp. 1471–1495, June 2004.

[17] C. Rakopoulos, A. Dimaratos, E. Giakoumis, and D. Rakopoulos, "Exhaust emissions estimation during transient turbocharged diesel engine operation using a two-zone combustion model," vol. 49, pp. 125–149, Jan. 2009.

[18] H. Hiroyasu, T. Kadota, and M. Arai, "Development and use of a spray combustion modeling to predict diesel engine efficiency and pollutant emissions : Part 2 computational procedure and parametric study," vol. 26, no. 214, pp. 576–583, 1983.

[19] H. Hiroyasu, "Diesel engine combustion and its modeling," (Tokyo, Japan), pp. 53–75, Sept. 1985.

[20] H. Hiroyasu, O. Furukawa, M. Arai, S. Iida, and H. Motonaga, "Development and use of a spray combustion modeling to predict diesel engine efficiency and pollutant emissions : Part 3 an analysis by the method of system-model transformation," vol. 26, no. 214, pp. 584–591, 1983.

[21] G. Stiesch, *Phänomenologisches Multizonen-Modell der Verbrennung und Schadstoffbildung im Dieselmotor*. PhD thesis, Universität Hannover, Düsseldorf, 1999.

[22] G. Stiesch and G. Merker, "A phenomenological heat release model for direct injection diesel engines," in *CIMAC, Proceedings of the 22nd CIMAC International Congress on Combustion Engines*, vol. 2, (Copenhagen), pp. 423–430, May 1998.

[23] D. Jung and D. N. Assanis, "Quasidimensional modeling of direct injection diesel engine nitric oxide, soot, and unburned hydrocarbon emissions," vol. 128, no. 2, p. 388, 2006.

[24] D. Jung and D. N. Assanis, "Multi-zone DI diesel spray combustion model for cycle simulation studies of engine performance and emissions," SAE Technical Paper 2001-01-1246, SAE International, Warrendale, PA, Mar. 2001.

[25] D. Jung and D. N. Assanis, "Reduced quasi-dimensional combustion model of the direct injection diesel engine for performance and emissions predictions," *KSME International Journal*, vol. 18, pp. 865–876, May 2004.

[26] Y. H. Im and K. Y. Huh, "Phenomenological combustion modeling of a direct injection diesel engine with in-cylinder flow effects," vol. 14, no. 5, p. 569581, 2000.

[27] C. Rakopoulos, K. Antonopoulos, and D. Rakopoulos, "Multi-zone modeling of diesel engine fuel spray development with vegetable oil, bio-diesel or diesel fuels," *Energy Conversion and Management*, vol. 47, pp. 1550–1573, July 2006.

[28] C. Rakopoulos, K. Antonopoulos, D. Rakopoulos, and D. Hountalas, "Multi-zone modeling of combustion and emissions formation in DI diesel engine operating on ethanoldiesel fuel blends," *Energy Conversion and Management*, vol. 49, pp. 625–643, Apr. 2008.

[29] A. M. Kulkarni, G. M. Shaver, S. S. Popuri, T. R. Frazier, and D. W. Stanton, "Computationally efficient whole-engine model of a cummins 2007 turbocharged diesel engine," vol. 132, no. 2, p. 022803, 2010.

[30] T. Cerri, A. Onorati, and E. Mattarelli, "1D engine simulation of a small HSDI diesel engine applying a predictive combustion model," vol. 130, no. 1, p. 012802, 2008.

[31] M. M. A. A. Al-Sood, M. Ahmed, and Y. M. Abdel-Rahim, "Rapid thermodynamic simulation model for optimum performance of a four-stroke, direct-injection, and variable-compression-ratio diesel engine," *Int J Energy Environ Eng*, vol. 3, pp. 1–13, Dec. 2012.

[32] A. Marchenko, A. Osetrov, O. Linkov, and D. Samoilenko, "Simulation of biofuels combustion in diesel engines," in *Biodiesel - Feedstocks, Production and Applications* (Z. Fang, ed.), InTech, Dec. 2012.

[33] D. T. Hountalas, D. A. Kouremenos, E. G. Pariotis, V. Schwarz, and K. B. Binder, "Investigation concerning the effect of post fuel injection on the performance and pollutants of heavy duty diesel engines using a multi-zone combustion model," in *Thermo- and Fluid Dynamic Processes in Diesel Engines 2* (J. H. Whitelaw, F. Payri, C. Arcoumanis, and J. M. Desantes, eds.), pp. 257–283, Berlin, Heidelberg: Springer Berlin Heidelberg, 2004.

[34] Z. Gao and W. Schreiber, "A phenomenologically based computer model to predict soot and NOx emission in a direct injection diesel engine," *International Journal of Engine Research*, vol. 2, pp. 177–188, June 2001.

[35] S. Kumar, M. Kumar Chauhan, and Varun, "Numerical modeling of compression ignition engine: A review," *Renewable and Sustainable Energy Reviews*, vol. 19, pp. 517–530, Mar. 2013.

[36] T. Ahmad and A. Alkidas, "A simple correlation for mixing and combustion rates in diesel engines," (Tokyo, Japan), pp. 393–403, Sept. 1985.

[37] M. Ishida, Z. Cheni, H. Ueki, and D. Sakaguch, "Combustion analysis by two-zone model in a DI diesel engine," (Yokohama, Japan), pp. 309–314, July 1994.

[38] B. T and P. Mehta, "A multi-zone diesel combustion model using eddy dissipation concept," (Kyoto, Japan), pp. 135–140, July 1998.

[39] B. Xiao, C.-j. Tong, and B.-z. Li, "Combustion modelling and performance prediction of medium speed diesel engine," (Tokyo, Japan), Sept. 1985.

[40] H. Tanabe, H. Sugihara, M. Kawakami, N. Iida, H. Fujimoto, and G. Sato, "Heat release model based on combustion phenomena," (Tokyo, Japan), pp. 383–392, Sept. 1985.

[41] X. Xue and J. A. Caton, "Detailed multi-zone thermodynamic simulation for direct-injection diesel engine combustion," *International Journal of Engine Research*, Feb. 2012.

[42] X. Xue and J. Caton, "Nitric oxide and soot emissions determined from a multi-zone thermodynamic direct-injection diesel engine combustion model," *International Journal of Engine Research*, Dec. 2012.

[43] Asay, Richard J., *A five-Zone model for direct injection diesel combustion.* Brigham young university, Brigham, 2003.

[44] E. Pariotis, G. Kosmadakis, and C. Rakopoulos, "Comparative analysis of three simulation models applied on a motored internal combustion engine," *Energy Conversion and Management*, vol. 60, pp. 45–55, Aug. 2012.

[45] C. Baumgarten, *Mixture formation in internal combustion engines.* Berlin: Springer, 2006.

[46] M. M. Elkotb, "Fuel atomization for spray modelling," *Progress in Energy and Combustion Science*, vol. 8, no. 1, pp. 61–91, 1982.

[47] S. S. Sazhin, "Advanced models of fuel droplet heating and evaporation," *Progress in Energy and Combustion Science*, vol. 32, no. 2, pp. 162–214, 2006.

[48] E. Wakil, O. Uyehara, and P. Myers, *A Theoretical Investigation of the Heating-up Period of Injected Fuel Droplets Vaporizing in Air.* Technical note 3179 National Advisory Committee for Aeronautics, National Advisory Committee for Aeronautics, 1954.

[49] G. L. Borman and J. H. Johnson, "Unsteady vaporization histories and trajectories of fuel drops injected into swirling air," SAE Technical Paper 620271, SAE International, Warrendale, PA, Jan. 1962.

[50] W. Ranz and W. Marshall, "Evaporation from drops," *Chem. Eng. Prog*, vol. 48, no. 3, pp. 141–146, 1952.

[51] F. P. Incropera, A. S. Lavine, and D. P. DeWitt, *Fundamentals of Heat and Mass Transfer.* John Wiley & Sons, Apr. 2011.

[52] Y. Ding, *Characterising Combustion in Diesel Engines: using parameterised finite stage cylinder process models.* PhD thesis, TU Delft, Delft University of Technology, Dec. 2011.

[53] Edwin Knobbe and Douwe Stapersma, "Some new ideas for performing heat release analysis," in *23 - Congres International des Machines a Combustion (CIMAC)*, (Hamburg), 2001.

[54] D. Stapersma, *Diesel Engines*, vol. 4: Emissions and Heat Transfer. The Netherlands: TU Delft / Royal Netherlands Naval College, 5th ed., 2009.

[55] D. N. Assanis, Z. S. Filipi, S. B. Fiveland, and M. Syrimis, "A predictive ignition delay correlation under steady-state and transient operation of a direct injection diesel engine," *Journal of Engineering for Gas Turbines and Power*, vol. 125, no. 2, p. 450, 2003.

[56] D. Stapersma, "Zeldovich mechanism for NO formation," Tech. Rep. KIM-PFS-2012-189, Issue A, Royal Netherlands Naval College, Jan. 2012.

[57] G. L. Borman and K. W. Ragland, *Combustion engineering*. McGraw-Hill, Jan. 1998.

[58] A. H. LEFEBVRE and J. S. CHIN, "Steady-state evaporation characteristics of hydrocarbon fuel drops," *AIAA Journal*, vol. 21, no. 10, pp. 1437–1443, 1983.

[59] C. L. Yaws, "Yaws' handbook of thermodynamic and physical properties of chemical compounds."

Glossary

List of Acronyms

TU Delft	Delft University of Technology
CFD	computational fluid Mechanics
CRR	combustion reaction rate
IC	inlet valve closed
EO	exhaust valve open
SOI	start of injection
SOC	start of combustion
TDC	Top Dead Centre
BDC	Bottom Dead Centre
DI	direct injection
CR	common rail injections system
PL	plunger injection system
ROHR	rate of heat release
EGR	exhaust gas recirculation
SMD	sauter mean diameter
CI	compression ignition
SDPO	ship design, propulsion and operation
MT	Marine Technology
imep	indicated mean effective pressure
NECA	NO_x emission control area

Symbol

A	area	m^2
A_B	bore area	m^2
A_{eff}^{inj}	effective injection area	m^2
AF_{st}	stoichiometric air-fuel ratio	m^2
C_D	discharge coefficient	[-]
D_B	bore	m
D_{fa}	binary diffusivity fuel in air	m^2/s
E	activation energy	J
E_{kin}	kinetic energy	J
H	enthalpy	J
H_u	lower heating value	J
$\dot{H}$	enthalpy flow	J/s
I_{hv}	heat value of fuel	J
L_{min}	stoichiometric air-fuel ratio	[-]
L_p	stroke	m
N_{drop}	number of droplets	[-]
Nu	Nusselt number	[-]
P	preparation rate	kg/s
P_i	indicated power	W
Q_{comb}	combustion heat	J
$\dot{Q}_{comb}$	combustion heat flow	W
$\dot{Q}_{loss}$	heat loss flow	W
$\dot{Q}_{loss}$	super heat flow	W
Q_B	heat release	J
Q_f	heat from fuel	J
Q_i	heat input	J
R	chemical reaction rate	kg/s
R	gas constant	J/kg/K
R_u	universal gas constant	J/mol/K
Re	Reynolds number	[-]
RR_m	premixed combustion rate	kg/s
RR_p	mixing combustion rate	kg/s
Sh	Sherwood number	[-]
Sc	Schmidt number	[-]
T	temperature	K
U	internal energy	J
$\dot{U}$	internal energy flow	J/s
V	Volume	m^3
V_s	stroke volume	m^3
W_T	Power transfer	W
X	normalized reaction rate	[-]
Z	normalized rate of combustion	[-]
a	Vibe parameter linked to combustion efficiency	[-]

b_k	Weight factors in multiple Vibe function	[-]
c	concentration	mol/m^3
c_m	mean piston speed	m/s
c_p	specific heat at constant pressure	J/kg/K
c_v	specific heat at constant volume	J/kg/K
d_{nozzle}	nozzle diameter	m
e_F	specific energy of flow	J/kg
h	specific enthalpy	J/kg
$h^{'}$	normalized plunger displacement	[-]
$\tilde{h_D}$	mass transfer coefficient	m/s
k	Reaction speed constant	[-]
k	turbulent kinetic energy	J
l	connecting rod length	m
m	mass	kg
m_B	fuel mass	kg
$m_{f,comb}$	fuel to be combusted	kg
m_k	Form factors in multiple Vibe function (k=1,2,3,..)	[-]
m_L	air mass	kg
$\dot{m}$	mass flow	kg/s
n	number of droplets	[-]
n_{end}	engine speed	rev/s
n_{noz}	number of nozzles	[-]
p	pressure	Pa
p_{vap}	vapour pressure	Pa
r	crank length	m
r_c	effective compression volume ratio	[-]
r_e	effective expansion volume ratio	[-]
t	time	s
t_{comb}	duration of combustion	s
t_{inj}	duration of injection	s
u	specific internal energy	J/kg
v	velocity	m/s
v_{tip}	spray tip velocity	m/s
u_{comb}	heat of combustion	J
x	mass fraction	[-]
y	mole fraction	[-]

Greek symbols

α_{drop}	heat transfer coefficient droplet	W/m^2/K
$\alpha_{g\rightarrow w}$	heat loss to the walls coefficient	W/m^2/K
Δh_R	reaction enthalpy	J/kg
ϵ	geometric compression ratio	[-]
η_{comb}	Combustion efficiency	[-]
η_{ind}	indicated efficiency	[-]
θ	normalized temperature	[-]

κ	thermal conductivity	W/m/K
λ	air excess ratio	[-]
λ_{CR}	radius to length ratio	[-]
μ	multiplication factor	[-]
μ	dynamic viscosity	kg/m/s
ν	kinematic viscosity	m^2/s
ξ	fuel burn rate (or combustion reaction rate)	kg/s
ρ	density	kg/m3
σ	air/fuel ratio	[-]
τ	Normalized time	[-]
τ	characteristic time scales	s
τ_{id}	ignition delay	ms
ϕ	equivalence ratio	[-]
φ	crank angle	deg

Subscript

0	trapped conditions
1	flame zone
2	bulk zone
a	fresh air
bu	burnt
cyl	cylinder
e	equilibrium
f	fuel
g	gas
inj	injection
m	mean value in evaporation layer
max	maximum
nof	no fuel
ref	reference
sg	stoichiometric gas
$wall$	cylinder walls (crown, liner or head)
$+$	forward direction
$-$	reverse direction

Superscript

in	into the system
out	out of the system
$comb$	combustion
ref	reference
ent	entrainment
$exit$	leaving flame zone
$evap$	evaporation
liq	liquid
inj	injection